THE UNIVERSITY OF CHICAGO

CHAPERONES REMODEL STRESS-INDUCED BIOMOLECULAR CONDENSATES

A DISSERTATION SUBMITTED TO
THE FACULTY OF THE DIVISION OF THE BIOLOGICAL SCIENCES
AND THE PRITZKER SCHOOL OF MEDICINE
IN CANDIDACY FOR THE DEGREE OF
DOCTOR OF PHILOSOPHY

GRADUATE PROGRAM IN BIOCHEMISTRY AND MOLECULAR BIOPHYSICS

BY
HANEUL YOO

CHICAGO, ILLINOIS
DECEMBER 2021

To my parents, Chul Ho and Jung Ja.

TABLE OF CONTENTS

LIST OF FIGURES

LIST OF TABLES

ACKNOWLEDGMENTS

I am grateful that I was able to meet and work with people who inspire me to become a better person and a scholar. First and foremost, I thank my advisor, D. Allan Drummond, for all the support, patience, and trust he showed me throughout my time in his lab. Because of his mentorship, I was able to get everything I wanted to get out of my graduate training and more. I thank both the former and current members of the Drummond lab (Chris Katanski, Josh Riback, Cat Triandafillou, Jared Bard, Sammy Keyport, Caitlin Wong, Hendrik Glauninger, Kyle Lin, and Rosalind Pan) for making the lab a fun place to come and do good science; I learned a lot from watching them and talking science with them over many lunches and experiments. The professors I met at the University of Chicago were extremely supportive. I especially thank Tobin Sosnick, Michael Rust, David Pincus, Joe Piccirilli and Jingyi Fei for their insightful questions, support, and guidance. I thank Shani Charles, Lisa Anderson, and other administrators and staffs in the Biochemistry and Molecular Biology Department for making it possible for all of us to work here. I thank my friends in Chicago for all the precious memories that make me smile. Finally, I thank my parents and brother for their endless love and support. I could not have come this far without them.

ABSTRACT

Stresses such as heat shock trigger formation of protein aggregates and induction of a disaggregation system composed of molecular chaperones. Recent work reveals that several cases of apparent heat-induced aggregation, long thought to be the result of toxic misfolding, instead reflect evolved, adaptive biomolecular condensation, with chaperone activity contributing to condensate regulation. Here I show that the yeast disaggregation system directly disperses heat-induced biomolecular condensates of endogenous poly(A)-binding protein (Pab1) orders of magnitude more rapidly than aggregates of the most commonly used misfolded model substrate, firefly luciferase. Beyond its efficiency, heat-induced condensate dispersal differs from heat-induced aggregate dispersal in its molecular requirements and mechanistic behavior. This work establishes a bona fide endogenous heat-induced substrate for long-studied heat shock proteins, rigorously isolates a specific example of chaperone regulation of condensates, and underscores needed expansion of the proteotoxic interpretation of the heat shock response to encompass adaptive, chaperone-mediated regulation.

CHAPTER 1

INTRODUCTION

The physical environment surrounding a cell is never constant but changes both regularly (e.g., daily cycles between day and night) and randomly (e.g., accidental increase in temperature, as happened to Ferruccio Ritossa's cells in 1962 leading to his discovery of the heat shock response [140, 141]). To survive in such fluctuating environment, cells evolved a remarkable capacity to sense and respond to various forms of environmental change. How do cells do this? This thesis aims to address this question by studying biomolecular condensates that form inside the cell in response to environmental stress.

Environmental stress such as heat shock or nutrient withdrawal triggers coalescence of specific endogenous proteins into higher-order structures without membrane or fixed-stoichiometry. Throughout the years, these structures have been called by various names including aggregates, assemblies, stress granules (SGs), puncta, or foci. In 2017, the term biomolecular condensates was proposed to collectively describe higher-order membraneless structures of concentrated biomolecules [11]. Biomolecular condensates are often associated with liquid-liquid phase separation (LLPS) [11]. One advantage of condensate formation by LLPS is that it allows proteins to undergo a switch-like transition from a diffusive to a condensed state [68, 196]. I discuss how cells harness the cooperative process of LLPS as a sensing mechanism in more detail in Chapter 2.

Whether LLPS is the dominant means to form biomolecular condensates *in vivo* and whether the liquid-likeness have functional importance remain unclear [196, 111]. For example, SGs and nucleolus in mammalian cells form via LLPS and are liquid-like [139, 57, 47], but the corresponding structures in fungi are solid-like [88, 6]. I use the term biomolecular condensates to refer to endogenous membraneless structures of concentrated biomolecules regardless of the mechanism of formation, reserving the term phase separation for cases where it has been demonstrated.

Heat shock is a primordial stress that reliably triggers a set of conserved molecular

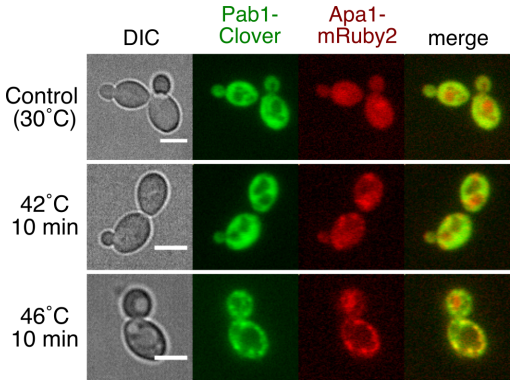

Figure 1.1: Heat shock triggers formation of biomolecular condensates. Confocal microscopy images of mock- or heat-treated budding yeast cells expressing Pab1-Clover and Apa1-mRuby2. Large Pab1-marked stress granules appear only in response to severe heat shock (46degreeC). Smaller condensates that form at milder heat shock temperature (42degreeC) are not visible but can be isolated by centrifugation [138]. The scale bar is 5 μm.

programs known as the heat shock response (HSR) [95]. The HSR involves 1) transcriptional activation of genes encoding heat shock proteins (Hsp) [125], many of which are molecular chaperones, and 2) formation of biomolecular condensates [27, 182]. Proteins enriched in heat-induced condensates are associated with RNA-binding and RNA helicase activities [182]. Heat-induced condensates of two endogenous proteins, Poly(A)-binding protein (Pab1) and Apa1, in budding yeast are shown in Figure 1.1.

An early and long-standing interpretation of these heat-induced condensates has been that they represent toxic aggregates of nonfunctional, un-/mis-folded proteins [181, 116, 95]. This interpretation is intuitive because it is well known that heat destabilizes protein [44]. However, a number of recent evidence from budding yeast challenge this interpretation and instead suggest condensate formation of at least several mature endogenous proteins represents a part of the evolved, adaptive cellular response to heat shock:

1) A specific set of endogenous mature proteins form condensates which fully reverse to functional units without degradation as cells recover from stress [182]. In the case of a heterotrimeric aminoacyl-tRNA synthetase complex, the complex retains both its enzymatic activity and specificity even after condensation *in vitro*. This shows that a

protein can still remain structurally stable and functional in heat-induced condensates.

2) If heat-induced condensates represent toxic aggregates, preventing their formation should increase cell's fitness. However, preventing condensation of Pab1 or DEAD-box helicase Ded1 decreased cell's fitness during stress [138, 72], indicating that condensation is adaptive.

3) Condensates of endogenous proteins are dispersed faster than that of exogenous misfolded protein (e.g., luciferase) [27, 88]. Dispersal of only the endogenous condensates correlates with the timing of translation resumption and cell cycle re-entry [27, 88], hinting a regulatory role of condensates.

It is important to note that the evidence for adaptive function of stress-induced condensates is restricted to endogenous mature proteins. Nascent polypeptides and newly synthesized proteins in the process of folding are thought to be highly susceptible to heat-induced misfolding and aggregation [10, 172, 92]. Expression and aggregation of exogenous, misfolding-prone reporter proteins (e.g., luciferase, Ubc9ts, and destabilized fluorescent proteins) compromise cellular fitness [51] and change the dynamics of endogenous condensates [108, 57].

While there are condensates which reverse autonomously when the environment returns to normal, some condensates require additional factor(s) for facilitated dispersal. Examples of condensate regulators whose activity has been demonstrated both *in vivo* and *in vitro* include nuclear-import receptors [59] and post-translational modifiers such as dual-specificity kinase (DYRK3) [190, 133] and lysine (de)acetylases [151]. The benefits of autonomous versus facilitated dispersal is further discussed in Chapter 2 [196].

We and others have hypothesized molecular chaperones, specifically the molecular disaggregation system, as direct regulators of heat-induced biomolecular condensates [182, 138, 89, 196, 176, 13, 166, 24]. This hypothesis is backed by many *in vivo* data which show delayed SG dispersal when one or more chaperones are inhibited or deleted [27, 183, 88, 89, 24]. A direct biochemical demonstration of heat-induced condensate dispersal by molecular chaperones

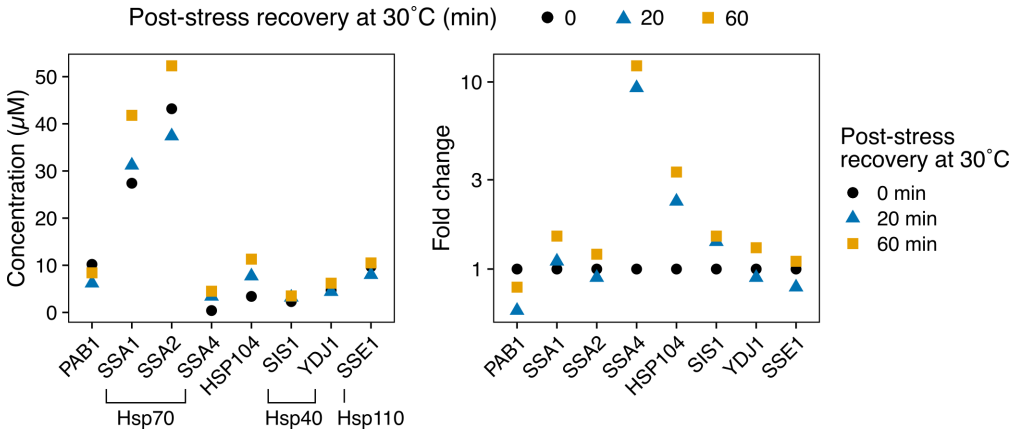

Figure 1.2: Endogenous concentrations of Pab1 and molecular chaperones during recovery.
Estimated absolute concentrations (left) and fold-change in concentrations (right) of Pab1 and molecular chaperones after a 10 minute, 42°C heat shock. Concentrations are estimated using measurements of absolute protein concentration in budding yeasts growing at 30°C [29] and fold change in concentration following acute heat shock [182]. Ssa1/2 and Ssa4 are constitutively-expressed and heat-inducible Hsp70 paralogs, respectively. Sis1 and Ydj1 are type II and type I Hsp40s, respectively. Sse1 is a nucleotide exchange factor for Hsp70.

has been missing. I provide this data in Chapter 3 [195].

In Chapter 3 [195], I use biochemical reconstitution to demonstrate that the molecular disaggregation system consisting of three chaperones (Hsp104, Hsp70, and Sis1) is both necessary and sufficient for complete dispersal of heat-induced Pab1 condensates *in vitro*. Comparative studies of Pab1 condensates and aggregates of misfolded luciferase reveal key differences in their engagement with chaperones. Importantly, I find that chaperones are much more efficient at dispersing Pab1 condensates than luciferase aggregates, which is consistent with the faster dispersal of endogenous condensates observed *in vivo* [27, 88]. I construct and simulate kinetic models of the reconstituted system, which provides an insight about the mechanism by which chaperones detect condensed substrate and why Hsp70s—the most abundant cytosolic chaperone enzymes (Figure 1.2)—need to be present in excess for efficient condensate dispersal.

CHAPTER 2

CELLULAR SENSING BY PHASE SEPARATION: USING THE PROCESS, NOT JUST THE PRODUCTS

This chapter was published as: Yoo et al. 2019. [196]

2.1 Abstract

Phase separation creates two distinct liquid phases from a single mixed liquid phase, like oil droplets separating from water. Considerable attention has focused on how the products of phase separation—the resulting condensates—might act as biological compartments, bioreactors, filters, and membraneless organelles in cells. Here, we expand this perspective, reviewing recent results showing how cells instead use the process of phase separation to sense intracellular and extracellular changes. We review case studies in phase separation-based sensing and discuss key features, such as extraordinary sensitivity, which make the process of phase separation ideally suited to meet a range of sensory challenges cells encounter.

2.2 Introduction

Phase separation is a process through which a single phase composed of mutually soluble components demixes into two or more distinct phases (Fig. 1A), as with oil and water. In biology, liquid–liquid phase separation has emerged as a means to form coherent structures with a range of potential functions [68, 161, 11, 65]. Structures resulting from phase separation have been given various names, including membraneless organelles or biomolecular condensates, reflecting the breadth of scenarios in which they occur and the potential functions they may fulfill. The nucleolus provides a canonical example of a membraneless organelle, compartmentalizing key steps in ribosome production within the nucleus without membrane boundaries. The vertebrate nucleolus displays liquid-like behaviors [43, 19], and its structure arises in part from phase separation [43, 184].

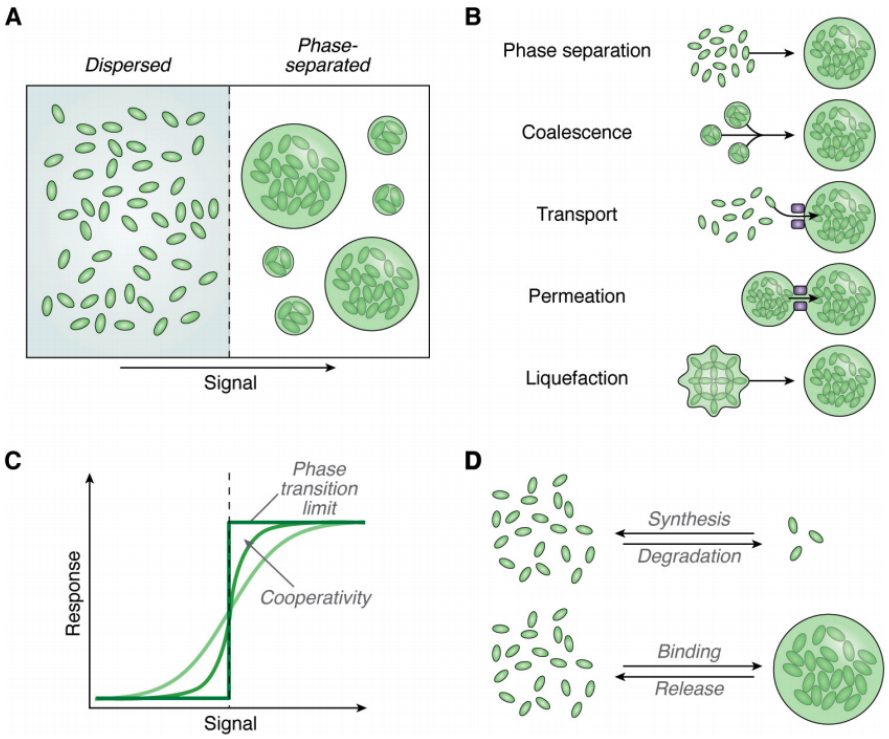

Figure 2.1: Distinguishing the process and the products of phase separation. (A) Phase separation of a single-phase solution into dense (droplet) and dilute (surrounding medium) phases. (B) Mechanisms for forming large fluid structures. This list is not exhaustive. Some mechanisms involve pre-existing phase-separated subunits, whereas others do not involve phase separation at all. (C) Phase boundaries represent a sharp thermodynamic transition, making them well-suited for sensing small changes in important conditions. (D) Efficiency and kinetics of large-state changes can differ markedly depending on implementation. (Top) synthesis and degradation processes (e.g. by changes in mRNA or protein synthesis and turnover) take minutes to hours and substantial energy expenditure. (Bottom) phase separation processes (e.g. phase separation of cGAS upon binding DNA) rearrange matter in place, allowing rapid changes on a system-wide scale in seconds, in many cases spontaneously.

Efforts to determine cellular functions for phase separation have focused primarily on its products: the resulting condensates, their material states such as liquid or gel, and the composition and dynamics of the cellular bodies hypothesized to form by phase separation. In this view, phase separation is a means to generate condensates, which are the functional entities: compartments, filters, depots, reaction vessels, factories, force generators, regulators of cell signaling, and more [150, 63, 169, 93, 124, 35, 46, 191, 74, 168, 90, 148, 98, 18].

However, the existence of a large fluid organelle does not imply that it formed by phase

separation or even that phase separation occurred during organelle assembly. There are many processes by which large liquid-like structures may form: phase separation; coalescence of smaller structures; transport processes, including those involving active transporters such as pumps and insertases or local synthesis; permeation involving docking and regulated transport between structures, liquefaction (melting or dissolution of a solid structure), or other processes (Fig. 1B).

In certain cases, such as coalescence and permeation, phase separation may generate the subunits being assembled, but the assembly process is distinct from phase separation. The distinction is critical: the hypothesis that, for example, a membraneless organelle forms by phase separation is biologically and physically quite distinct from the hypothesis that this organelle forms by coalescence of phase-separated subassemblies. By analogy, imagine a child displaying a castle she has just constructed out of stackable plastic bricks. To tell her that the castle was formed by injection molding (the process used to make the bricks) rather than by her painstaking assembly process would be an obvious and grave error.

The same distinctions between processes of formation and the resulting product matter in biology. For example, lipid droplets are fluid organelles. Their constituents, lipids, spontaneously phase-separate in the cytosol—they are literally oil in water. However, lipid droplets do not form by such spontaneous processes; instead, they bud from the endoplasmic reticulum. New molecules may also later be added to lipid droplets via coalescence, permeation, and local production at the surface [189]. Lipid droplets are separate phases but do not form by phase separation.

Each alternative formation process presents distinct features, such as kinetics, energy requirements, and mechanisms for regulation, yet they result in the same product: in this case, a fluid organelle. That multiple processes can result in the same product is familiar: there are alternative recipes for the same dish, different manufacturing processes for the same car, and different approaches to write the same document. Although some processes may yield a subtly different outcome (a tastier dish, a more coherent letter), other alternative

processes may differ only in their efficiency, speed, reliability, yield, cost, compactness of encoding, and so on, resulting in effectively indistinguishable products. When alternative processes can yield the same product, two questions arise. Are there scenarios in which one process, such as phase separation, might be favored over alternative processes? And are there situations in which the process may be as important, or even more important, for biological function than the resulting product? Cellular sensing of internal and external variables provides a set of biological scenarios where, recent work suggests, both questions may be answered affirmatively.

In this minireview, we address why and how biological systems exploit the cooperativity and efficiency of the process of phase separation, and phase transitions more broadly, for cellular sensing. Phase transition refers to any transition between one phase of matter to another, for example from liquid water to solid ice. Liquid–liquid phase separation, or phase separation for short, specifically refers to transition of a single liquid phase to two or more distinct liquid phases. Both phase transitions and phase separation have the shared feature of extraordinary cooperativity that allows system-wide changes in response to small changes in the environment and the ability to rearrange matter in place, in many cases without energy expenditure. Cells can exploit these features for specific biological functions [145]. We review three recent case studies that exemplify this in the context of cellular sensing: 1) poly(A)-binding protein (Pab1) in sensing thermal stress [138]; 2) Sup35 in sensing change in intracellular pH during starvation [45]; and 3) cGMP–AMP synthase (cGAS)2 in sensing cytosolic DNA [35]. In all three case studies, the process of phase separation plays critical sensing roles; functions played by the product of phase separation remain either enigmatic or, in the case of cGAS, are involved in the response pathway downstream of sensing. Before reviewing each case study in detail, we first discuss features of phase separation in more detail and how these features make phase separation ideally suited to solve a range of sensory challenges.

2.3 Phase separation in environmental sensors

To survive and thrive, all organisms must sense features of their environment and internal state—particularly when conditions take a turn for the worse. For primordial environmental conditions such as temperature, oxygen concentration, and nutrient availability, individual cells in an organism retain the capacity to sense stressful changes [95, 114, 106, 25]. We know this largely because cellular responses to such stresses are universally conserved. The stress-induced formation of cytoplasmic clusters of RNA and protein appears to be universal in eukaryotes [27, 40, 87, 182, 82, 67].

Temperature provides an instructive example of how small changes in a physical environmental parameter can lead to dramatic biological consequences. How eukaryotes sense temperature at the molecular level has remained surprisingly unclear [157]. A major challenge is to explain how small changes on the temperature scale—such as the two or three degrees, a mere 1% in absolute terms—are converted into dramatic system-wide changes. For example, eggs of the red-eared slider turtle incubated at 26 °C produce all males, at 31 °C produce all females, and at 29.2 °C produce an equal male/female ratio [28]. Such temperature-dependent sex determination is common, yet the mechanism behind this extraordinary sensitivity remains unknown. More prosaically but no less consequentially, the mechanism by which a few degrees' increase in temperature produces a thousand-fold induction of heat-shock genes also remains incomplete [114].

In contrast, we are constantly confronted with dramatic system-wide behavior sensitive to a fraction of a degree: the freezing of water into ice and its vaporization into steam. Melting, freezing, vaporization, separation, and other phase boundaries (Fig. 1A) mark transitions in which individual molecules cooperate to change their state in response to a small change in the relevant variable, such as temperature or pH or the concentration of a ligand. Hypersensitive behavior is expected at a phase boundary, providing a tantalizing class of potential solutions to otherwise tricky problems in sensory biology.

Unlike the two-dimensional phase diagram shown in Fig. 1C, a phase diagram for a

biomolecule may have multiple dimensions, each of which can be modulated to regulate phase behavior. For example, the intracellular environment of yeast undergoes dynamic changes when the cell encounters stress: the cellular ATP level drops [7]; the intracellular pH drops by 0.5–1 pH unit [117, 187, 73]; the cellular volume shrinks and the intracellular environment becomes more crowded [77]; and the cytoplasm transitions from viscous fluid to a more glass-like state [77, 117]. These parameters—concentrations of specific mRNAs, ATP, protons, and crowders—have been demonstrated to affect the phase boundaries of proteins that undergo phase separation [138, 173, 126, 94, 101, 198, 31]. Post-translational modification following stress can also trigger or modulate phase separation [169, 93, 124]. Other changes, such as production of cytoprotective metabolites like glycerol and trehalose [16] and production of molecular chaperones, are also likely to affect the phase boundary and contribute to the accuracy and adaptability of the sensing system through signal integration. Understanding the phase response of proteins to both changes in concentrations of cellular components and intensive system properties such as temperature is of great interest; some factors, such as the volume fraction of components, are under cellular control, whereas others are products of the environment [145]. Ultimately, these intracellular environmental changes and resulting phase behaviors appear likely to contribute to major stress-induced functional changes: global translational attenuation [27, 26], arrest of the cell cycle [88], and induction of a transcriptional program.

Below, we review three specific case studies in detail. All three case studies highlight the two properties of phase separation most relevant to sensing. First, phase separations are highly cooperative, enabling switch-like responses to small changes (Fig. 1C). Second, phase changes rearrange existing cellular matter without the need for creation or destruction, raising the possibility that such processes can execute changes with less expenditure of time and energy than processes involving synthesis and degradation (Fig. 1D). If, as in the figure, only monomers or only demixed molecules are active, regulating activity can be achieved in seconds, in some cases spontaneously, without any need for de novo synthesis of mRNA

or protein molecules, which take minutes and substantial energy. Similar logic underlies the utility of post-translational control in rapid cellular responses [160], and indeed, protein phase separation is a mode of post-translational control. Phase separation in general, and environmentally sensitive spontaneous phase separation in particular, may thus provide an ideal mechanism for mounting an immediate response to an abrupt environmental insult which, only on a longer time scale, would be accompanied by changes in transcription, translation, and turnover.

2.3.1 Case study 1: temperature sensing by phase separation of poly(A)-binding protein

Temperature presents a universal challenge to all living organisms, which typically inhabit a narrow thermal range and can survive only brief excursions outside this range. All cellular life induces production of so-called heat-shock proteins in response to a nonlethal rise in temperature. All eukaryotes form stress granules, cytosolic clusters of RNA and protein, at the upper extreme of survivable heat shock. Severe heat stress causes proteostasis catastrophe and accumulation of misfolded proteins, which lead to induction of the heat-shock response and other protein quality control processes such as endoplasmic reticulum-associated protein degradation [27, 51, 96, 167]. Despite these well-studied responses to thermal stress, how temperature is mechanistically sensed in eukaryotes remains largely unknown.

A study by Riback, Katanski et al. [138] revealed that poly(A)-binding protein (Pab1 in yeast; PABPC1 in humans), a highly conserved RNA-binding protein component of stress granules, undergoes phase separation to form a hydrogel in response to physiological thermal stress both in vivo and in vitro (Fig. 2). In yeast, Pab1's phase separation is tuned to occur at the organism's heat-shock temperature by modulatory hydrophobic residues in its proline-rich domain. Phase separation is mediated by its RNA-binding domains, and Pab1 releases RNA during phase separation.

The ability of Pab1 to autonomously sense a mere 3% change in absolute temperature,

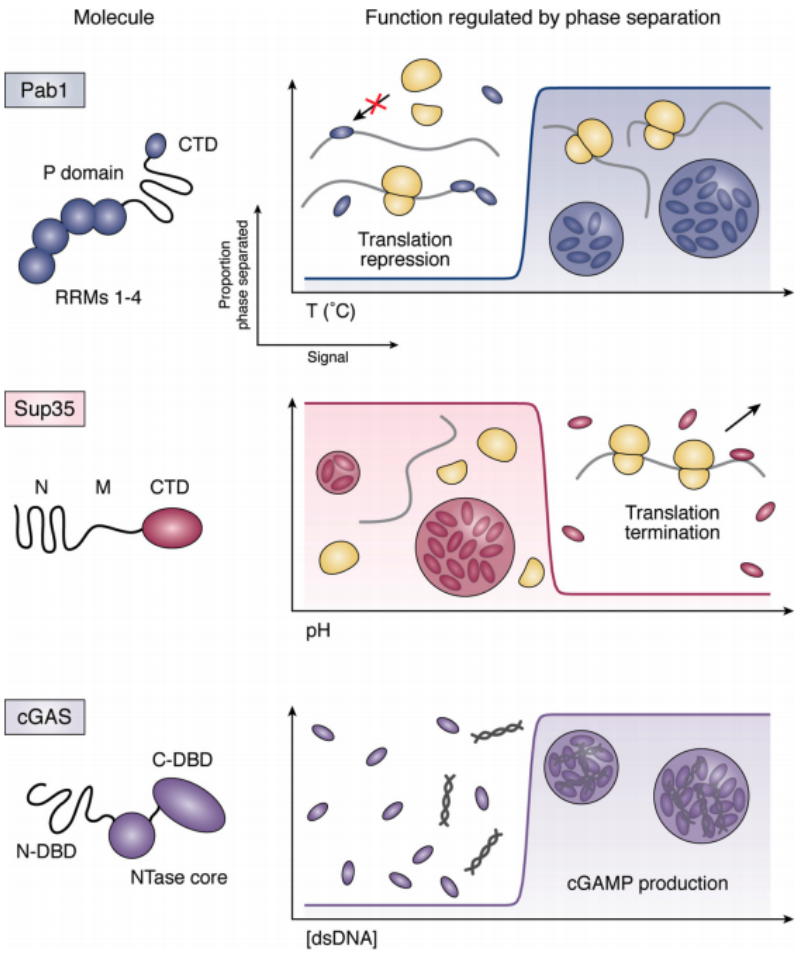

Figure 2.2: Proposed functions of phase separation–based sensory systems. The following abbreviations are used: CTD, C-terminal domain; P domain, proline-rich domain; RRM, RNA recognition motif; N, N-terminal prion domain; M, middle domain; DBD, DNA-binding domain; NTase core, nucleotidyltransferase domain.

from robust growth (30 °C/303 K) to stress (40 °C/313 K), makes Pab1's phase separation one of the most thermosensitive biomolecular processes yet found [138]. The standard way to characterize temperature sensitivity in biology is the Q10 value, the ratio of any two biological properties of a system at temperatures 10 °C apart [157]. Typical biological reactions have Q10 values of roughly 2–3, meaning a 2–3-fold change over a 10 °C range [137]. In contrast, the rate of radial growth of Pab1 phase-separated assemblies has a Q10 of 350 at 36 °C [138]. Pab1's assembly rate is smoothly graded as a function of temperature, indicating that Pab1 senses the magnitude of thermal stress as well as its presence or absence. Pab1's phase separation is also highly sensitive to pH, a physiologically relevant feature because heat shock

is accompanied by a pH drop [187], and other stresses, such as energy depletion, involve only a pH change [117]. Interestingly, the magnitude of cytosolic acidification correlates with the severity of heat stress [186]. Thus, Pab1 may be able to integrate both thermal and intracellular pH information to accurately sense both the presence and magnitude of thermal stress. Crucially, preventing Pab1's stress-triggered phase separation compromises growth during stress [138], indicating that phase separation is adaptive.

Although the function remains speculative, Pab1's phase separation may regulate translation, translationally repressing heat-shock mRNAs by binding their A-rich 5 UTRs before stress and following recovery, but derepressing these mRNAs upon releasing RNA during stress-triggered phase separation [138]. In this mechanism, the sensitivity to temperature and pH, which is required for sensing, is provided by the process of phase separation. Further studies are needed to establish the function(s) of Pab1's phase separation.

2.3.2 Case study 2: starvation sensing by phase separation of Sup35

As sessile organisms, yeast cells depend on their current environment for nutrients; when nutrients run out, growth stops, and when nutrients become plentiful, growth must rapidly restart. Correspondingly, cells rapidly arrest translation during starvation [157] and resume translation during refeeding. How do cells regulate translational activities during stress? And more broadly, how do cells sense and adapt to a changing environment?

Sup35 is a translation terminator factor in yeast and is also one of the classic yeast prions [129, 127]. Inheritance of phenotypic variations through prions has been studied extensively as an evolved adaptation mechanism in fungal species [177, 60, 179, 2, 49, 36]. For example, prion formation of Sup35 leads to translation read-through, which has been hypothesized to provide cells a means to expose hidden genetic variations, some of which might have adaptive value [179]. Like other prions, Sup35 has a disordered, low-complexity domain enriched in polar and aromatic amino acids [103]. This prion domain (PrD) mediates formation of fibrillar, amyloid-like Sup35 prion conformation [54, 81], but a recent study by Franzmann et

al. [45] uncovered its additional role in mediating phase separation of Sup35.

The PrD of Sup35 can mediate phase separation of Sup35 into nonfibrillar structures in energy-depleted yeast cells by sensing the intracellular pH (Fig. 2) [45], which drops during starvation and other stresses. Sup35 consists of the N-terminal PrD (N), a charged middle domain (M), and a C-terminal GTPase domain. The GTPase domain is essential for soluble Sup35's function as a translation terminator. Sensing of pH is mediated by the charged M domain; removal of the negative charges from the M domain abolishes the pH-dependent phase behavior of Sup35. Yeast cells expressing Sup35 without NM domains recover growth and translational activity more slowly after starvation compared with WT. Whether these differences come from loss of phase separation or loss of another NM domain activity remains open. In energy-depleted yeast cells, Sup35 readily dissolves upon re-addition of glucose in an Hsp104-independent manner [45]. This pH-dependent, reversible phase separation of Sup35 is likely to provide a fast and efficient mechanism to sense energy depletion and possibly other stresses that trigger reduction in the intracellular pH.

What is the fitness benefit of Sup35 phase separation versus prion formation? Franzmann et al. [45] showed that a strain carrying Sup35 prions recovers more slowly from the stationary phase compared with a strain without Sup35 prions. Are phase separation and prion formation two distinct evolved mechanisms to sense and/or react to different forms and/or severity of stress? Are phase separation and prion formation mutually exclusive? More studies are necessary to address these questions and delineate distinct functions between the two processes.

2.3.3 Case study 3: cytosolic DNA sensing by phase separation of cGMP–AMP synthase (cGAS)

In eukaryotes, cellular DNA resides in the nucleus, and introduction of cytosolic DNA upon microbial or viral infection or after severe genomic damage triggers the innate immune response. The enzyme cGAS, a DNA-binding enzyme that converts GTP and ATP into

cGAMP [170], is responsible for the detection of this aberrant cytosolic DNA. cGAMP activates the adaptor protein STING, which induces type I interferons and other cytokines [192].

Du and Chen [35] discovered that DNA sensing by cGAS involves phase separation. The N terminus of cGAS is disordered and positively charged. The C terminus contains a structured nucleotidyltransferase domain. Both termini bind indiscriminately and cooperatively to DNA. Longer DNA, which allows more multivalent DNA–cGAS interaction than shorter DNA, promotes cGAS phase separation better than shorter DNA. In buffer with physiological concentrations of salt and zinc, even nanomolar concentrations of cGAS are capable of phase-separating in response to similar concentrations of DNA. ATP and GTP partition into cGAS droplets, and the cGAMP synthesis activity of cGAS increases upon phase separation.

Phase separation of cGAS illustrates how the process and product of phase separation may play separate but coupled roles: phase separation provides the sensitivity and conditional behavior, whereas the resulting compartment accelerates specific biochemical reactions. When the cytosolic DNA concentration exceeds the critical concentration, which depends on both the length of the cytosolic DNA and cytosolic zinc concentration, cGAS phase-separates and sequesters the cytosolic DNA into a confined space [35]. The resultant cGAS droplet acts as a microreactor for synthesizing cGAMP for downstream signaling.

Whether the product can be spontaneously reversed or requires additional factors is unclear. The authors noticed that the fluorescence recovery after photobleaching (FRAP) recovery rate of cGAS droplets decreased with increasing time, suggesting that the cGAS droplets gradually transition into a gel-like state. Further studies on how cells regulate both the formation and dissolution of cGAS droplets by, for example, changing cytosolic zinc concentration or molecular chaperones are necessary.

2.4 Direct versus indirect sensing

The case studies presented here are paradigms for sensing achieved via phase behavior, yet they have important differences that typify the diversity of mechanisms by which phase separation can achieve threshold detection and adaptation. Some proteins, such as Pab1 and cGAS, may directly sense a signal (heat or DNA) and undergo a phase separation as a result. In other cases, a molecule might undergo phase separation in response to a downstream signal or secondary messenger; this appears to be the case for Sup35 and in some scenarios for Pab1, in which the signal being sensed is a decrease in the intracellular pH in response to energy depletion.

This observation opens the possibility that previous results, although not identified as sensing by phase separation, may fall into one of these categories. For example, the RNA-binding protein Whi3, which regulates cell-cycle progression, has been implicated in the process in which yeast cells resume budding after nonproductive mating attempts [23]. The authors note that Whi3 forms "super-assemblies" in such cells. Given that the protein contains a domain known to contribute to phase separation in other systems and that a homologous RNA-binding protein has been shown to phase-separate in vitro [198], it is plausible that Whi3 acts as a phase-separating sensor for the cellular state of unproductive mating. Notably, the molecular chaperone Ssa1 was shown to interact with the assembled form of Whi3, providing a plausible mechanism for resetting the sensing system (adaptation). Further research is needed to determine whether the protein actually undergoes phase separation and, if so, what signal directly triggers the change.

Components of a larger sensing system may display phase behavior that can confer threshold detection indirectly. A recent study in budding yeast by Simpson-Lavy et al. [165] may represent such a case in a glucose-sensing system. The study demonstrates that glucose-dependent release of Std1 from its binding partner Sip1 leads to the formation of Std1 cytoplasmic focus, which sequesters the catalytic component of AMP-activated protein kinase (SNF1 in yeast; AMPK in human) from the nucleus to switch the mode of metabolism

from respiration to fermentation. Std1 has an asparagine-rich disordered region, which is both necessary and sufficient for the cytoplasmic focus formation in vivo, and displays a relatively fast FRAP. The authors propose that, in the presence of glucose, activated Vhs1 kinase phosphorylates Sip1 to release Std1. More experiments need to be done to determine whether Std1 forms cytosolic focus via phase separation, aggregation, or a combination of processes described in Fig. 1B.

A similar process was also recently reported for another important stress-associated transcription factor in yeast [69]. Snf5, a component of the SWI/SNF complex responsible for the expression of many glucose-repressed genes, has a poly-Q stretch that the authors find is crucial for transcriptional activation. Strikingly, although removal of the domain represses transcriptional output, replacement of the domain with an exogenous domain that aggregates in a pH-sensitive manner partially rescues this phenotype. The authors note that the poly-Q stretch is in close proximity to several histidines, and it may act as a pH-sensor that responds to starvation-associated acidification. However, more in vitro data are needed to determine whether the protein or complex truly undergoes phase separation in a pH-dependent fashion.

Finally, we have proposed that temperature and pH sensing may be carried out by proteins having phase diagrams like Pab1, with state changes depending on both variables, for induction of the transcriptional response regulated by heat-shock factor 1 (Hsf1) [138]. Hsf1 is constitutively bound by molecular chaperones, and stress produces as-yet-unidentified molecular species (speculated to be unfolded proteins), which titrate away these chaperones, activating Hsf1. Phase-separating proteins, such as Pab1, can substitute for unfolded proteins in this model, potentially linking phase separation to transcriptional induction. Sensing of pH would, as above, represent indirect sensing of stresses that compromise ATP production, membrane integrity, or other aspects of pH homeostasis.

2.5 Autonomous versus facilitated reversal

Many studies of conditional phase separation have focused on whether the process is reversible, generally in the context of returning the environment to its initial state and asking whether demixed molecules disperse. Although this is, of course, a point of curiosity, reversibility has deeper significance in regulation, taking on a different meaning if dispersal is spontaneous or, alternatively, if it depends on factors that are induced by the conditional signal.

Some phase-separated structures, like Sup35, are autonomously dispersed when the signal returns below the threshold. Others, like Pab1, require molecular chaperones for facilitated dispersal [27]. The type of stress can also dictate whether a protein phase-separates into a spontaneously reversible structure as illustrated by poly(U)-binding (Pub1); heat-induced Pub1 droplets require Hsp104, whereas pH-induced Pub1 droplets spontaneously dissolve upon reversing pH [89]. What are the benefits and costs of autonomous versus facilitated reversal? One benefit of autonomous reversal may be that a cell can immediately resume growth when the environment returns to favorable conditions, such as with nutrient withdrawal and replenishment. Interestingly, a list of metabolic enzymes has been reported to form reversible cytoplasmic foci or filaments upon stress [119, 131, 12, 100, 76], and at least some of these metabolic enzymes have been shown to undergo autonomous reversal [12, 100]. Reversal indicates (senses) that the stress is over.

In contrast, facilitated reversal by signal-induced factors may be useful for programming a timed or graded response. In the case of chaperones induced by stress, the dispersal of Pab1, Pub1, and other such proteins reveals that the cell has obtained sufficient free levels of chaperones to effect dispersal. In other words, facilitated reversal indicates the completion of the stress response rather than the end of the stress.

2.6 Nucleation and growth versus spinodal decomposition processes

Phase separation can occur by two mechanisms: nucleation and growth and by spinodal decomposition [38]. In nucleation and growth, an energetically unfavorable nucleation step must be first accomplished, followed by spontaneous growth of the dense phase of nuclei that have formed. In spinodal decomposition, the nucleation step is itself spontaneous, such that nuclei appear throughout the solution, and the entire system spontaneously and simultaneously separates. Pab1 shows clear signs of being in the nucleation and growth regime under physiological conditions, preferentially forming new assemblies on top of existing assemblies [138]. Nucleation and growth offer biological systems the opportunity to regulate each step separately and to control the location where phase-separated structures form by controlling the location of nucleus formation. By contrast, spinodal decomposition might help ensure a synchronized, system-wide switch as soon as a biological condition is reached. These alternative processes of phase separation itself thus open possibilities for alternative biological control mechanisms.

2.7 Concluding remarks

Given the universal need for sensing in biology, we expect sensory phase separation to be exploited widely. Although our case studies are eukaryotic, a few examples of phase separation in bacteria have been reported recently [1, 113]. The field is wide open and filled with opportunities to discover more examples of sensory phase separation in different cell types and in different contexts, to dissect out the underlying molecular mechanism of sensory phase separation, to investigate how multiple sensory inputs are simultaneously integrated or processed separately, and to illuminate the costs and benefits of these molecular sensory strategies.

We end by emphasizing that the process of phase separation itself has features distinct

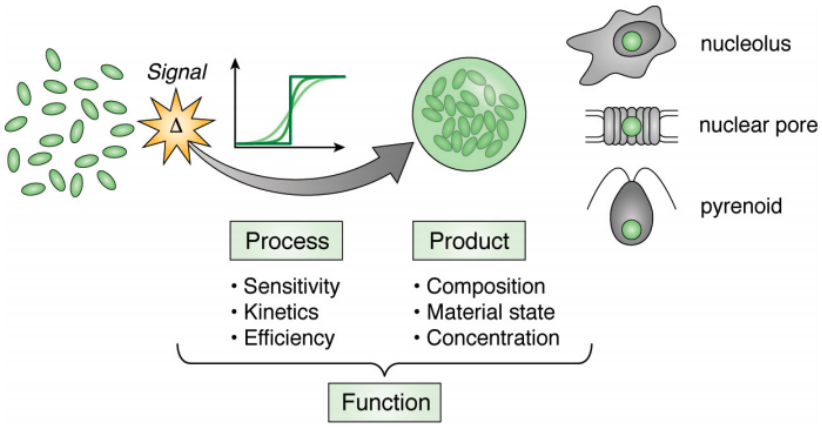

Figure 2.3: Distinct features of the process and the products of phase separation. Both may carry out functions, and specific functions (such as sensing, signal transduction, and isolation of events in time) may rely mainly on features of the process, whereas other specific functions (such as colocalization, filtration, and isolation in space) depend primarily on the products.

from its products that make it uniquely well-suited to certain biological functions (Fig. 3). A prominent body of existing work on the products of phase separation exists, such as the nucleolus where key steps in ribosome assembly are compartmentalized [43, 19], the pyrenoid where CO2-fixing enzymes are defended by colocalized radical scavengers [46], and the nuclear pore where selective transport (filtration) regulates access to and from the nucleus [154, 155]. As in the case studies highlighted here, we anticipate many more studies uncovering functional roles exploiting the unusual sensitivity, efficiency, kinetics, and other temporal features that characterize the process of phase separation.

2.8 Author contributions

HY, CT, and DAD conceived of the general outline of the review. HY and CT did literature search. HY wrote the initial draft with inputs from CT. CT and DAD made figures. HY, CT, and DAD edited the manuscript for final publication.

CHAPTER 3

CHAPERONES DIRECTLY AND EFFICIENTLY DISPERSE STRESS-TRIGGERED BIOMOLECULAR CONDENSATES

This chapter was published as: Yoo et al. 2021. [195]

3.1 Abstract

Stresses such as heat shock trigger formation of protein aggregates and induction of a disaggregation system composed of molecular chaperones. Recent work reveals that several cases of apparent heat-induced aggregation, long thought to be the result of toxic misfolding, instead reflect evolved, adaptive biomolecular condensation, with chaperone activity contributing to condensate regulation. Here I show that the yeast disaggregation system directly disperses heat-induced biomolecular condensates of endogenous poly(A)-binding protein (Pab1) orders of magnitude more rapidly than aggregates of the most commonly used misfolded model substrate, firefly luciferase. Beyond its efficiency, heat-induced condensate dispersal differs from heat-induced aggregate dispersal in its molecular requirements and mechanistic behavior. This work establishes a bona fide endogenous heat-induced substrate for long-studied heat shock proteins, rigorously isolates a specific example of chaperone regulation of condensates, and underscores needed expansion of the proteotoxic interpretation of the heat shock response to encompass adaptive, chaperone-mediated regulation.

3.2 Introduction

In all cellular life, a sudden increase in temperature—heat shock—causes formation of intracellular aggregates and production of heat shock proteins, many of which act as molecular chaperones [125]. An early and long-standing interpretation of these observations, which follow a wide range of so-called "proteotoxic stresses" is that molecular chaperones are

produced to protect cells from the toxic effects of stress-induced misfolded proteins and their aggregates [95, 116, 181].

Supporting this view, the molecular disaggregation system, which includes molecular chaperones Hsp100, Hsp70, and Hsp40, has been demonstrated to disperse aggregates of model substrates such as heat-misfolded firefly luciferase and restore their function *in vitro* [53, 55]. Decades of biochemical studies on these model substrates have uncovered the general mechanism of disaggregation as follows (reviewed in detail by [112]): First, J-domain proteins such as Hsp40 target Hsp70 to specific substrates while simultaneously stimulating Hsp70's ATPase activity [91, 99, 75, 41]. Second, substrate-bound Hsp70 recruits and de-represses the AAA+ disaggregase Hsp100 [142, 21, 159, 61]. Third, Hsp100 threads substrate delivered by Hsp70 through its central channel to extract the substrate from aggregates [62, 50, 9]. Lastly, the threaded substrate is released from Hsp100 and undergoes either spontaneous or Hsp70/40-assisted folding to regain its native structure [70].

A surprising and universal feature of biochemical studies of model misfolded substrate dispersal has been the use of—and in the case of Hsp70, a requirement for—substantial excesses of molecular chaperones over their substrates to achieve only limited dispersal. This is unlike a typical enzymatic reaction, although Hsp70 and Hsp104 are well-characterized enzymes and no chaperones are consumed during the disaggregation reaction.

An important possibility is that model substrates are not fully accurate models of endogenous substrates—and remarkably, the endogenous heat-induced substrates of the disaggregation system have largely eluded biochemical study. Alongside nascent polypeptides and prion fibers [163, 71], heat-induced aggregates of misfolded mature proteins are considered major substrates of the disaggregation system. However, no endogenous mature protein has yet been identified to misfold in response to physiological heat shock in eukaryotes. As a consequence, a central element in our understanding of the heat shock response—that molecular chaperones directly engage and disperse endogenous aggregates induced by heat shock—has remained untested. A corollary is that the degree to which model thermolabile

proteins, such as luciferase, accurately model endogenous aggregating proteins has been difficult to assess.

Recent work suggests that the proteotoxicity model, and the view that heat shock induces widespread protein misfolding, must be expanded. A proteome-wide study in budding yeast showed that a specific set of mature proteins form fully reversible aggregates in response to sublethal heat shock [182]. Closer inspection revealed that several cases of this apparent aggregation reflect evolved, adaptive biomolecular condensation [138, 72]. For example, physiological heat shock temperature and pH changes cause poly(A)-binding protein (Pab1), an abundant and broadly conserved eukaryotic RNA-binding protein, to phase separate and form gel-like condensates *in vitro* [138]. Suppressing Pab1 condensation reduces cell fitness during prolonged heat stress, indicating that condensation is adaptive [138]. Similarly, heat-induced phase separation of translation initiation factor and DEAD-box helicase Ded1 confers an adaptive benefit to cells by promoting translational switch from housekeeping to stress-induced transcripts [72]. As illustrated by these studies, heat-induced biomolecular condensates of endogenous, mature proteins appear to be fundamentally different from misfolded protein aggregates in both mechanism of formation and, most importantly, fitness consequences.

Here we will use the term biomolecular condensates to refer to endogenous membraneless structures of concentrated biomolecules [11] regardless of the condensation mechanism, reserving the term phase separation for cases where it has been shown. We use the term aggregates to refer to amorphous clumps of misfolded proteins, which are commonly deleterious to cells,[51] and which differ from endogenous condensates whose fitness consequences are adaptive in several cases.

Substantial *in vivo* evidence indicates that endogenous heat-induced condensates interact with the disaggregation system. All members of the yeast disaggregation system (Hsp104/Hsp70/Hsp40) co-localize with stress granules, which contain both Pab1 and Ded1 [27, 183, 88, 89]. Deletion or inhibition of any member of the system, or the Hsp70 nucleotide

exchange factor (NEF) Hsp110 (Sse1/2), delays dissolution of stress granules during stress recovery [27, 183, 88, 89]. Interestingly, dispersal of endogenous stress granules precedes dispersal of exogenously expressed misfolded protein aggregates [27, 88] and only the former correlates with the resumption of translation activity and the cell cycle [27, 89].

We and others have hypothesized that heat-induced biomolecular condensates are major endogenous substrates of molecular chaperones [182, 138, 89, 196, 176, 13, 166]. However, the questions of whether molecular chaperones directly engage heat-induced biomolecular condensates, and whether and how functional engagement differs between adaptive condensates and aggregates of model misfolded substrates, have remained unanswered.

Here, we address these major open questions by reconstituting *in vitro* the dispersal of heat-induced Pab1 condensates by their cognate disaggregation system. We use independent methods to demonstrate that Hsp104, Hsp70, and the type II Hsp40 Sis1 are necessary and sufficient for complete dispersal of Pab1 condensates back to functional monomers. Comparative studies of Pab1 condensates and aggregates of misfolded luciferase reveal four key differences. First, and most strikingly, chaperones which show slow and incomplete dispersal of luciferase aggregates disperse Pab1 condensates rapidly and completely. Second, unlike luciferase [22], Pab1 does not require co-condensation with small heat shock protein Hsp26 for subsequent efficient dispersal. Third, unlike luciferase for which type I (Ydj1) and type II (Sis1) Hsp40 show synergistic activity [121, 122], Pab1 condensate dispersal depends only on Sis1 and is antagonized by Ydj1. Fourth, we show that unlike luciferase, Pab1 is only partially threaded by Hsp104 and readily regains its function upon dispersal.

Finally, we investigate the dispersal system's puzzling dependence on excess Hsp70 for optimal activity, which we find also applies to Pab1 condensate dispersal. Combining biochemical experiments with modeling, we show that the required presence of multiple, closely-spaced Hsp70s for Hsp104 recruitment and activation suffices to render the disaggregation system sensitive to the relative Hsp70 level.

Our results establish heat-induced biomolecular condensates of Pab1 as direct endogenous

substrates of the disaggregation system, and reveal that many important conclusions drawn from studying aggregates of "model" misfolded proteins do not generalize to endogenous condensates. Whether the remarkable efficiency of Pab1 dispersal is itself a general feature of native substrates remains to be seen. Further study of how chaperones engage with adaptive, endogenous substrates, and how this engagement differs from foreign or proteotoxic substrates, appears likely to yield substantial new insights into the mechanistic features and biological roles of this ancient molecular system.

3.3 Results

3.3.1 Heat shock causes Pab1 condensation, which is not spontaneously reversible

In budding yeast, Pab1 forms RNase-resistant, sedimentable condensates after physiological heat shock [182, 138]. Condensates of mature, endogenous proteins disperse to their pre-stress soluble form within an hour, without degradation, as cells recover at 30°C [182, 27].

Consistent with previous results, 20 minutes of heat shock at 42°C caused a roughly five-fold increase in the proportion of large sedimentable Pab1 compared to the pre-shock level (Figure 3.1A-C). This fraction decreased as the cells recovered at 30°C and reached the pre-shock level by 60 minutes. RNase treatment to release sedimentable species formed by RNA-protein interaction decreased the fraction of Pab1 sedimented at 100,000 g spin, but did not change the fraction of Pab1 sedimented at 8,000 g spin (Figure 3.1B), as previously reported [138]. These results confirm that under these conditions Pab1 rapidly forms RNase-resistant assemblies which persist upon return to pre-shock temperatures *in vivo*.

To reconstitute Pab1 condensates *in vitro*, we treated purified Pab1 at 42°C for 20 minutes in a physiological buffer at pH 6.8, which is about the measured pH of budding yeast cytoplasm during the same heat shock [176] (Figure 3.1D). We examined the size distribution

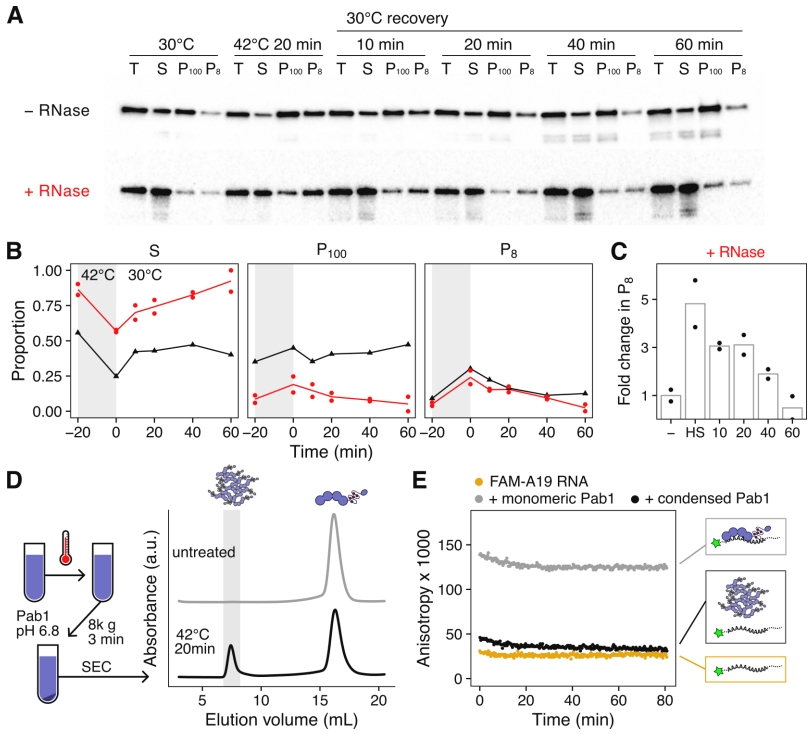

Figure 3.1: Heat shock causes Pab1 condensation, which is not spontaneously reversible.
(A) Western blot against Pab1 isolated from yeast cells before and after 20 minutes of heat shock at 42°C, and during post-stress recovery at 30°C. Cell lysates were incubated with or without RNase I_f and centrifuged at 8,000 g and 100,000 g to separate the supernatant (S) from the pellet (P_8 and P_{100}). (B) Quantification of (A). Red and black colors correspond to the RNase- or mock-treated sample, respectively. (C) Relative change in the fraction of large sedimentable Pab1 (P_8) after heat shock and during recovery compared to pre-shock level. (D) Schematic description of *in vitro* Pab1 condensate purification process and the representative SEC traces for untreated and heat shocked Pab1. Only the heat shocked sample contains Pab1 condensates, which elute in the void volume shaded in gray. (E) Fluorescence anisotropy of 5' labeled 19-mer poly(A) RNA (A19) in the absence or presence of Pab1. Pab1 condensates have substantially reduced RNA binding capacity than the equimolar amount of monomeric Pab1. No spontaneous reversal of Pab1 condensates was observed at physiological recovery condition (pH 7.3 buffer at 30°C).

of Pab1 in the soluble fraction using size exclusion chromatography (SEC) and saw a clear division of Pab1 into two peaks: one peak corresponding to Pab1 monomers and another peak in the void volume corresponding to Pab1 condensates larger than 5,000 kDa (Figure 3.1D). About 30% of total recombinant Pab1 shifted to the void peak after heat shock, consistent with about 25% of total cellular Pab1 sedimented at 8,000 g spin (Figure 3.1B). Because a previous study indicated that misfolded proteins can nucleate stress granule formation *in*

vivo [88], we tested whether heat shocking Pab1 in the presence of firefly luciferase increases the condensation yield. Indeed, we found that heat shocking Pab1 in the presence of 100-fold lower amount of thermolabile firefly luciferase, but not thermostable BSA, increased the condensation yield to about 50% (Figure 3.8A-C).

Condensation requires Pab1's folded RNA recognition motifs (RRMs) and excess RNA inhibits Pab1 condensation *in vitro* [138], suggesting a competition between Pab1's condensation and RNA-binding activity. Consistent with this, heat shock reduces the association of Pab1 with RNA *in vivo* [20]. We measured the RNA-binding capacity of Pab1 condensates isolated from SEC using fluorescence anisotropy. For 1:1 binding of Pab1 to RNA, we made 19-mer poly(A) RNA (A19) and labeled the 5' end of the RNA with fluorescein. Indeed, Pab1 condensates showed significantly reduced RNA binding activity compared to monomers (Figure 3.1E).

As expected, unlike Pab1 condensates formed *in vivo*, Pab1 condensates formed *in vitro* remained stable and RNA-binding incompetent even after dilution into pH 7.3 buffer at 30°C (Figure 3.1E), consistent with a requirement for cellular disaggregation machinery as repeatedly indirectly demonstrated. Thus, we next investigated whether the reversal of Pab1 condensates to RNA-binding monomers depends on direct engagement the molecular disaggregation system.

3.3.2 Hsp104, Hsp70, and type II Hsp40 are necessary and sufficient for complete dispersal of Pab1 condensates in vitro

To monitor the dispersal Pab1 condensates into functional monomers, we developed a fluorescence anisotropy-based assay in which the increase in fluorescence anisotropy of labeled A19 RNA indicates RNA binding by Pab1 (Figure 3.2A). We mixed Pab1 condensates and labeled A19 with molecular chaperones Hsp104, Ssa2 (Hsp70), Ydj1 and Sis1 (type I and II Hsp40, respectively), and Sse1 (Hsp110). In the absence of ATP, no change in fluorescence anisotropy was observed. In contrast, in the presence of 5 mM ATP, fluorescence anisotropy

quickly increased and reached a plateau after about 5 minutes, marking the completion of Pab1 dispersal (Figure 3.2A).

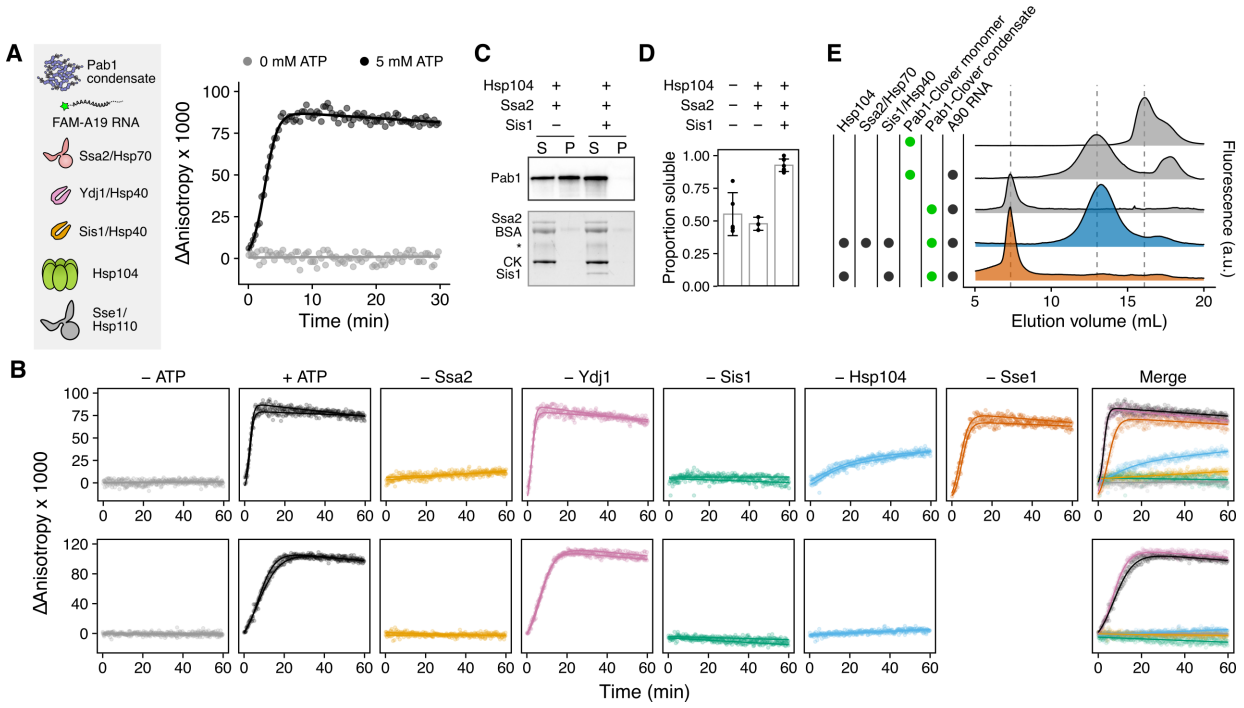

Figure 3.2: Hsp104, Hsp70, and Sis1 are necessary and sufficient for complete dispersal of Pab1 condensates *in vitro*.
(A) Schematic representation of Pab1 condensate, labeled A19 RNA, and molecular chaperones used in the fluorescence anisotropy assay. Solid line is the fit of experimental data points to the logistic equation. (B) Time-resolved fluorescence anisotropy of A19 in the presence of Pab1 condensates and a specific set of molecular chaperones. All chaperones shown in (A) except the component specified at the top of each column were included in the experiments shown in the top row. The same experiment repeated in the absence of Sse1 is shown in the bottom row. Fitted data points from two independent experiments are shown. Merged data points and a solid line fitted to the merged data are shown. (C) Western blot of Pab1 after sedimentation. Total protein image of the corresponding lanes is shown as a loading control at the bottom. CK stands for creatine kinase. Asterisk indicates unknown contaminant. (D) Quantification of Pab1 sedimentation results. (E) Fluorescence-detection SEC (FSEC) profiles of Pab1-Clover. The dashed lines mark the peaks corresponding to Pab1-Clover condensates (7.3 mL), RNA-bound Pab1-Clover monomers (13 mL), and free monomers (16 mL).

We next tested which set of molecular chaperones are necessary and sufficient for complete Pab1 dispersal *in vitro* by removing one component of the chaperone mix at a time and monitoring the effect on Pab1 dispersal (Figure 3.2B). We used excess molecular chaperones

except Sse1, which becomes inhibitory when present in excess [79], to help ensure even weak disaggregation activity would be detected. Condensate dispersal in the absence of Sse1 absolutely required ATP, Ssa2, Sis1, and Hsp104 (Figure 3.2B; bottom). When Sse1 was present, removal of Hsp104 led to a much slower and incomplete dispersal of Pab1 (Figure 3.2B; top). This is consistent with the weak disaggregation activity of Hsp110/70/40 observed against amorphous aggregates and amyloid fibrils [162]. Sse1 and Ydj1 were dispensable in the presence of Hsp104, Ssa2, and Sis1 for both condensates formed in the absence or presence of luciferase (Figure 3.8D).

The same chaperone requirement pattern was observed when we repeated the assay with Ssa1 and Ssa4, which are respectively the constitutively expressed and heat-inducible paralogs of Ssa2 (Figure 3.10 and Figure 3.9A-C). The overall dispersal rate was slower with Ssa4 than with Ssa2, which is consistent with the weaker activity of stress-inducible human Hsp70 observed against amyloid fibrils [48, 156].

We verified our fluorescence anisotropy results using two additional independent methods. First, we examined solubilization of Pab1 using sedimentation. About half of Pab1 condensates isolated from SEC remained in the supernatant after 100,000 g spin in the absence of chaperones, suggesting some condensates are too small to be pelleted (Figure 3.2C and 3.2D). Incubating Pab1 condensates with the minimal disaggregation system (Hsp104, Ssa2, Sis1) completely solubilized Pab1. In contrast, Pab1 solubility remained unchanged from background levels when the condensates were incubated with an incomplete disaggregation system.

Next, we prepared Pab1-Clover condensates and examined their size distribution by fluorescence-detection SEC (FSEC). Pab1-Clover condensates remained stable when incubated for an hour at 30°C in the absence of any molecular chaperones or in the presence of an incomplete disaggregation system (Figure 3.2E). After incubation with the minimal complete disaggregation system, however, the condensate peak disappeared and a new peak corresponding to RNA-bound Pab1-Clover appeared. A similar experiment performed

with unlabeled Pab1 using SEC and western blot confirmed that small Pab1 condensates remain stable and are reversed back to monomers only upon incubation with the complete disaggregation system (Figure 3.10B-C).

In summary, the results from three independent methods consistently indicate that Hsp104, Hsp70, and type II Hsp40 Sis1 are necessary and sufficient for complete dispersal of Pab1 condensates *in vitro*. These results are consistent with the *in vivo* observations that deletion or inhibition of Hsp104, Hsp70, or Hsp40 delays dispersal of Pab1 condensates [27] and of stress granules marked by Pab1 [27, 183, 88, 89].

Pab1 condensates and misfolded protein aggregates exhibit different chaperone dependence for dispersal

The mechanism of substrate dispersal by the disaggregation system has been extensively studied using non-native model substrates. The most commonly used model substrate is firefly luciferase, which readily misfolds *in vitro* at elevated temperatures and whose light-producing enzymatic activity can be easily and accurately measured as a readout for the extent of protein refolding. Therefore, we used luciferase as a benchmark heat-misfolded substrate and studied how Pab1 dispersal differs from luciferase disaggregation. We first focused on two chaperone-related features of luciferase disaggregation which we could recapitulate: 1) dependence on co-aggregation with excess Hsp26 for more efficient disaggregation [22] and 2) synergistic disaggregation in the presence of both type I and II Hsp40s, Ydj1 and Sis1 (Figure 3.3B) [121, 122].

Heat-induced aggregation of luciferase in the presence of five-fold excess Hsp26 facilitated subsequent disaggregation and reactivation of luciferase (Figure 3.3A) as previously reported [22]. To investigate the effect of Hsp26 on Pab1, we subjected Pab1 to a more severe heat shock condition (46°C for 20 minutes at pH 6.4) in the absence or presence of increasing concentrations of Hsp26. Hsp26 suppressed Pab1 condensation and sedimentation in a concentration-dependent manner (Figure 3.11A-B). Dynamic light scattering (DLS) also

revealed that Hsp26 suppresses nucleation of Pab1 (Figure 3.11C-D). Thus, unlike luciferase which readily co-aggregates with Hsp26 under physiological heat shock conditions, Pab1 condensation is suppressed by Hsp26. Most importantly, unlike luciferase aggregates, Pab1 condensates formed in the absence of Hsp26 are rapidly and completely dispersed by the disaggregation system (Figure 3.2).

We next investigated whether Pab1 dispersal is accelerated in the presence of both Ydj1 and Sis1, as with luciferase. Ydj1 is a type I Hsp40 which has an highly conserved N-terminal J domain followed by G/F-rich region, zinc-finger domain, C-terminal domains, and a dimerization domain [80]. Type II Sis1 largely resembles the architecture of Ydj1 but lacks the zinc-finger domain. To quantify the maximal rate of dispersal in the presence of either or both types of Hsp40s, we converted the fluorescence anisotropy to Pab1 concentration using a calibration curve (Figure 3.11E and Eq. 3.3) and extracted the rate (Eqs. 3.4 and 3.5). The rate of dispersal did not improve when both Sis1 and Ydj1 were added to Pab1 condensates compared to when only Sis1 was added (Figure 3.3B-C). Instead, Ydj1 slightly inhibited Pab1 dispersal in a concentration-dependent manner (Figure 3.3D and 3.3E). These results indicate that, unlike luciferase aggregates for which Sis1 and Ydj1 show synergistic activity, Sis1 and Yd1j show antagonistic activity for Pab1 condensates.

3.3.3 The disaggregation system restores Pab1 condensates far more efficiently than misfolded protein aggregates

The poor activity of the disaggregation system against aggregates of model substrates has been observed since the first biochemical reconstitution of the system [53, 55]. Even with co-aggregation with 5-fold excess Hsp26, less than half of luciferase activity is regained after a two-hour incubation with 37.5-fold excess Hsp104 and Ssa2 (Figure 3.3B). Indeed, the standard *in vitro* disaggregation protocol requires the use of 10- to 100-fold excess molecular chaperones over substrates to obtain moderate to good yield (Figure 3.6C). We found that when sub-stoichiometric concentration of Hsp104 (0.5×) and closer to stoichiometric

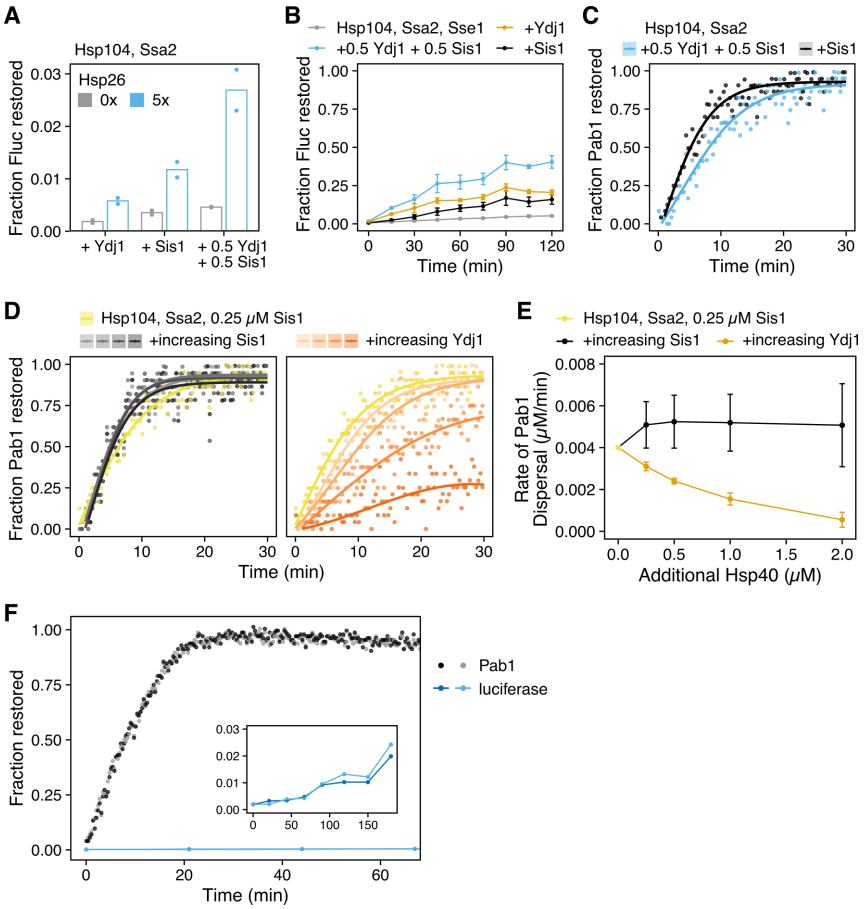

Figure 3.3: Pab1 condensates and misfolded protein aggregates exhibit different chaperone dependence for dispersal.
(A) Fraction of functional luciferase after a two-hour incubation of luciferase aggregates (0.2 μM) with Hsp104 (0.1 μM; 0.5x), Ssa2 (1 μM; 5x), and Hsp40 (0.5 μM total; 2.5x). Luciferase was aggregated either in the absence or presence of 5-fold excess Hsp26. (B) Reactivation of 20 nM aggregated luciferase in the presence of excess Hsp104 (0.75 μM; 37.5x), Ssa2 (0.75 μM; 37.5x) and Sis1 (0.25 μM; 12.5x). Either Sis1 (black), Ydj1 (orange), or both (blue) were used as co-chaperones. Mean and standard deviation were calculated from two independent experiments with duplicates in each experiment. (C) Pab1 dispersal using either Sis1 (black) or a combination of Sis1 and Ydj1 (blue) as co-chaperones. (D) Titration of either Sis1 (left; gradients of black) or Ydj1 (right; gradients of orange) to reactions containing 0.2 μM Pab1 condensates, 0.05 μM Hsp104, 0.5 μM Ssa2, and 0.25 μM Sis1. The amount of additional Hsp40 added was 0.25, 0.5, 1, and 2 μM. (E) The average maximal rate of dispersal and standard deviations quantified from three independent titration experiments, one of which is shown in (D). (F) Restoration of 0.2 μM of Pab1 or luciferase by 0.1 μM Hsp104 (0.5x), 1 μM Ssa2 (5x), and 0.5 μM Sis1 (2.5x). The inset shows zoomed-in refolding kinetics of luciferase over three hours.

concentrations of Ssa2 (5×) and Sis1 (2.5×) are used, Pab1 dispersal still completes within 20 minutes while less than 1% of luciferase is reactivated after an hour (Figure 3.3F). The heat

shock condition used to prepare Pab1 condensates and luciferase aggregates was identical except for the initial concentration (2 μM luciferase in the presence of five-fold excess Hsp26 versus 25 μM Pab1).

What causes this large difference in restoration efficiency between Pab1 and luciferase? To gain insight into the potential sources of this discrepancy, we turned to computational kinetic modeling.

3.3.4 Higher disaggregation rate and partition coefficient lead to more efficient substrate restoration in silico

Pab1 condensation requires the folded RRMs, and condensation involves only minor unfolding of secondary structures [138]. We hypothesized that separation of specific RRM interactions and subsequent folding of the re-solvated Pab1 into native structure may be more efficient compared to the restoration of luciferase aggregates. To test this hypothesis within our model, we synthesized existing simulation studies [132, 30, 120, 194, 56, 8, 188] to build what we call a cooperative model of the disaggregation system (Figure 3.4A and 3.12A). The cooperative model captures the current model of Hsp104 regulation by Hsp70, in which binding of more than one Hsp70 is required to activate Hsp104 [159, 21]. Many of the rate parameters involved, especially in the refolding step, have been measured using bacterial chaperones and model substrates or peptides (Table 3.1). We assumed that these parameters are generally consistent in the eukaryotic system, and that the same model architecture can be used for both luciferase and Pab1. For details of this ordinary differential equation model, see Methods.

We examined how varying each of the following parameters affected the substrate restoration yield: 1) rate of disaggregation by Hsp104, 2) efficiency of the released substrate from regaining its native structure, which we define as the partition coefficient, and 3) substrate affinity for Hsp70. Modulation of each parameter over 1-2 orders of magnitude substantially affected the restoration yield, measured from 0 to 1 (Figure 3.4B, D, E). A large difference in

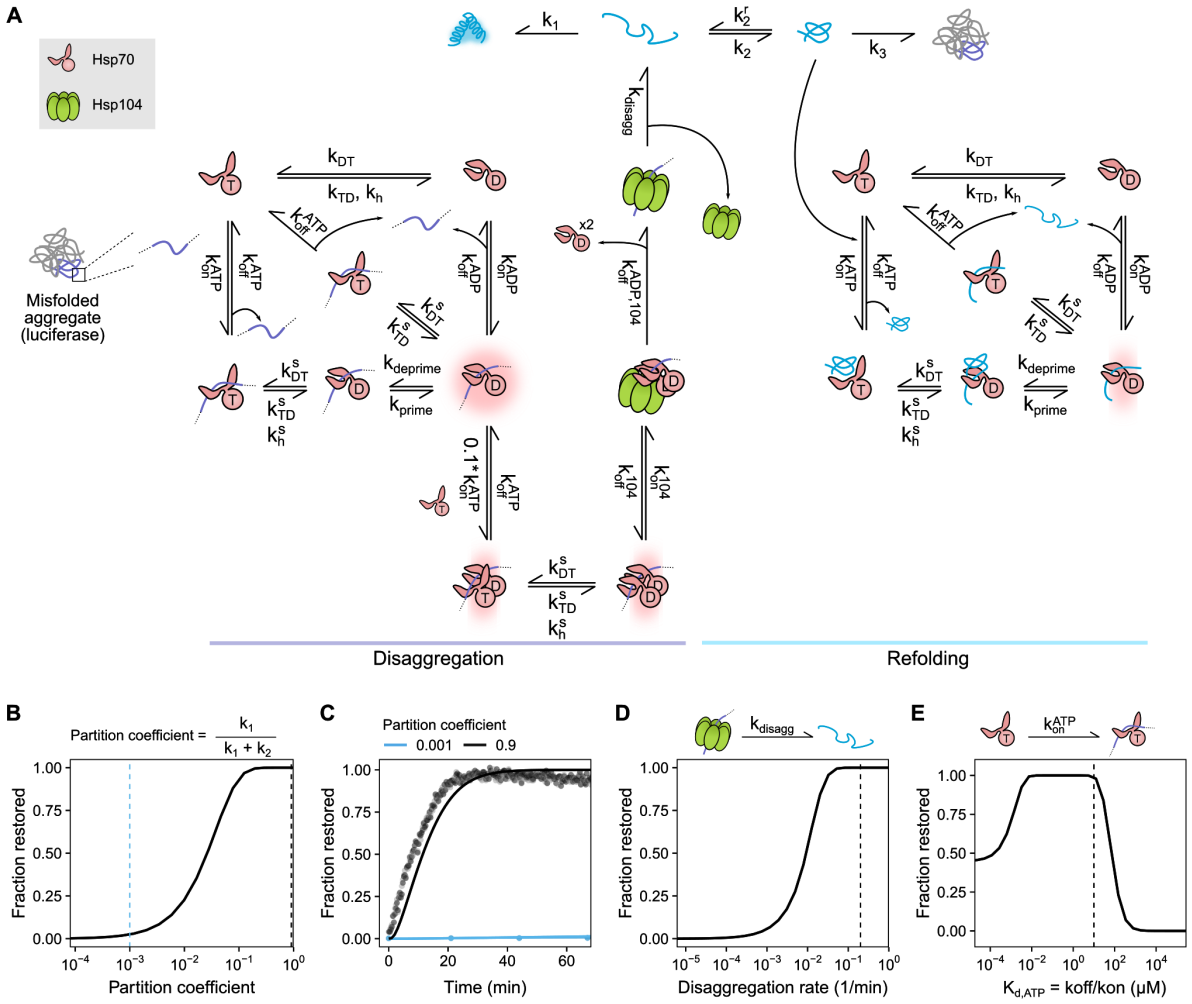

Figure 3.4: Higher disaggregation rate and folding partition coefficient lead to more efficient substrate restoration *in silico*.
(A) Cooperative model of the disaggregation system. For more details, see Methods and Figure 3.12. (B) Summary of model output in terms of fraction substrate restored as a function of partition coefficient. Dashed lines indicate the partition coefficient used to simulate Pab1 (black) and luciferase (light blue) results in (C). For all simulation experiments in this figure, fraction restored at 2 hours is shown. The starting simulation condition was 0.2 μM substrate, 0.1 μM Hsp104, and 1 μM Hsp70. (C) Simulated substrate dispersal kinetics with either high (black) or low (light blue) partition coefficients. Simulation results (solid line) are overlaid on top of Pab1 and luciferase experimental data from Figure 3.3F. (D) Simulated fraction substrate restored as a function of disaggregation rate. (E) Simulated fraction substrate restored as a function of Hsp70(ATP) substrate affinity. Dashed lines in (D) and (E) indicate the default value used in the simulation experiments.

partition coefficient alone reproduced the Pab1 and luciferase dispersal data (Figure 3.4C). The simulation also revealed Hsp70 affinity as a potential factor which can contribute to the observed difference in dispersal efficiency.

Because Hsp104 is associated with both the disaggregation rate and the partition coefficient of a substrate, e.g., through complete threading vs. partial threading of a substrate, we decided to investigate experimentally and compare how Hsp104 engages with Pab1 condensates and luciferase aggregates.

3.3.5 Pab1 is partially threaded by Hsp104

Substrate threading through the central channel of Hsp104 is a common mechanism for protein disaggregation [174]. Complete threading requires complete substrate unfolding. To probe the folding state of Pab1 and luciferase during their release from Hsp104, we used a mutated version of a bacterial chaperonin, GroEL, which traps unfolded protein [185] (Figure 3.5A). We verified that this GroEL variant traps unfolded luciferase released during disaggregation and prevents folding (Figure 3.5B).

We then tested whether Pab1 becomes unfolded during dispersal by dispersing Pab1ΔP in the presence of excess GroEL trap. We used Pab1ΔP (55 kDa) because most GroEL substrates are known to have molecular weight less than 60 kDa [66] and full-length Pab1 (64 kDa) exceeds that limit. Pab1ΔP lacks the disordered P domain but retains the ability to phase separate [138]. Pab1ΔP condensates were readily dispersed by the disaggregation system, indicating that the P domain is dispensable for the condensate's engagement with chaperones (Figure 3.5C). The rate of dispersal was almost identical for Pab1ΔP dispersed in the absence or presence of GroEL trap. However, when we chemically denatured both full-length Pab1 and Pab1ΔP in 8 M urea and refolded the proteins in buffer containing no or 10-fold excess GroEL trap, both constructs refolded to the same level regardless of the presence of GroEL trap (Figure 3.5D). This indicated to us that GroEL trap is unable to engage with fully unfolded Pab1 and thus not applicable to investigating the folding state of

Pab1.

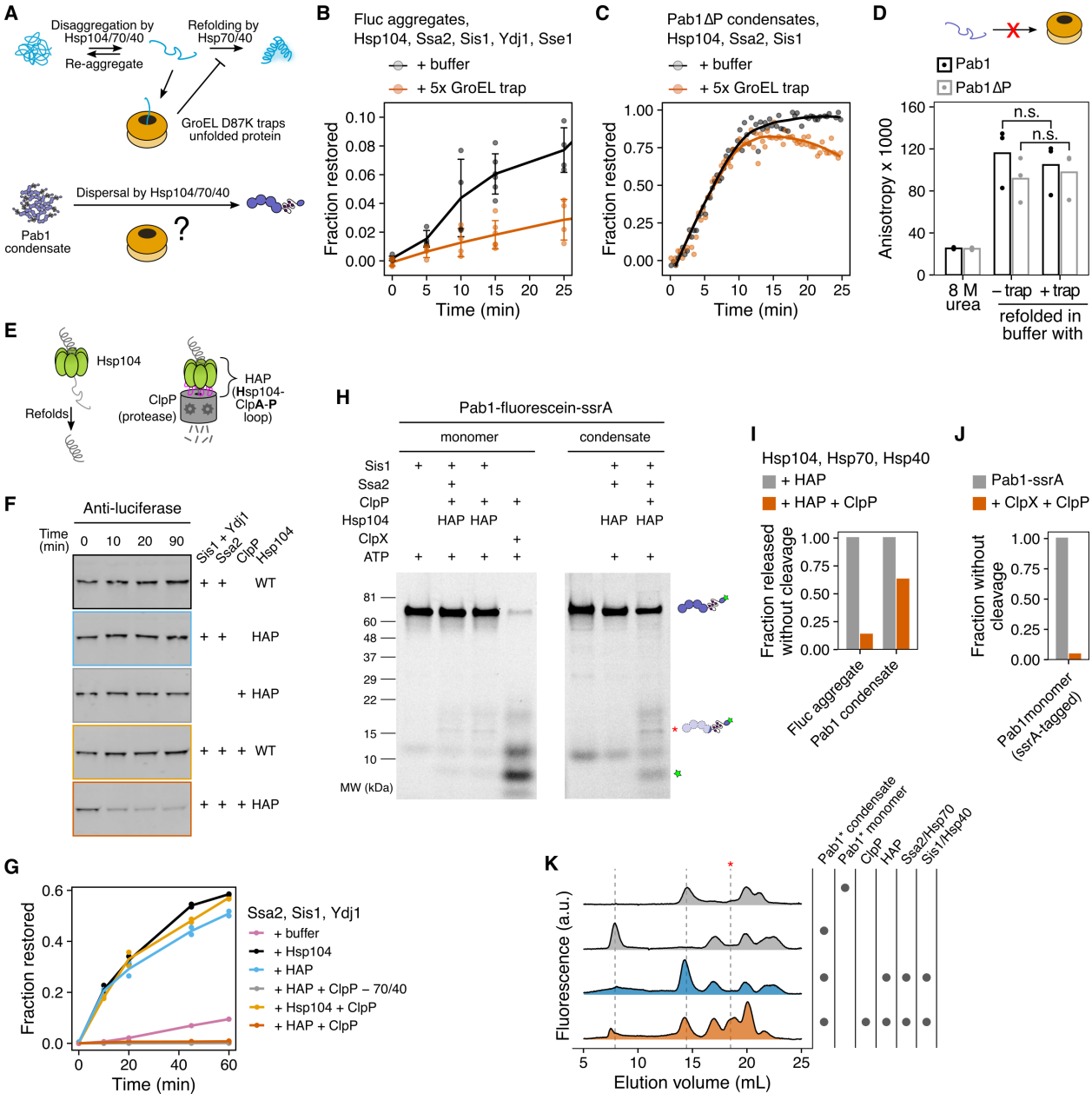

Figure 3.5: Pab1 is partially threaded by Hsp104.
(A) Schematic description of GroEL trap system. (B) Luciferase disaggregation in the absence or presence of 5-fold excess GroEL trap. Mean and standard deviation were calculated from three independent experiments. (C) Pab1ΔP dispersal in the absence or presence of 5-fold excess GroEL trap. Solid lines represent smoothed data from a representative experiment. The decrease in the signal in the presence of GroEL trap after 10 min is due to RNA degradation. (D) Refolding of urea-denatured Pab1 (black) and Pab1ΔP (gray) in buffer containing no or 10-fold excess GroEL trap. (E) Schematic description of HAP/ClpP system. (F) Chemically aggregated luciferase were incubated with the indicated components and the extent of luciferase degradation was visualized by western blot.

To circumvent the limitation of the GroEL trap, we turned to the HAP/ClpP system [174]. HAP (Hsp104-ClpA-P loop) is an engineered Hsp104 that interacts with the bacterial peptidase ClpP to form a proteolytic system (Figure 3.5E). HAP behaved like wild type Hsp104 and quickly degraded luciferase in the presence of ClpP (Figure 3.5F-G), consistent with a previous report that luciferase is fully threaded and degraded by HAP/ClpP [62]. HAP also behaved like wild type Hsp104 during Pab1 dispersal (Figure 3.13A-B).

If complete threading of Pab1 were required for condensate dispersal, we would expect to see complete degradation of Pab1 by HAP/ClpP. We made condensates using Pab1-fluorescein-ssrA and examined the degradation pattern after dispersal using SDS-PAGE (Figure 3.5H and Figure 3.13C-D) and FSEC (Figure 3.5K). A mixed group of full-length and degraded Pab1 populations were observed after dispersal. The appearance of full-length Pab1 monomers suggested partial translocation of Pab1 by HAP and release before Pab1 enters the proteolytic chamber of ClpP (Figure 3.5I and Figure 3.5K). We confirmed that ClpP can degrade Pab1 using ClpX, which recognizes the ssrA degradation tag and unfolds the substrate for ClpP (Figure 3.5H and Figure 3.5J). Specific degradation fragments appeared upon incubation of HAP/ClpP and chaperones with Pab1 condensates, but also to a lesser extent with Pab1 monomers, suggesting a basal level of interaction between Pab1 and HAP/ClpP (Figure 3.5H). Similar C-terminal fragments containing a part of the P domain and the C-terminal domain of Pab1 appeared for Pab1-Clover and Pab1-fluorescein without the ssrA tag (3.11E and Figure 3.11H). However, much less full-length monomer appeared for Pab1-Clover than Pab1-fluorescein-ssrA (Figure 3.13F), suggesting that a fluorescent label can affect the processing by HAP/ClpP. We also examined the N-terminal fragments using fluorescein-Pab1 and saw appearance of both large fragments of the RRMs and small peptides (Figure 3.13G). HAP/ClpP fails to completely disperse condensates of Pab1-Clover (Figure 3.13F), which limited our ability to quantify the fraction of Pab1 released without cleavage for these constructs.

Together, these results show that, unlike luciferase which requires complete threading

and unfolding by HAP for disaggregation, partial threading of Pab1 still leads to condensate dispersal. This is consistent with the partial threading mechanism proposed for proteins with a mixture of misfolded and folded domains [62, 171] and the lack of major secondary structure changes in Pab1 at condensation temperature [138]. However, we cannot rule out the possibility that wild type Hsp104 processes unlabeled Pab1 differently from what we observed with HAP and labeled Pab1 constructs.

3.3.6 Cooperative binding of Hsp70 targets condensates for dispersal

How does the disaggregation system recognize Pab1 condensates? To address this question, we first performed a series of fluorescence anisotropy Pab1 dispersal assays with varying chaperone concentrations and quantified the maximal rate of dispersal (Figure 3.6A and 3.6B). Pab1 condensate dispersal was most robust to the Hsp104 concentration, showing half-maximal dispersal rate at 1:10 Hsp104:Pab1 ratio. Excess Sse1 was inhibitory and Sse1 worked most optimally at sub-stoichiometric level, consistent with previous observations [79, 188]. Pab1 condensate dispersal was most sensitive to the concentrations of Sis1 and Ssa2. In particular, the rate of dispersal plummeted as the Ssa2 concentration approached the stoichiometric level (Figure 3.6A).

Indeed, the disaggregation system's dependence on super-stoichiometric Hsp70 for optimal activity has been a long-standing puzzle. Earlier studies investigating this problem with a reconstituted bacterial disaggregation system found that DnaK (bacterial Hsp70) has to be present in excess for maximal disaggregation yield [55, 14]. We surveyed *in vitro* disaggregation studies in the literature and found that this dependence on excess Hsp70 is widespread across studies, precise conditions, and substrates (Figure 3.6C), and our results are no exception.

We decided to investigate why excess Hsp70 over substrate is needed for what is still a catalytic series of reactions. We titrated Ssa2 over a narrow window around the stoichiometric Hsp70:Pab1 ratio and monitored Pab1 dispersal reaction for eight hours (Figure 3.6E). We

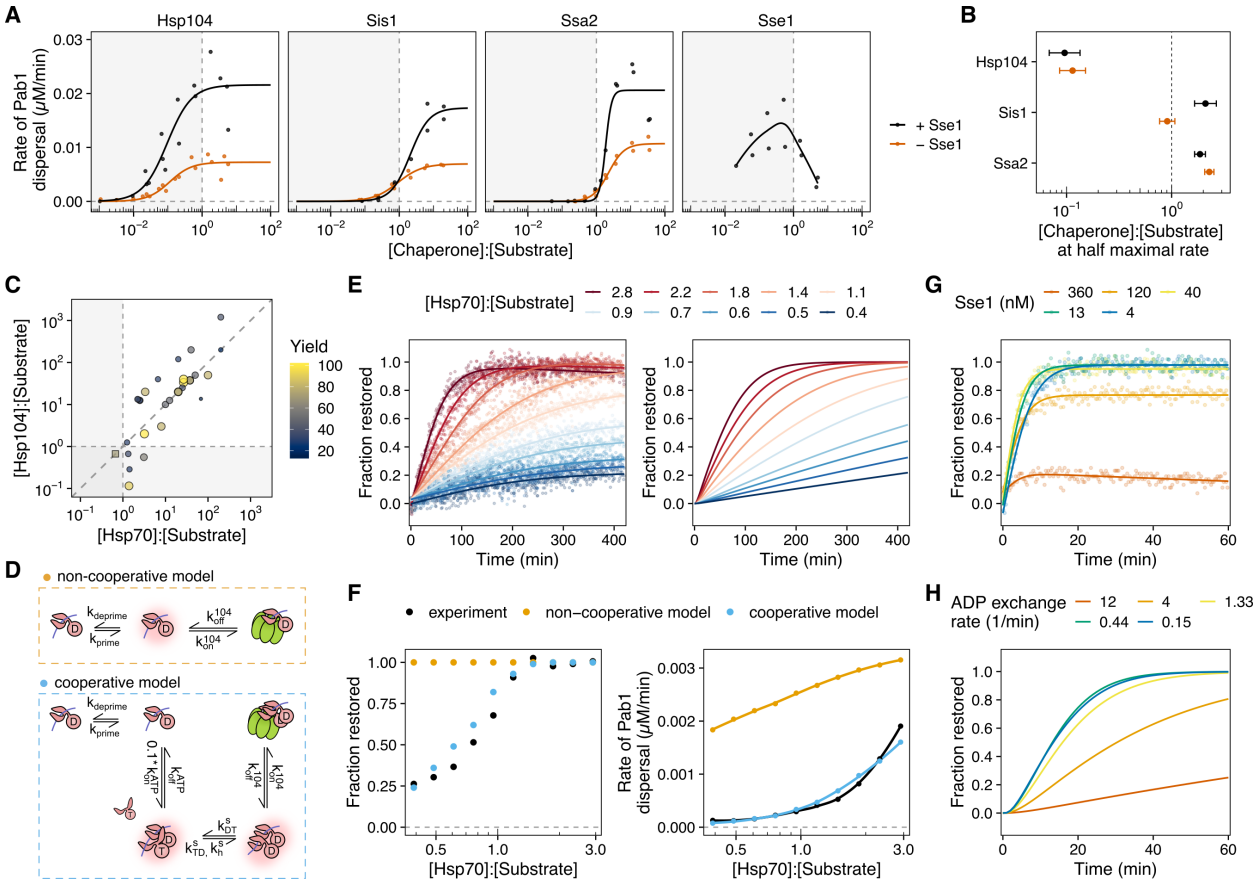

Figure 3.6: Cooperative binding of Hsp70 labels condensates for disaggregation. (A) Maximal rate of Pab1 dispersal in the presence (black) or absence (brown) of Sse1. Solid lines in Hsp104, Sis1, and Ssa2 panels represent logistic fit to the data. Solid line in Sse1 panel is the smoothing line. The baseline concentrations of the proteins were 0.2 μM Pab1, 0.5 μM Ssa2, 0.5 μM Sis1, 0.2 μM Hsp104, and 0.1 μM Sse1. Shaded area denotes the sub-stoichiometric region. The lower rate with the highest Hsp70 concentration is due to RNA degradation. (B) Relative chaperone concentration at half-maximal dispersal rate, extracted from the fits in (A). Error bars represent standard errors around the estimated parameter. (C) Survey of disaggregation studies in the literature. Maximal yield of disaggregation experiments and the relative amount of Hsp104 and Hsp70 used in the experiment are shown. Color and size of each data point correspond to the yield. Circles represent studies with wild type Hsp104. One square data point in the sub-stoichiometric Hsp70 area represents a study which used a hyperactive D484K variant of Hsp104. (D) Schematic comparison of the cooperative and non-cooperative models. (E) Pab1 dispersal monitored by fluorescence anisotropy (left) and the simulated Pab1 dispersal results from the cooperative model (right). (F) Quantitative comparison of Pab1 dispersal data (black) to the simulated results from the cooperative (blue) and non-cooperative models (orange). Fraction restored at the end of the 8 hour experiment (left) and the maximal rate of dispersal (right) were used for comparison. (G) Representative Sse1 titration Pab1 dispersal data. (H) Simulation of Pab1 dispersal with different ADP nucleotide exchange rates using the cooperative model.

also simulated the cooperative model (Figure 3.4A) using the same chaperone concentrations used in the *in vitro* experiment (Figure 3.6E). The cooperative model recapitulated the disaggregation system's Hsp70-sensitive Pab1 dispersal activity (Figure 3.6F). This model reflects the results from recent studies which indicate that interaction with more than one Hsp70 is required for activation of Hsp104 [21, 159]. Indeed, simulation of non-cooperative model, in which single Hsp70 is sufficient to recruit and activate Hsp104, resulted in high Pab1 dispersal activity even with sub-stoichiometric Hsp70 (Figure 3.6D and 3.6F).

The cooperative model was also able to recapitulate the general trend seen in the Hsp104 and Ssa2 titration experiments (Figure 3.6A and Figure 3.12B). Although Sis1 and Sse1 were not explicitly included in the model, modulating the ATP hydrolysis rate and ADP exchange rate allowed us to mimic the effect of titrating Sis1 and Sse1, respectively (Figure 3.12B). Interestingly, although we were able to recapitulate the inhibitory effect of Sse1 with high ADP exchange rate, modulating ADP exchange rate was not enough to recapitulate the facilitative effect of sub-stoichiometric Sse1 (Figure 3.6G and Figure 3.6H).

These results converge on a picture in which the presence of multiple, closely spaced Hsp70 molecules on the surface of condensates provide a molecular marker labeling condensates for Hsp104-dependent dispersal, as proposed in the bacterial disaggregation system by [159]. Our simulation results indicate that a cooperative Hsp70 effect on Hsp104 binding and activation suffices to explain the disaggregation system's intrinsic sensitivity to the level of Hsp70.

3.4 Discussion

We demonstrated that the yeast disaggregation system composed of molecular chaperones Hsp104, Hsp70, and Hsp40 can directly reverse heat-induced biomolecular condensates of Pab1 back to functional monomers *in vitro*. This establishes heat-induced biomolecular condensates of Pab1 as endogenous substrates of the molecular disaggregation system. Through comparative studies of Pab1 and the model substrate firefly luciferase, we uncovered a number of distinctions in the way chaperones engage with each substrate. The most notable

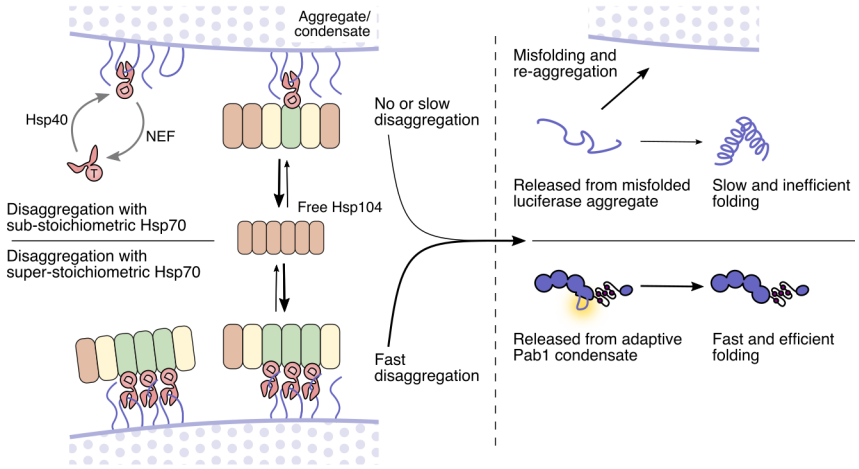

Figure 3.7: Model of Pab1 dispersal by the Hsp104/Hsp70/Hsp40 disaggregation system.
Productive recruitment and activation of Hsp104 depend on the presence of multiple closely spaced Hsp70 molecules on the surface of aggregate/condensate, a condition which is most likely to be achieved with excess Hsp70. Luciferase is fully threaded by Hsp104 and released as unfolded protein; This leads to slow and inefficient folding because unfolded protein is prone to misfolding and re-aggregation. In contrast, Pab1 is released after partial threading by Hsp104 and readily re-folds into native structure, resulting in faster and more efficient folding compared to luciferase. The schematic of Hsp104 with repressed (red) and activated (green) protomers is adapted from [21].

distinction was the large difference in the restoration efficiency between Pab1 condensates and luciferase aggregates. Our results show that partial threading of Pab1 by Hsp104 during dispersal can contribute to this large difference in the restoration efficiency. Finally, we find that efficient Pab1 dispersal depends on the presence of excess Hsp70, which serves as a condensate detector through cooperative recruitment and activation of Hsp104 near the surface of condensates (Figure 3.7).

3.4.1 Heat-induced biomolecular condensates are endogenous substrates of the molecular disaggregation system

In yeast, heat-induced biomolecular condensates including stress granules adopt a solid-like characteristic [88, 138]. Timely dispersal of endogenous condensates depends on molecular chaperones [27, 183, 88, 89], and the timing of dispersal correlates with resumption of active

cellular translation and growth [27, 88, 89]. These *in vivo* observations strongly suggest heat-induced biomolecular condensates are the endogenous substrates of the molecular disaggregation system. However, direct biochemical evidence for chaperone-mediated condensate dispersal has been missing.

In this study, we showed using *in vitro* reconstitution that the Hsp104/70/40 disaggregation system directly engages and disperses heat-induced condensates of Pab1. The contrast between Pab1 condensates and luciferase aggregates on multiple important dimensions (requirements for specific chaperones and for small heat-shock proteins, rate and yield of dispersal, the nature of engagement with Hsp104) demonstrates that luciferase, and by extension other similarly behaving "model" misfolded proteins, have severe limitations as models of endogenous heat-induced chaperone substrates. Whether the authentic substrate Pab1 is itself a suitable model for other endogenous substrates remains an important open question.

We also showed that Hsp110, Hsp70, and Hsp40 can disperse Pab1 condensates. This alternative disaggregation system is also capable of disaggregating luciferase aggregates and amyloid fibrils, although with much weaker disaggregation activity than with Hsp104 [162]. The disaggregation activity of the Hsp110/70/40 system is conserved in animals [162, 188], which lack cytosolic Hsp104 [39], suggesting a potential evolutionary and biochemical bridge to chaperone-mediated condensate dispersal in animals.

3.4.2 Different engagement of molecular chaperones with biomolecular condensates and misfolded protein aggregates

Co-aggregation of luciferase with Hsp26 keeps luciferase in a near-native conformation, generates smaller aggregates, and facilitates aggregate interaction with Hsp70 [22, 180, 200]. However, Hsp26 is almost undetectable in cells pre-stress [22]. Because biomolecular condensation of endogenous proteins occurs within a few minutes of heat stress [182], Hsp26 is unlikely to be involved in condensate regulation during the initial exposure to stress. We showed that Hsp26 prevents condensation of Pab1 *in vitro*. Human small heat shock protein

Hsp27 has also been shown to repress phase separation of FUS [97]. Post-stress accumulation of Hsp26 in cells may be involved in desensitization of the cells to sustained or repeated stress by modulating the phase boundary of endogenous mature proteins.

The canonical type I (Ydj1; DNAJA2 in humans) and type II Hsp40 (Sis1; DNAJB1) chaperones show synergistic activity toward luciferase aggregates [121, 122]. This synergistic activity stems from the preference of type I and II Hsp40 chaperones for small (200-700 kDa) and large (>5,000 kDa) aggregates, respectively [122], although how aggregates of different sizes can be distinguished at the molecular level remains unclear. Sis1 and Ydj1 also exhibit different amino acid sequence preference [75] and different mode of binding Hsp70, the latter of which has been shown to be responsible for amyloid disaggregation activity unique to type II chaperones [41]. The inability of Ydj1 to support Pab1 dispersal could be due to the large size of Pab1 condensates, the lack of Ydj1 binding sites among the exposed region of Pab1 in condensates, dependence on the Hsp70 binding mode unique to type II Hsp40, or any combination of these.

The antagonistic effect of Ydj1 on Sis1 suggests a competition between the two co-chaperones for Hsp70. In cells, stress-induced phosphorylation of Hsp70 reprograms Hsp70's substrate specificity, e.g., by preventing Hsp70 from interacting with Ydj1 but not with Sis1 [178]. Similar post-translational modifications may also regulate the activity of the disaggregation system toward specific substrates.

Hsp104 functions by threading substrate through its central channel [50]. However, both our simulation and biochemical experiments suggest Pab1 is partially threaded by Hsp104. A partial threading activity of Hsp104 and its bacterial homolog ClpB has been reported previously, where both proteins selectively thread misfolded moiety of the substrate while leaving the natively folded domains intact [62, 171]. We hypothesize that partial threading of the locally "unfolded" region of Pab1, possibly the same or near the region mediating Pab1 condensation interaction, allows for condensate dispersal without substantial protein unfolding.

3.4.3 Hsp70 clusters are a potential condensate-specific marker for Hsp104

Efficient dispersal of Pab1 condensates depends on the presence of excess Hsp70. Nearby Hsp70s, which would be rare on monomers but common on condensates, both increase Hsp104 binding and stimulate additional Hsp104 activity. In this sense, consistent with an insightful proposal from [159] working in the homologous bacterial system, Hsp70 clusters provide an active label for engagement and activation of powerful dispersal machinery only in spatial proximity to condensed substrates.

Cooperative action of Hsp70 in substrate unfolding has been proposed to explain the requirement of excess Hsp70 during glucose-6-phosphate dehydrogenase (G6PDH) disaggregation [14]. We find by simulation that cooperative action of Hsp70 in the recruitment and activation of Hsp104 is sufficient to reproduce the *in vitro* Hsp70 titration data.

We also found that, in the cooperative model, modulating the ADP exchange rate alone was not enough to reproduce the facilitative effect of Sse1 (Figure 3.6H). A recent study by [188] uncovered an additional function of human Hsp110 in promoting local clustering of Hsp70 on the substrate surface. A similar function in the yeast Hsp110, Sse1/2, may explain the discrepancy between our model and the data.

3.4.4 Biomolecular condensates in the cellular heat shock response

Engagement of molecular chaperones, especially Hsp40 and Hsp70, with stress-induced biomolecular condensates provides a tangible means to explain how yeast cells integrate multiple physical cues from the environment to sense temperature. In yeast, the transcriptional heat shock response is triggered when Hsp70, which is bound repressively to the transcriptional factor Hsf1, is titrated away by stress-induced substrates [199, 86, 130, 107, 42].

S. cerevisiae cultured at 30°C begins mounting the transcriptional heat shock response when the temperature is raised above 36°C. The identities of these stress-induced substrates remain elusive. Although misfolding-prone nascent or newly synthesized polypeptides are known to help trigger the response, suppression of protein synthesis is not sufficient to

suppress the transcriptional response, implying the existence of mature substrates which, we recently showed, also like depend on stress-associated intracellular acidification for formation [176]. Notably, condensation of Pab1 and other heat-sensitive proteins is strongly pH-sensitive [138, 72, 89]. Here, we provide an additional important piece of circumstantial evidence for the model of stress-triggered condensation as an activator of Hsf1: heat-induced condensates of Pab1 are authentic chaperone substrates which depend on Hsp70 for dispersal. Thus, Pab1 can autonomously transduce physiological heat shock temperatures into biomolecular condensation, dependent on pH, and recruit molecular chaperones including Hsp70. In short, Pab1—and by extension presumably others of the dozens of previously identified heat-condensing proteins [182, 26], including more than a dozen which condense in response to a 37°C heat shock—now appears to have all the characteristics needed to act as an inducer of the transcriptional heat shock response. An important conceptual difference is that while the proteotoxicity model has invoked toxic misfolding, biomolecular condensation is known to be an evolved, adaptive response [138, 72].

3.4.5 Molecular chaperones as biomolecular condensate remodelers

In this work, we show that molecular chaperones can regulate biomolecular condensates by acting as dispersal factors. This expands the list of known condensate dispersal factors, which currently includes the dual specificity kinase DYRK3 [190] and nuclear-import receptor karyopherin-β2 [59]. The functional repertoire of molecular chaperones in biomolecular condensate regulation is likely to be much broader than just dispersal. For example, Hsp104, Hsp70, and Hsp40 in yeast are required for condensate formation of SNF1 kinase activator Std1 during fermentation [165]. Another example is Hsp27, which partitions into liquid-like FUS condensates upon stress-induced phosphorylation and prevents amyloid transition of FUS [97]. Illumination of the roles of molecular chaperones as facilitators, remodelers, and dispersers of biomolecular condensates—and the mechanisms and biological consequences of this regulation—presents an enormous opportunity for expanding our understanding of these

ancient molecules.

3.5 Methods

3.5.1 Data and Code Availability

Experimental data and code for analysis

All data analysis and visualization were performed with R (version 3.5.2) in RStudio [143]. The raw and processed data, and the custom scripts for data process, data analysis, and figure generation will be available on Data Dryad.

Code for simulation and data analysis

Simulation was performed with Python (version 3.7.7) in Jupyter notebook [85]. The code is available on GitHub (`https://github.com/haneulyoo/sim_disagg_2021`).

3.5.2 Experimental Model and Subject Details

Yeast strain and growth conditions

S. cerevisiae strain BY4741 (MATa ura3Δ0 leu2Δ0 his3Δ1 met15Δ0) cells were cultured in yeast extract peptone dextrose (YPD) media in shaking baffled flasks at 30°C. The strain background used was S288C.

Bacteria strain and growth conditions

Unless specified otherwise under Chemicals, Peptides, and Recombinant proteins of the Key Resources Table, all recombinant proteins used in this work are expressed in and purified from *E. coli* BL21(DE3). Cells were first grown in Luria broth (LB) at 37°C for 12 to 16

hours and then inoculated to 1-2 L Terrific Broth (TB) culture. Specific growth condition used for each recombinant protein is described in Method Details.

Purification of Pab1 and Pab1 variants

Protein expression and purification protocols were adapted with modification from [138]. N-terminally 8xHis-tagged Pab1 constructs were transformed into an *E. coli* strain BL21(DE3) and grown overnight at 37°C. The overnight culture was used to inoculate 1L Terrific Broth (TB). Cells were grown until the optical density at 600 nm (OD_{600}) reached between 0.4 and 0.6 and then the flask was moved into a 30°C incubator. After 30 minutes, 0.2 mM IPTG was added to induce protein expression. Cells were harvested after 4 hours and lysed by sonication in His binding buffer (20 mM HEPES pH 7.3, 150 mM KCl, 2.5 mM $MgCl_2$, 20 mM imidazole, 10 % glycerol, and 1 mM BME) supplemented with 1 Pierce protease inhibitor tablet (Thermo Fisher A32965). Lysate was cleared by spinning at 20,000 g for 15 minutes. Cleared lysate was loaded onto a 5 mL HisTrap FF column (Thermo Fisher 17525501) equilibrated with His binding buffer on an AKTA FPLC system. Protein was eluted with a 20 mL gradient from 0 to 100 % His elution buffer (20 mM HEPES pH 7.3, 150 mM KCl, 2.5 mM $MgCl_2$, 400 mM imidazole, 10 % glycerol, and 1 mM BME). Fractions containing Pab1 were buffer exchanged into a Q binding buffer (20 mM HEPES pH 7.3, 50 mM KCl, 2.5 mM $MgCl_2$, 10 % glycerol, and 1 mM DTT) and loaded onto a 5 mL HiTrap Heparin HP column (GE Healthcare 17040701) to remove nucleic acids. Nucleic acid-free protein was eluted over a 20 mL gradient from 0 to 100 % Q elution buffer (20 mM HEPES pH 7.3, 1 M KCl, 2.5 mM $MgCl_2$, 10 % glycerol, 1 mM DTT). Fractions of interest were combined with an aliquot of a homemade tobacco etch virus (TEV) protease and dialyzed against 1 L His binding buffer overnight to remove the N-terminal tag and to lower the salt concentration. On the next day, the dialyzed solution was loaded again onto a 5 mL HisTrap FF column and the flow-through which contains the cleaved protein was collected. The protein was concentrated and loaded onto a Superose 6 10/300 GL column (GE Healthcare)

equilibrated with SEC/Storage buffer (20 mM HEPES pH 7.3, 150 mM KCl, 2.5 mM $MgCl_2$, and 1 mM DTT). Monomeric proteins were pooled together, further concentrated if necessary, and stored at -80°C. Protein concentration was measured using Bradford assay (Bio-Rad 5000201).

Purification of Hsp70 chaperones

We adapted with minor modifications the protocol provided by Zachary March in James Shorter's group. N-terminally 6xHis-SUMO-tagged Hsp70 proteins were transformed into an *E. coli* strain BL21(DE3) and grown overnight at 37°C. The overnight culture was used to inoculate 1L Terrific Broth (TB). Cells were grown until OD_{600} between 0.4 and 0.6 and then the flask was moved into a 18°C incubator. After 30 minutes, 0.2 mM IPTG was added to induce protein expression overnight. Cells were harvested after 14 - 18 hours and lysed by sonication in Hsp70 His binding buffer (50 mM HEPES pH 7.3, 750 mM KCl, 5 mM $MgCl_2$, 20 mM imidazole, 10 % glycerol, 1 mM BME, and 1 mM ATP) supplemented with 1 Pierce protease inhibitor tablet. Cleared lysate was loaded onto a 5 mL HisTrap FF column equilibrated with Hsp70 His binding buffer on an AKTA FPLC system. After loading, the column was washed with more Hsp70 His binding buffer until the UV reading returned to a steady, baseline level. The column was further washed with about 20 mL high ATP buffer (50 mM HEPES pH 7.3, 750 mM KCl, 5 mM $MgCl_2$, 20 mM imidazole, 10 % glycerol, 1 mM BME, and 20 mM ATP) and incubated in this buffer for at least 30 minutes. The high ATP buffer was washed out with Hsp70 His binding buffer and the protein was eluted with a 20 mL gradient from 0 to 100 % Hsp70 His elution buffer (50 mM HEPES pH 7.3, 750 mM KCl, 5 mM $MgCl_2$, 400 mM imidazole, 10 % glycerol, 1 mM BME, and 1 mM ATP). The fractions of interest were combined and dialyzed against 1 L Hsp70 His binding buffer for at least 2 hours to remove excess imidazole. An aliquot of homemade SUMO protease Ulp1 was added to the dialysis bag. Dialysis was continued overnight at 4°C. Next day, the cleaved protein was recovered by running the dialyzed solution through His column and collecting flow-through.

Flow-through fractions containing tag-free Hsp70 proteins were combined, diluted in Hsp70 Q binding buffer (20 mM HEPES pH 7.3, 50 mM KCl, 5 mM $MgCl_2$, 0.5 mM EDTA, 2 mM DTT, and 1 mM ATP), and loaded onto an equilibrated 5 mL HiTrap Q HP anion exchange column (GE Healthcare 17115401). Hsp70 was eluted over a 50 mL gradient from 0 to 100 % Hsp70 Q elution buffer (20 mM HEPES pH 7.3, 1 M KCl, 5 mM $MgCl_2$, 0.5 mM EDTA, 2 mM DTT, and 1 mM ATP). Fractions containing Hsp70 were determined by SDS-PAGE. We observed a peak with a left shoulder or two closely overlapping peaks around 25 mS/cm. Both peaks contained Hsp70, but only the later peak fractions exhibited activity in both luciferase and Pab1 disaggregation assays. We combined the fractions corresponding to the second peak, concentrated, and buffer exchanged the protein into Hsp70 storage buffer (50 mM HEPES pH 7.3, 150 mM KCl, 5 mM $MgCl_2$, 10 % glycerol, 2 mM DTT, and 1 mM ATP). Protein concentration was measured using Bradford assay. Protein aliquots were snap-frozen in liquid nitrogen and stored at -80°C.

Purification of sortase A enzymes

Wild-type [58] (used for N-terminal labeling) and heptamutant sortase A [64] (used for C-terminal labeling) were purified using the same protocol. Constructs were transformed into *E. coli* strain BL21(DE3), grown in 1 L of TB until they reached an OD_{600} of 0.6. Protein production was induced with 0.5 mM IPTG. The cells were incubated overnight at 18°C, and harvested in His binding buffer (20 mM HEPES pH 7.5, 150 mM KCl, 2.5 mM $MgCl_2$, 20 mM imidazole, 10 % glycerol, and 1 mM BME), supplemented with protease inhibitors and Pierce Universal Nuclease (Thermo Scientific PI88702). Cells were lysed by sonication, clarified by centrifugation at 20,000 g for 30 minutes, then bound to 5 mL of Ni-NTA resin (Thermo Scientific 88222) for 1 hour at 4°C. The resin was washed with 100 mL of His binding buffer, then the protein was eluted in 20 mL of His elution buffer (20 mM HEPES pH 7.5, 150 mM KCl, 2.5 mM $MgCl_2$, 250 mM imidazole, and 1 mM BME). The protein was concentrated in a spin concentrator, then loaded onto a Superdex 200 16/60 column (GE

Healthcare) equilibrated in buffer (20 mM HEPES pH 7.5, 150 mM KCl, 2.5 mM $MgCl_2$, 10 % glycerol, and 0.5 mM TCEP). Fractions corresponding to the monomeric protein were pooled together, concentrated, and aliquoted for storage at -80 °C.

Purification of ClpX and ClpP

The purification of ClpXΔN and ClpP were done as previously described [104]. A plasmid encoding a linked trimer of ClpXΔN with an N-terminal 6xHis affinity tag was transformed into *E. coli* BL21(DE3) and grown in 1 L of TB until OD_{600} of 0.6. Protein production was induced with 0.5 mM IPTG. Cells were harvested after 4 hours at 37°C and resuspended in His binding buffer (20 mM HEPES pH 7.5, 100 mM KCl, 400 mM NaCl, 20 mM imidazole, 10% glycerol, and 1 mM BME), supplemented with protease inhibitors and Pierce Universal Nuclease (Thermo Scientific PI88702). Cells were lysed by sonication, clarified by centrifugation at 20,000 g for 30 minutes, then bound to 5 mL of Ni-NTA resin (Thermo Scientific 88222) for 1 hour at 4°C. The resin was washed with 100 mL of His binding buffer, then the protein was eluted in 20 mL of His elution buffer (20 mM HEPES pH 7.5, 100 mM KCl, 400 mM NaCl, 250 mM imidazole, 10% glycerol, and 1 mM BME). The protein was concentrated in a spin concentrator, then loaded onto a Superdex 200 16/60 column (GE Healthcare) equilibrated in buffer (20 mM HEPES pH 7.5, 300 mM KCl, 0.1 mM EDTA, 10 % glycerol and 1 mM DTT). Fractions corresponding to the monomeric protein were pooled together, concentrated and aliquoted for storage at -80°C. Protein concentration was determined by measuring A_{280}.

A plasmid encoding ClpP with a C-terminal 6xHis affinity tag was transformed into *E. coli* BL21(DE3), grown in 1 L of TB until OD_{600} of 0.6. Protein production was induced with 0.5 mM IPTG, and cells were harvested after 4 hours at 37°C, and resuspended in His binding buffer (20 mM HEPES pH 7.5, 100 mM KCl, 400 mM NaCl, 20 mM imidazole, 10% glycerol, and 1 mM BME), supplemented with Pierce Universal Nuclease (Thermo Scientific PI88702). Protease inhibitors were omitted. Cells were lysed by sonication, clarified by centrifugation

at 20,000 g for 30 minutes, then bound to 5 mL of Ni-NTA resin (Thermo Scientific 88222) for 1 hour at 4°C. The resin was washed with 100 mL of His binding buffer, then the protein was eluted in 20 mL of His elution buffer (20 mM HEPES pH 7.5, 100 mM KCl, 400 mM NaCl, 250 mM imidazole, 10% glycerol, and 1 mM BME). The protein was then bound to a 5 mL HiTrap MonoQ column equilibrated in low salt buffer (50 mM Tris-HCL pH 8.0, 50 mM KCl, 10 mM $MgCl_2$, 0.1 mM EDTA, 10% glycerol, and 1 mM BME), washed with 20 mL of low salt buffer and then eluted using a 100 mL gradient between low salt buffer and high salt buffer (50 mM Tris-HCL pH 8.0, 200 mM KCl, 10 mM $MgCl_2$, 0.1 mM EDTA, 10% glycerol, and 1 mM BME). The protein was concentrated in a spin concentrator, then loaded onto a Superdex 200 16/60 column (GE Healthcare) equilibrated in buffer (20 mM HEPES pH 7.5, 200 mM KCl, 0.1 mM EDTA, 10 mM $MgCl_2$, 10 % glycerol and 1 mM DTT). Fractions corresponding to the monomeric protein were pooled together, concentrated and aliquoted for storage at -80°C. Protein concentration was determined by measuring A_{280}.

Purification of remaining recombinant proteins

The rest of the recombinant proteins used in this paper were expressed with an N-terminal 6xHis-SUMO tag in *E. coli* strain BL21(DE3) and purified as described for Pab1, but using anion exchange instead of Heparin column.

Fluorescein labeling of Pab1

Fluorescein labeling of Pab1 termini was done using sortase catalyzed ligation of labeled peptides. For N-terminal labeling, 6xHis-TEV-GGG-Pab1 was purified using the same protocol described for wild-type Pab1 above. The labeling was done in SEC buffer (20 mM HEPES 7.3, 150 mM KCl, and 2.5 mM $MgCl_2$) as a 500 μL reaction with 100 μM Pab1, 20 μM wild-type sortase A, 0.5 mM TCEP, 10 mM $CaCl_2$ and 0.5 mM 5-FAM-HHHHHHLPETGG peptide (Biomatik). After an hour incubation at room temperature, labeled protein was separated from free peptide on a 5 mL HiTrap Desalting column equilibrated in aggregation

buffer (20 mM HEPES pH 6.8, 150 mM KCl, 2.5 mM $MgCl_2$, and 1 mM DTT). The C-terminally labeled Pab1 was prepared similarly, but the labeling reaction was done with the following condition: 100 μM Pab1, 20μM heptamutant sortase A, 0.5 mM TCEP, and 0.5 mM GGGK(FAM)AANDENYALAA or GGGK(FAM) peptide (Biomatik).

In vivo Total/Soluble/Pellet (TSP) assay

Yeast cells were diluted to OD_{600} of approximately 0.001 in 250 mL YPD and incubated at 30°C until OD_{600} reached between 0.3 and 0.4. 30 mL of the cell culture was harvested as the pre-shock sample by spinning in a 50 mL conical tube at 3,000 g for 5 minutes at room temperature (RT). The cell pellet was resuspended in 1 mL of cold soluble protein buffer (SPB; 20 mM HEPES pH7.3, 120 mM KCl, 2 mM EDTA, 0.2 mM DTT, 1:100 PMSF, and 1:100 protease inhibitors cocktail IV (MilliporeSigma 539136)), transferred to a pre-chilled 1.5 mL microcentrifuge tube, and centrifuged again at 5,000 g for 30 seconds at RT. Supernatant was removed and the pellet was resuspended in 170 μL SPB. Two 100 μL aliquots from the resuspended sample were snap-frozen in liquid nitrogen. The remaining cell culture was vacumm filtered and the cell pellet was transferred to a 50 mL conical tube. The conical tube was placed in a 42°C water bath to heat shock the cells. After 20 minutes, the cell pellet was resuspended in 220 mL of pre-warmed 30°C YPD media. 30 mL of this culture was harvested as the heat shock sample and processed as described earlier. The remaining cell culture was transferred to a 1 L flask and the cells were recovered in a 30°C water bath. Recovery samples were collected at different time points and processed in the same way as the pre-shock sample. Cells were lysed by cryomilling and fractionated as described in [182], with minor modifications on spin conditions. Briefly, cell lysates were cleared at 3,000 g for 30 seconds. 150 μL of the cleared lysate was transferred to a new 1.5 mL tube. To remove RNA, RNase I_f (NEB M0243S) was added to the final concentration of 0.3 units/μL and the sample was incubated at RT for 30 minutes. 50 μL of the sample was transferred to a new tube, mixed with Total protein buffer (TPB; 20 mM HEPES pH 7.3, 150 mM NaCl, 5 mM

EDTA, 3% SDS, 1:100 PMSF, 2 mM DTT, and 1:1000 protease inhibitors IV (MilliporeSigma 539136)), and spun at 6,000 g for 1 minute to collect Total protein sample. Pellet samples were collected by spinning the remaining 100 μL sample at 8,000 g for 5 minutes (P_8) and at 100,000 g for 20 minutes (P_{100}) at 4°C, and resuspending the pellet in Insoluble protein buffer (IPB; TPB with 8 M urea). Supernatant from this last spin was collected as the Soluble protein sample. Pab1 in each sample were visualized by SDS-PAGE and western blot as described in [182] using mouse monoclonal anti-Pab1p antibody (EnCor Biotechnology MCA-1G1) and Image Lab software (Bio-Rad).

In vitro Total/Soluble/Pellet (TSP) assay

Reaction mixture containing Pab1 condensates and molecular chaperones were prepared and incubated at 30°C for an hour either in the absence or presence of 5 mM ATP. The reaction mixture (Table 3.2) were centrifuged at 100,000 g for 20 minutes at 4°C. Supernatant was collected as the soluble fraction sample. Buffer (20 mM HEPES pH 7.3, 150 mM KCl, 2.5 mM $MgCl_2$, 0.01 % Triton X-100, 0.5 mg/mL BSA, and 1 mM DTT) was added to the pellet and the sample was centrifuged again under the same condition. After removing the supernatant, the pellet was directly resuspended in 1x Laemmli buffer. Pab1 in each sample was visualized by SDS-PAGE and western blot as described in [182] using Image Lab software (Bio-Rad).

Preparation of Pab1 condensates

Pab1 monomers were buffer exchanged into aggregation buffer (20 mM HEPES pH 6.8, 150 mM KCl, 2.5 mM $MgCl_2$, and 1 mM DTT) and diluted to make a 500 μL sample of 25 μM Pab1. The sample was sometimes supplemented with 100-fold lower firefly luciferase to increase yield. The sample was incubated in a 42°C water bath for 20 minutes at pH 6.8. Under this heat shock condition, the solution remained clear and minimal protein pelleting was observed after a 3 minute centrifugation at 8,000 g. N-terminally fluorescein labeled Pab1

aggregates were prepared at 39°C. The supernatant was loaded onto a Superose 6 10/300 GL column (GE Healthcare) equilibrated with SEC/Storage buffer (20 mM HEPES pH 7.3, 150 mM KCl, 2.5 mM $MgCl_2$, and 1 mM DTT). Void fractions containing small Pab1 assemblies (>5,000 kDa) were collected. About half of the loaded protein eluted in the void volume while the remaining protein eluted as monomers. Concentration of Pab1 condensates in each void fraction was measured using Bradford assay and/or SDS-PAGE with Pab1 standards of known concentrations. Protein aliquots were snap-frozen in liquid nitrogen and stored at -80°C.

Monitoring Pab1 dispersal using fluorescence anisotropy

Because Pab1 binds 12-mer poly(A) with full affinity and has a binding footprint of roughly 25 nucleotides [149], we used 19-mer poly(A) RNA to get 1:1 binding of Pab1 to RNA. Pab1 condensates, molecular chaperones, and 5' labeled A19 RNA (FAM-A19 or Atto550-A19) were diluted to desired concentrations in disaggregation buffer (20 mM HEPES pH 7.3, 150 mM KCl, 2.5 mM $MgCl_2$, 0.5 mg/mL BSA, 0.01 % Triton X-100, and 1 mM DTT). The reaction mixture (Table 3.2) was supplemented with 5 mM ATP, and 8 mM creatine phosphate (CP) and 1 μM creatine kinase (CK) for ATP regeneration. The reaction mixture was also supplemented with 2 % SUPERase RNase Inhibitor (Thermo Fisher AM2694) to prevent RNA degradation. The final reaction volume was 15 μL. Calibration samples were prepared by adding known concentrations of monomeric Pab1 to a fixed concentration of FAM-A19 used in the reaction samples, typically 200 nM.

A new calibration curve was measured each time an experiment was performed. The reaction mixtures were added to non-binding surface 384-well plate (Corning CLS3575). The plate wells were sealed with a plate sealer (Thermo Fisher 235307) to prevent liquid evaporation. Fluorescence anisotropy was measured every 20 second in Spark microplate reader (TECAN) using excitation/emission wavelengths of 485 nm/535 nm, each with a bandwidth of 20 nm, at 30°C. Disaggregation buffer was used as blank. G factor was calibrated

with a solution of free 6-iodoacetamidofluorescein to produce a fluorescence polarization reading of 20 mP.

Anisotropy data fitting and analysis

The reaction data were fitted with the following logistic equation:

$$y = d + \frac{m}{1 + e^{-a(x-b)}} - x * c \tag{3.1}$$

where d, m, a, b, and c are fitting parameters. The negative linear term accounts for the chaperone concentration-dependent signal decay, which comes from RNA-degrading contaminants co-purified with chaperones.

To extract maximal rate of Pab1 dispersal, the fluorescence anisotropy values were first converted to the concentration of RNA-binding competent monomeric Pab1 using the calibration curve. Fluorescence anisotropy data of the calibration samples were fitted with the following equation:

$$y = \min + (\max - \min)\frac{(RNA + Pab1^n + d) - \sqrt{(RNA + Pab1^n + d)^2 - 4(RNA * Pab1^n)}}{2 * RNA} \tag{3.2}$$

Min and max refer to the fluorescence anisotropy values of the calibration samples with no or saturating amount of monomeric Pab1, respectively. The values of d and n extracted from the calibration fit were used to convert fluorescence anisotropy values in the reaction samples to concentrations of Pab1 with this rearranged equation (3.2):

$$Pab1 = \sqrt[n]{\frac{((y - \min)^2 * \frac{RNA}{\max - \min} - (y - \min) * (RNA + d))}{y - \max}} \tag{3.3}$$

The converted data were fitted again with equation (3.1). Maximal rate of dispersal was calculated by computing the extracted fit parameters to the derivative of equation (3.1) when

x = b:

$$\frac{dy}{dx} = \frac{a * m * e^{-a(x-b)}}{(1 + e^{-a(x-b)})^2} - c \tag{3.4}$$

$$\text{rate}_{max} = \frac{a * m}{4} - c \tag{3.5}$$

Note that, because Pab1 condensates exhibit substantially reduced but non-zero binding to FAM-A19 in a concentration-dependent manner, the maximal rate of dispersal quantified from fluorescence anisotropy data may be systematically underestimating the true rate of dispersal.

To convert the y-axis from Pab1 concentration to fraction restored Pab1, we first subtracted background signal using the negative control data (no ATP). Background-subtracted data were divided by the total concentration of Pab1, which was approximated by taking the mean of highest 50-100 data points, i.e., data points in the plateau region of the positive control. Total Pab1 concentration in the reaction had to be approximated this way for more accurate quantification because we noticed that Pab1 condensates adhere to plastic, causing loss of about 30-50% substrate during transfer. To compensate for this, 1.5 to 2-fold excess Pab1 was added to aim for, e.g., the final concentration of 0.2 μM Pab1 in the reaction. The same total Pab1 concentration was used to normalize reactions prepared from the same master mix. The presence of 5 mM ATP slightly lowered the fluorescence anisotropy baseline compared to the no ATP control, and this led to negative starting values for all ATP-containing reactions after background subtraction; All traces were shifted upward by the same amount to make the positive control reactions to start around the value of zero.

The rate data in Figure 3.6A were fitted with a logistic equation:

$$y = \frac{a}{1 + e^{-b(x-c)}} \tag{3.6}$$

with a, b, and c as fitting parameters. We used the total Pab1 concentration to calculate the

ratio of chaperone to substrate.

Fluorescence-detection size-exclusion chromatography (FSEC)

Small Pab1-Clover condensates were prepared and mixed with chaperones, ATP, ATP regeneration system, and SUPERase RNase Inhibitor as described above for wild type Pab1 (Table 3.2). The reaction samples (120 μL per run) were incubated at 30°C for an hour. 120 μL of the sample was loaded to a Superdex 200 10/300 GL column (GE Healthcare) equilibrated with filtered running buffer (20 mM HEPES pH 7.3, 150 mM KCl, 2.5 mM $MgCl_2$, and 1 mM DTT) using Akta system. Fluorescence was measured by a fluorescence detector (JASCO FP-2020 Plus) connected to the Akta system.

Luciferase reactivation assay

Recombinant firefly luciferase was aggregated by incubating 2 μM of luciferase with 10 μM Hsp26 in aggregation buffer (20 mM HEPES pH 6.8, 150 mM KCl, 2.5 mM $MgCl_2$, and 1 mM DTT) at 42°C for 20 minutes. After cooling on ice for 2 minutes, the aggregates were diluted to 0.2 μM in the disaggregation buffer (20 mM HEPES pH 7.3, 150 mM KCl, 2.5 mM $MgCl_2$, 0.5 mg/mL BSA, 0.01 % Triton X-100, and 1 mM DTT) supplemented with 5 mM ATP, 8 mM CP, 1 μM CK, and specified concentrations of chaperones (Table 3.2). The mixed sample was incubated at 30°C. At each time point, 2 μL of the reaction sample was added to 18 μL of luciferin mix (Promega E1500), and luminescence was measured using Spark microplate reader (TECAN) with integration time of 1 second. Luminescence of 0.2 μM native luciferase supplemented with 1 μM Hsp26 in disaggregation buffer was used to compute reactivation yield.

For faster disaggregation using excess molecular chaperones (Figure 3.3B), 33.8 nM luciferase was heat shocked in the presence of 169 nM Hsp26 at 42°C for 20 minutes in low-salt aggregation buffer (25 mM HEPES pH 7.3, 50 mM KCl, 0.1 mM EDTA, and 1 mM DTT). Luciferase aggregates were diluted to the final concentration of 20 nM in the

disaggregation buffer containing chaperones (Table 3.2). Luminescence was measured as described above.

For disaggregation of chemically aggregated luciferase using HAP/ClpP system (Figure 3.5H and 3.5I), luciferase was diluted to 5 μM in low-salt urea buffer (25 mM HEPES pH 7.3, 50 mM KCl, 0.1 mM EDTA, 1 mM DTT, and 8 M urea) and incubated at 30°C for 30 minutes. Aggregation was induced by diluting luciferase 100-fold into the disaggregation buffer containing chaperones and HAP/ClpP (Table 3.2). Western blot samples were collected at the specified time points and stained using luciferase antibody (MilliporeSigma L0159). Blots were visualized using Odyssey CLx (LI-COR). Luminescence was measured as described above using mock-treated luciferase as normalization control.

Dynamic light scattering (DLS)

DLS measurements were performed using DynaPro NanoStar (Wyatt). Sample acquisition was done as described in [138]. All experiments, unless noted otherwise, were performed with 10 μM Pab1 in filtered DLS buffer (20 mM HEPES pH 6.8, 150 mM KCl, 2.5 mM $MgCl_2$, and 1 mM DTT). All protein samples used for DLS experiments were dialyzed against DLS buffer overnight at 4°C and cleared of aggregates by spinning at 20,000 g for 20 minutes.

GroEL trap assay

Pab1 dispersal and luciferase reactivation assays were done as described above, but in the presence of 5-fold excess GroEL trap (Table 3.2). For refolding experiment, 5 μM Pab1 was denatured in 8 M urea buffer (20 mM HEPES pH 6.8, 150 mM KCl, 2.5 mM $MgCl_2$, 1 mM DTT, and 8 M urea) and incubated at 30°C for 30 minutes. Pab1 was first diluted to 0.5 μM in refolding buffer (20 mM HEPES pH 7.3, 150 mM KCl, 2.5 mM $MgCl_2$, and 1 mM DTT) containing no or 10-fold excess GroEL trap, and then to 0.1 μM in the same respective refolding buffer with 0.1 μM FAM-A19. Pab1's RNA-binding activity was measured by fluorescence anisotropy.

Gel analysis of HAP/ClpP degradation

Digestion by the HAP/ClpP system was done in disaggregation buffer (20 mM HEPES pH 7.3, 150 mM KCl, 2.5 mM $MgCl_2$, 0.5 mg/mL BSA, 0.01 % Triton X-100, and 1 mM DTT) with 0.2 μM Pab1 condensate or monomer, 1.5 μM ClpP, 1 μM Hsp104 (WT or HAP), 0.5 μM Sis1, 1-2 μM Ssa2, 5 mM ATP, and 8 mM CP and 1 μM CK for ATP regeneration (Table 3.2). Reactions were run for 1 hour at 30°C, then quenched with Laemmli buffer and run on a Bio-rad TGX 4-20% SDS-PAGE gel. Fluorescent gels were imaged using a ChemiDoc (Bio-rad) and westerns were performed using a 1:5000 dilution of Rabbit anti-GFP antibody (Life A11122) and a 1:20,000 dilution of secondary (Donkey anti-Rabbit, LiCor 925-32213). Blots were visualized using Odyssey CLx (LI-COR).

The ClpXP digestion reaction was done for 30 minutes at 30°C with 0.2 μM Pab1-FAM monomer, 0.1 μM ClpX and 1 μM ClpP in disaggregation buffer.

Disaggregation data from the literature

The following data from 18 different studies [122, 34, 134, 197, 200, 105, 84, 136, 142, 32, 162, 62, 53, 135, 22, 55, 164, 37] were compiled for comparison: 1) substrate identity; 2) concentrations of substrate and molecular chaperones used; 3) maximum yield observed within the experimental time; 4) the names of molecular chaperones; and 5) reference to the source paper with DOI. Only the results from *in vitro* experiments were recorded. Studies reporting fold-change relative to negative control were omitted because yield cannot be determined from the given information for comparison. For a study which reports multiple disaggregation results with the same substrate, the concentrations of substrate and chaperones which give the highest maximal yield were recorded.

Modeling and simulation

In our model, free substrates exist in one of the following states: folded (S_f), unfolded (S_u), misfolded (S_m), and aggregated (S_a). Free Hsp70 exists either in an ATP-bound state ($Hsp70_{ATP}$) or an ADP-bound state ($Hsp70_{ADP}$), and each state can bind certain free substrates to form a complex (e.g., $Hsp70_{ATP}$:S_a). ATP hydolysis of $Hsp70_{ATP}$ in $Hsp70_{ATP}$:S_m complex results in substrate unfolding, a step we call "priming". For an aggregated substate, the same sequence of events do not result in any state transition but instead primes the complex ($Hsp70_{ATP}$:S_{ap}) for interaction with Hsp104. In the cooperative model, a second $Hsp70_{ATP}$ can bind $Hsp70_{ADP}$:S_{ap} complex to form a ternary complex ($Hsp70_{ATP,ADP}$:S_{ap}) and only the ternary complex with both Hsp70s in the ADP-bound state ($Hsp70_{ADP,ADP}$:S_{ap}) can engage with Hsp104 for disaggregation. For simplicity, we did not allow unfolding of a natively folded substrate.

The time evolution of the concentrations of all distinct species in the cooperative model was described using the following ODEs:

$$\begin{aligned}\frac{d[Hsp70_{ATP}]}{dt} = {} & k_{DT}[Hsp70_{ADP}] + k_{off}^{ATP}([Hsp70_{ATP} : S_a] + [Hsp70_{ATP} : S_{ap}] \\ & + [Hsp70_{ATP} : S_m] + [Hsp70_{ATP} : S_u] + [Hsp70_{ATP,ADP} : S_{ap}]) \\ & - [Hsp70_{ATP}](k_{on}^{ATP}([S_m] + [S_a]) + (k_{TD} + k_h) + 0.1k_{on}^{ATP}[Hsp70_{ADP} : S_{ap}])\end{aligned} \tag{3.7}$$

$$\begin{aligned}\frac{d[Hsp70_{ADP}]}{dt} = {} & (k_{TD} + k_h)[Hsp70_{ATP}] + k_{off}^{ADP}([Hsp70_{ADP} : S_{ap}] \\ & + [Hsp70_{ADP} : S_u]) + 2k_{off}^{ADP,104}[Hsp70_{ADP,ADP} : S_{ap} : Hsp104] \\ & - [Hsp70_{ADP}](k_{DT} + k_{on}^{ADP}([S_a] + [S_u]))\end{aligned} \tag{3.8}$$

$$\begin{aligned}\frac{d[Hsp104]}{dt} = {} & k_{off}^{104}[Hsp70_{ADP,ADP} : S_{ap} : Hsp104] + k_{disagg}[Hsp104 : S_{ap}] \\ & - [Hsp104][Hsp70_{ADP,ADP} : S_{ap}]k_{on}^{104}\end{aligned} \tag{3.9}$$

$$\frac{d[S_a]}{dt} = k_3[S_m] + k_{off}^{ATP}([Hsp70_{ATP} : S_a] + [Hsp70_{ATP} : S_{ap}]) + k_{off}^{ADP}[Hsp70_{ADP} : S_{ap}] \\ -[S_a](k_{on}^{ATP}[Hsp70_{ATP}] + k_{on}^{ADP}[Hsp70_{ADP}]) \tag{3.10}$$

$$\frac{d[Hsp70_{ATP} : S_a]}{dt} = k_{on}^{ATP}[Hsp70_{ATP}][S_a] + k_{DT}^{s}[Hsp70_{ADP} : S_a] \\ -[Hsp70_{ATP} : S_a](k_{off}^{ATP} + k_{TD}^{s} + k_{h}^{s}) \tag{3.11}$$

$$\frac{d[Hsp70_{ADP} : S_a]}{dt} = (k_{TD}^{s} + k_{h}^{s})[Hsp70_{ATP} : S_a] + k_{deprime}[Hsp70_{ADP} : S_{ap}] \\ -[Hsp70_{ADP} : S_a](k_{DT}^{s} + k_{prime}) \tag{3.12}$$

$$\frac{d[Hsp70_{ADP} : S_{ap}]}{dt} = k_{prime}[Hsp70_{ADP} : S_a] + k_{TD}^{s}[Hsp70_{ATP} : S_{ap}] \\ +k_{off}^{ATP}[Hsp70_{ATP,ADP} : S_{ap}] + k_{on}^{ADP}[Hsp70_{ADP}][S_a] \\ -[Hsp70_{ADP} : S_{ap}](k_{deprime} + k_{DT}^{s} + k_{off}^{ADP} + 0.1k_{on}^{ATP}[Hsp70_{ATP}]) \tag{3.13}$$

$$\frac{d[Hsp70_{ATP} : S_{ap}]}{dt} = k_{DT}^{s}[Hsp70_{ADP} : S_{ap}] - [Hsp70_{ATP} : S_{ap}](k_{off}^{ATP} + k_{TD}^{s}) \tag{3.14}$$

$$\frac{d[Hsp70_{ADP,ADP} : S_{ap} : Hsp104]}{dt} = k_{on}^{104}[Hsp70_{ADP,ADP} : S_{ap}][Hsp104] \\ -[Hsp70_{ADP,ADP} : S_{ap} : Hsp104](k_{off}^{104} + k_{off}^{ADP,104}) \tag{3.15}$$

$$\frac{d[Hsp104 : S_{ap}]}{dt} = k_{off}^{ADP,104}[Hsp70_{ADP,ADP} : S_{ap} : Hsp104] - [Hsp104 : S_{ap}]k_{disagg} \tag{3.16}$$

$$\frac{d[S_u]}{dt} = k_2^r[S_m] + k_{disagg}[Hsp104 : S_{ap}] + k_{off}^{ATP}[Hsp70_{ATP} : S_u] + k_{off}^{ADP}[Hsp70_{ADP} : S_u] - [S_u](k_1 + k_2 + k_{on}^{ADP}[Hsp70_{ADP}]) \tag{3.17}$$

$$\frac{d[S_m]}{dt} = k_2[S_u] + k_{off}^{ATP}[Hsp70_{ATP} : S_m] - [S_m](k_2^r + k_3 + k_{on}^{ATP}[Hsp70_{ATP}]) \tag{3.18}$$

$$\frac{d[S_f]}{dt} = k_1[S_u] \tag{3.19}$$

$$\frac{d[Hsp70_{ATP} : S_m]}{dt} = k_{on}^{ATP}[S_m][Hsp70_{ATP}] + k_{DT}^{s}[Hsp70_{ADP} : S_m] - [Hsp70_{ATP} : S_m](k_{off}^{ATP} + k_{TD}^{s} + k_h^s) \tag{3.20}$$

$$\frac{d[Hsp70_{ADP} : S_m]}{dt} = (k_{TD}^{s} + k_h^s)[Hsp70_{ATP} : S_m] + k_{deprime}[Hsp70_{ADP} : S_u] - [Hsp70_{ADP} : S_m](k_{DT}^{s} + k_{prime}) \tag{3.21}$$

$$\frac{d[Hsp70_{ADP} : S_u]}{dt} = k_{prime}[Hsp70_{ADP} : S_m] + k_{TD}^{s}[Hsp70_{ATP} : S_u] + k_{on}^{ADP}[Hsp70_{ADP}][S_u] - [Hsp70_{ADP} : S_u](k_{deprime} + k_{DT}^{s} + k_{off}^{ADP}) \tag{3.22}$$

$$\frac{d[Hsp70_{ATP} : S_u]}{dt} = k_{DT}^{s}[Hsp70_{ADP} : S_u] - [Hsp70_{ATP} : S_u](k_{off}^{ATP} + k_{TD}^{s}) \tag{3.23}$$

$$\frac{d[Hsp70_{ATP,ADP} : S_{ap}]}{dt} = 0.1k_{on}^{ATP}[Hsp70_{ATP}][Hsp70_{ADP} : S_{ap}] + 2k_{DT}^{s}[Hsp70_{ADP,ADP} : S_{ap}] - [Hsp70_{ATP,ADP} : S_{ap}](k_{off}^{ATP} + k_{TD}^{s} + k_h^s) \tag{3.24}$$

$$\frac{d[Hsp70_{ADP,ADP} : S_{ap}]}{dt} = (k^s_{TD} + k^s_h)[Hsp70_{ATP,ADP} : S_{ap}]$$
$$+k^{104}_{off}[Hsp70_{ADP,ADP} : S_{ap} : Hsp104] \quad (3.25)$$
$$-[Hsp70_{ADP,ADP} : S_{ap}](2k^s_{DT} + k^{104}_{on}[Hsp104])$$

The parameter values used for the simulation are listed in Table 3.1. Note that the current model lacks spatial information; an extension of this model allowing spatial segregation of aggregated substrates would allow investigating the effect of aggregate shape and/or size on the efficiency of the disaggregation system.

3.6 Supporting information

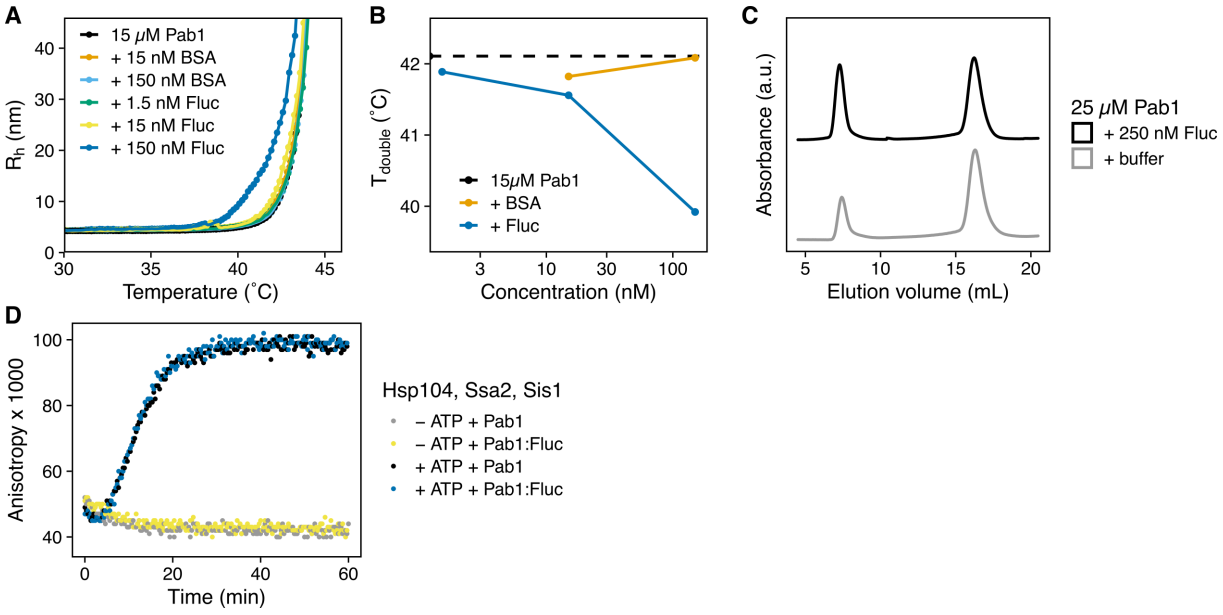

Figure 3.8: Misfolded protein can nucleate Pab1 condensation.
(A) DLS temperature ramp experiment with 15 μM Pab1 in the presence of increasing concentrations of firefly luciferase (Fluc) or BSA. (B) T_{double}, temperature at which the baseline R_h doubles, for the DLS temperature ramp experiment shown in (A) is plotted against the concentrations of the additives (either BSA or luciferase). Dashed line indicates T_{double} for Pab1 in the absence of any additives. (C) Representative SEC trace of Pab1 heat shocked in the absence or presence of 100-fold lower luciferase. Pab1 condensates and monomers elute around 7.5 mL and 16 mL, respectively. (D) Dispersal of Pab1 condensates formed in the presence or absence of 100-fold less luciferase. Condensation in the presence of 100-fold lower luciferase does not affect subsequent condensate dispersal by chaperones.

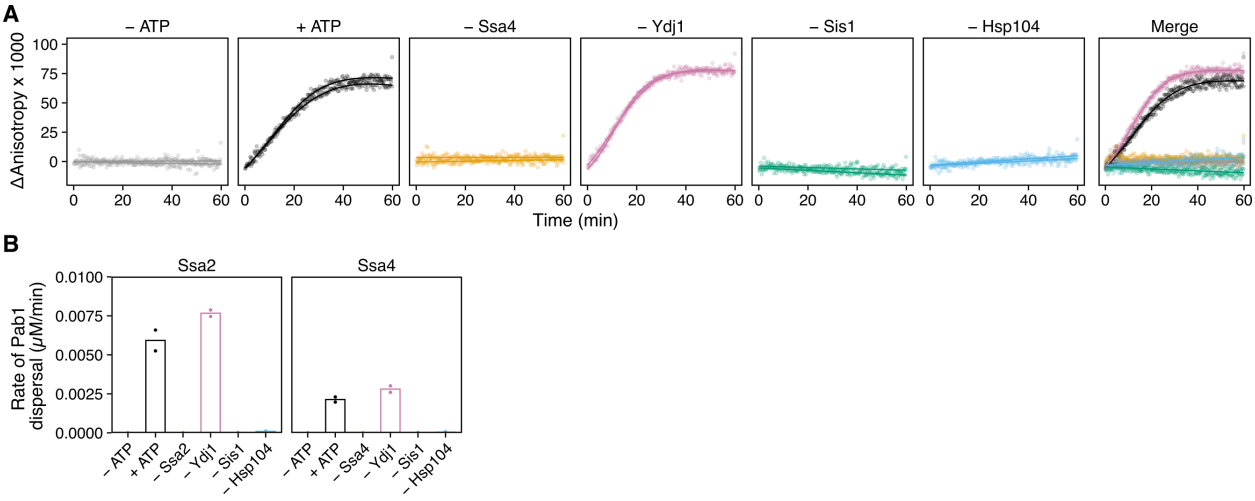

Figure 3.9: Ssa2 can be replaced by its heat-inducible paralog Ssa4 for Pab1 dispersal.

(A) Time-resolved fluorescence anisotropy of A19 in the presence of Pab1 condensates and molecular chaperones. All chaperones shown in Figure 3.2A, except Sse1, were included in the experiments. Ssa4 was added instead of Ssa2. Fitted data points from two independent experiments are shown. Merged data points and a solid line fitted to the average of each experimental condition is shown on the right. (B) Maximal rate of dispersal quantified from the dropout experiments in the absence of Sse1.

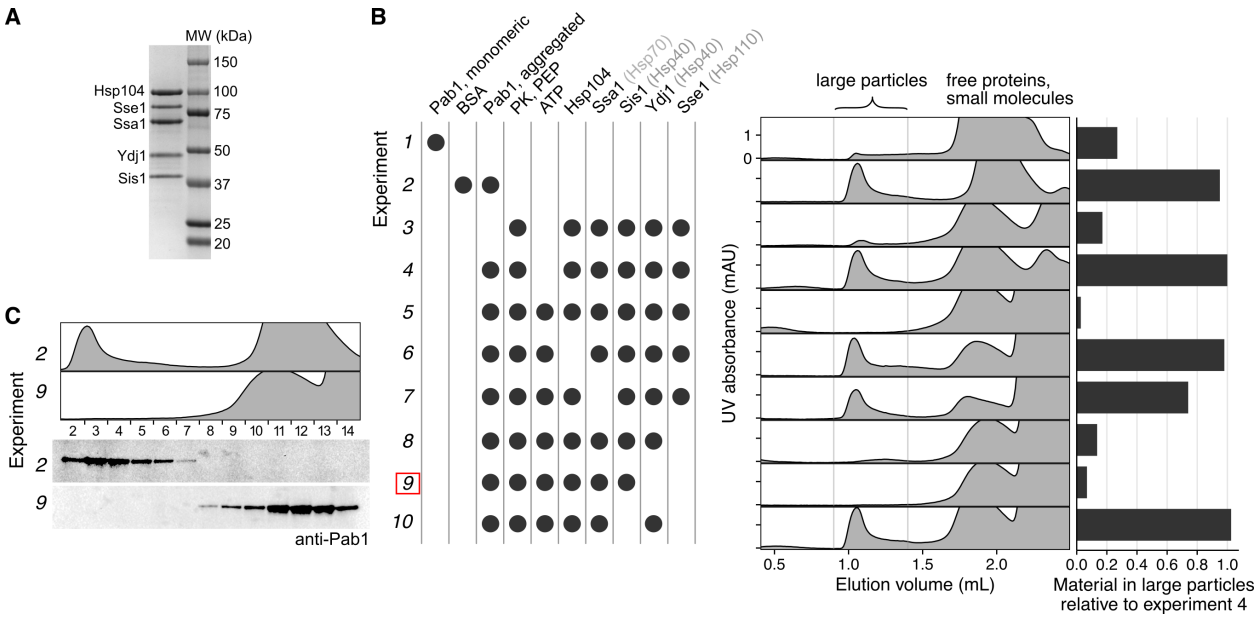

Figure 3.10: Hsp104, Hsp70, and Sis1 are necessary and sufficient for Pab1 dispersal.

(A) Purification of recombinant chaperones. (B) Dropout experiments to determine the components necessary for dispersal of Pab1 condensates. Pab1 dispersal reaction samples were examined by Superose 6 Precision Column. Red box highlights the minimal set composed of Hsp104, Ssa1, and Sis1. PK and PEP stand for pyruvate kinase and phosphoenolpyruvate, respectively. (C) Verification of Pab1 dispersal by western blot.

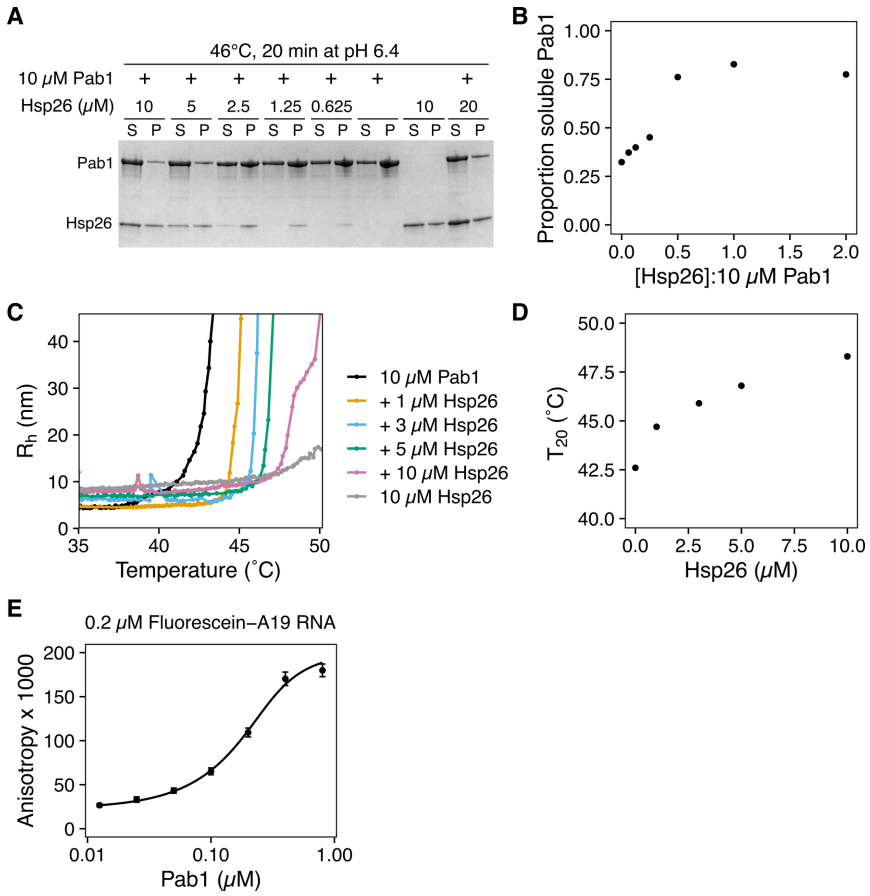

Figure 3.11: Hsp26 suppresses Pab1 condensation.
(A) Sedimentation of Pab1 in the absence or presence of increasing concentrations of Hsp26, visualized by Coomassie staining. (B) Quantification of proportion soluble Pab1 in (A) plotted against the ratio of Hsp26 to Pab1. (C) DLS temperature ramp experiment with 10 μM Pab1 with increasing concentrations of Hsp26 at pH 6.4. Note that the presence of Hsp26, which forms high molecular weight oligomers, shifts the DLS baseline upward. (D) Temperature at which Pab1's hydrodynamic radius crosses 20 nm in (C) is plotted against Hsp26 concentration. (E) A representative calibration curve showing the increasing fluorescence anisotropy of the labeled A19 RNA as a function of increasing concentration of monomeric Pab1. The calibration curve was used convert the y-axis from fluorescence anisotropy to Pab1 concentration and extract the rate of dispersal. The mean and standard deviation of 8 independent calibration data are shown. Data were fitted with equation 3.2.

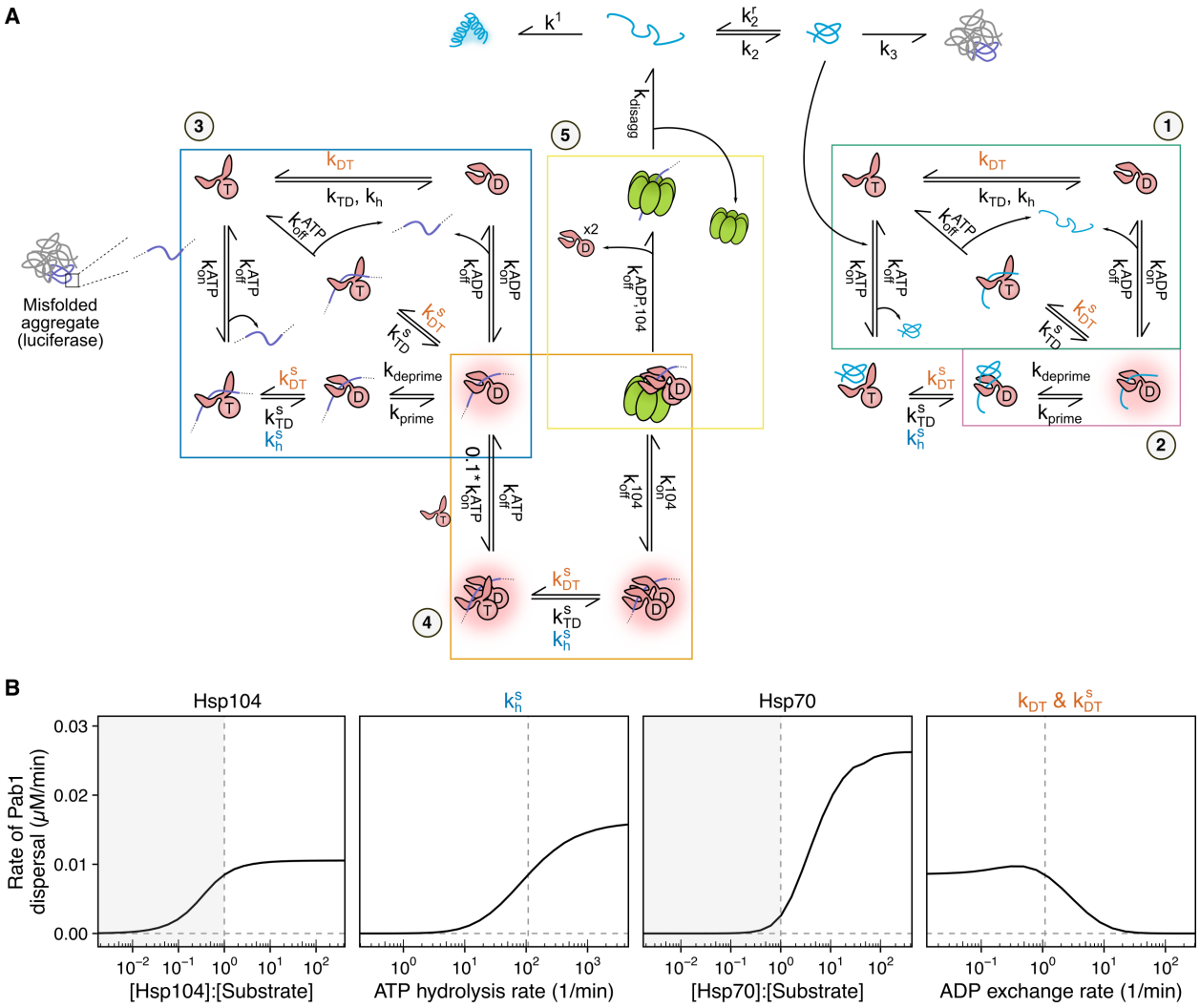

Figure 3.12: Cooperative model.
(A) (1) Biochemical model of ATP hydrolysis-coupled substrate binding and release from Hsp70 [30, 132, 120, 194]. Nucleotide exchange from ADP to ATP facilitates substrate release from Hsp70. (2) Hsp70 binding to a single misfolded protein leads to protein unfolding and expansion [70, 8]. We describe this step a "priming" step, and use pink halo to graphically represent the primed species. (3) Nucleotide state-coupled substrate binding of Hsp70 is assumed to be consistent with aggregated substrates. However, unlike with single misfolded proteins, aggregated proteins do not unfold upon Hsp70 binding and need Hsp104. (4) One Hsp70 molecule is insufficient to activate Hsp104 [159, 21]. Second Hsp70 binds the substrate with an order of magnitude lower affinity than the first Hsp70 due to the entropic penalty [188]. (5) Exact mechanism of substrate handover is unknown, but substrate handover is described as an irreversible step [132]. (B) Simulation of chaperone titration experiments shown in Figure 3.6A. Titration of Sis1 and Sse1 were simulated by varying the ATP hydrolysis rate of substrate-bound Hsp70 (kh_S) and ADP exchange rate (kDT and kDT_S), respectively, from the default level indicated by the dashed line.

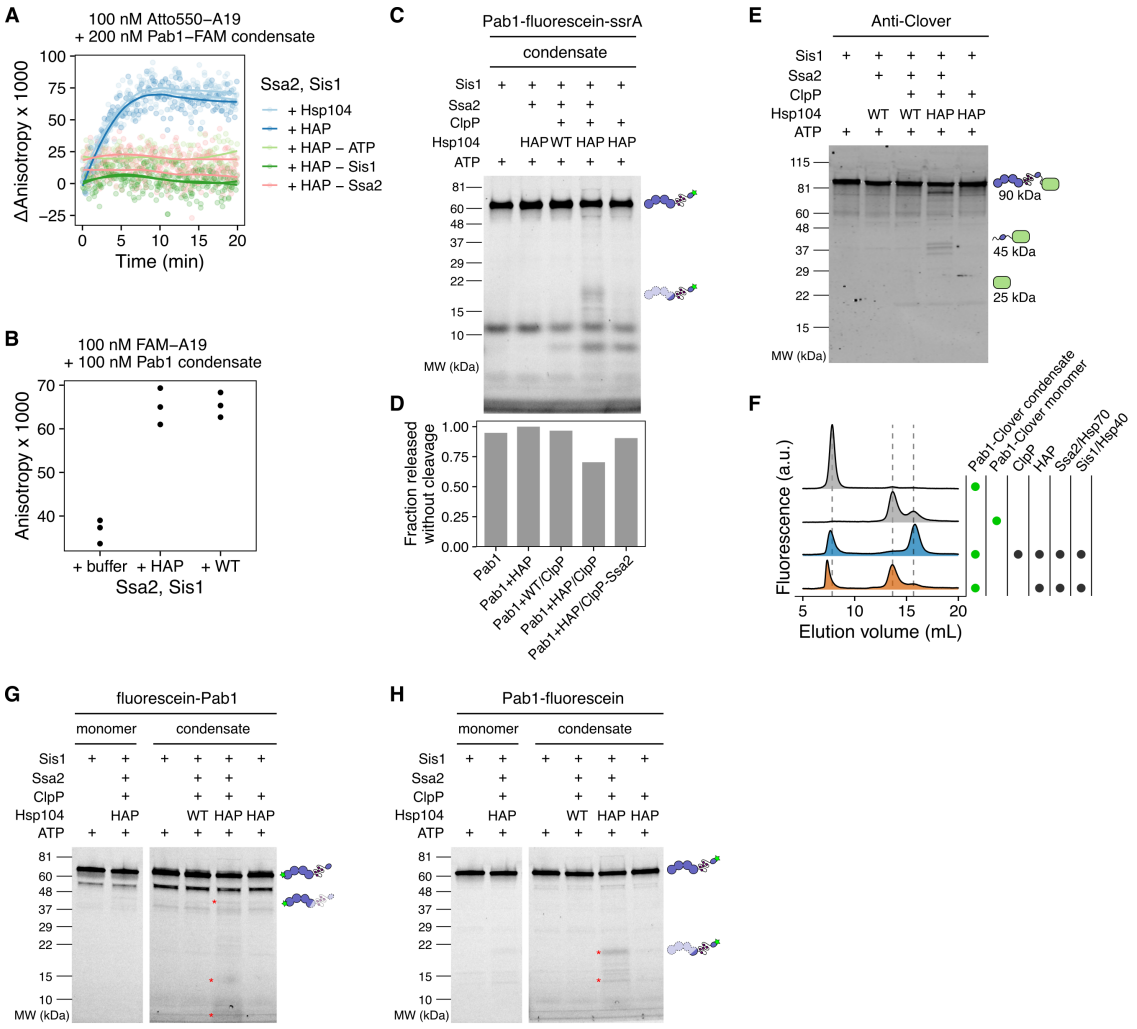

Figure 3.13: HAP/ClpP-specific cleavage of Pab1 constructs.
(A) Condensates of C-terminally fluorescein-labeled Pab1 were dispersed by the indicated components. Fluorescence anisotropy of Atto550-A19 RNA was monitored. (B) End-point measurement of unlabeled Pab1 condensate dispersal. FAM-A19 RNA was added after an hour of reaction incubation to measure fluorescence anisotropy. (C) A replicate of the condensate dispersal experiment shown in Figure 3.5H.(D) Quantification of full-length Pab1 band intensity in (C) normalized to the HAP control signal. The yield of dispersal was assumed to be the same as seen in the Figure 3.5K FSEC experiment. (E) Pab1-Clover condensates were incubated with the indicated components and examined by western blot. Schematics of full-length and truncated products, and their corresponding molecular weight are shown. (F) Pab1-Clover condensate was incubated with the indicated components for an hour and examined by FSEC. Dashed lines indicate the elution volume for Pab1-Clover condensates (7.8 mL), Pab1-Clover monomers (13.7 mL), and HAP/ClpP-specific cleavage products (15.7 mL). (G-H) SDS-PAGE gels of N- or C-terminally labeled Pab1 were visualized by detecting fluorescein fluorescence. Asterisks in indicate HAP/ClpP-specific cleavage products.

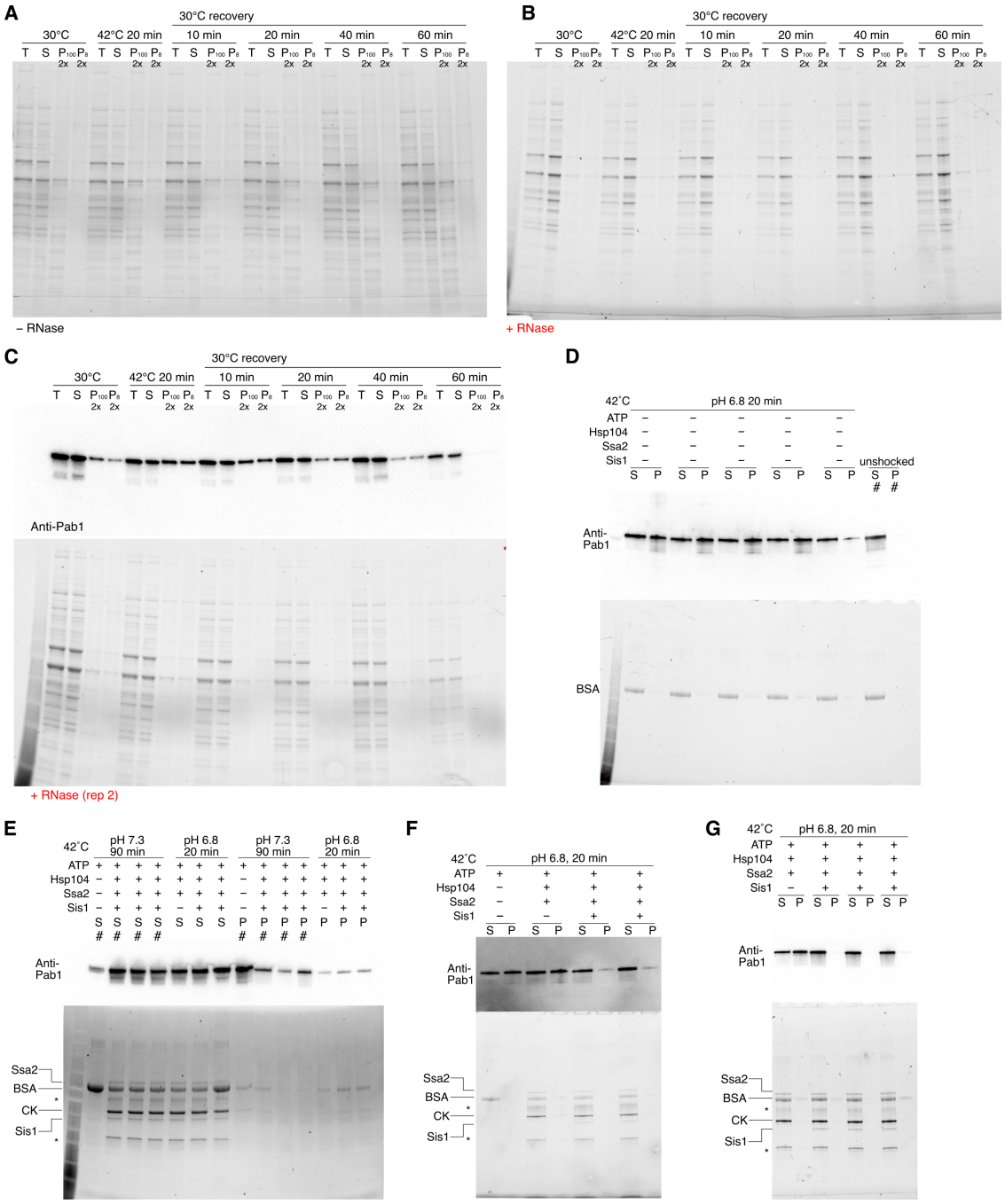

Figure 3.14: Uncropped stain-free total protein gel and western blot images. (A and B) SDS-PAGE gel of RNase treated (A) or untreated (B) yeast lysate samples. The corresponding anti-Pab1 western blot images are shown in (Figure 3.1A). (C) Replicate of (B). (D-G) Western blot (top) and SDS-PAGE images (bottom) of *in vitro* TSP experiments. Cropped images of (G) is shown in (Figure 3.2C). The quantification results are shown in (Figure 3.2D). Lanes marked with # were not quantified. CK stands for creatine kinase. Asterisks indicate unknown contaminant.

Table 3.1: Model parameters.

Name	Value	Unit	Description	Source
k_h	0.036	min^{-1}	ATP hydrolysis rate of free Hsp70	[110]*
k_h^s	108	min^{-1}	ATP hydrolysis rate of substrate-bound Hsp70	[91]*
k_{on}^{ATP}	12		Substrate onrate to $Hsp70_{ATP}$	[153, 52]*
k_{off}^{ATP}	120	min^{-1}	Substrate offrate to $Hsp70_{ATP}$	[153, 52]*
k_{on}^{ADP}	0.06		Substrate onrate to $Hsp70_{ADP}$	[109]*
k_{off}^{ADP}	0.0282	min^{-1}	Substrate offrate to $Hsp70_{ADP}$	[109]*
k_r^{ATP}	0.008	min^{-1}	ATP offrate from $Hsp70_{ATP}$	[146]*
k^{ATP}	7.8		ATP onrate to $Hsp70_{apo}$	[146]*
k_r^{ADP}	1.32	min^{-1}	ADP offrate from $Hsp70_{ADP}$	[175, 146]*
k^{ADP}	16		ADP onrate to $Hsp70_{apo}$	[146]*
k_{TD}, k_{TD}^s	0.0014	min^{-1}	Nucleotide exchange rate from ATP to ADP in free or substrate-bound Hsp70	Calculated as described in [30]
k_{DT}, k_{DT}^s	1.0951	min^{-1}	Nucleotide exchange rate from ADP to ATP in free or substrate-bound Hsp70	Calculated as described in [30]
k_{on}^{104}	30		Hsp104 onrate to $Hsp70_{ADP}$:substrate complex	Estimated from the K_d reported in [142]
k_{off}^{104}	60	min^{-1}	Hsp104 offrate from $Hsp70_{ADP}$:substrate:Hsp104 complex	Estimated from the K_d reported in [142]
$k_{off}^{ADP,104}$	100	min^{-1}	$Hsp70_{ADP}$ offrate after substrate handover to Hsp104	Free parameter
k_{disagg}	0.2	min^{-1}	Disaggregation rate	Estimated from the measurement in this study
k_{prime}	10	min^{-1}	Substrate remodeling rate	Free parameter
$k_{deprime}$	1	min^{-1}	Reverse substrate remodeling rate	Free parameter
k_1	10, 0.001	min^{-1}	Rate of transition from the unfolded Pab1/luciferase to the folded state	Free parameter
k_2	1	min^{-1}	Rate of transition from the unfolded state to the misfolded state	Free parameter
k_2^r	0.1	min^{-1}	Rate of transition from the misfolded state to the unfolded state	Free parameter
k_3	1	min^{-1}	Rate of transition from the misfolded state to the aggregated state	Free parameter

*Curated by Rios *et al.* [30].

Table 3.2: Reaction conditions for experiments shown in Chapter 3.

Panel	Reaction mixture*
1d	25 μM Pab1
1e	0.2 μM FAM-A19, 0.2 μM Pab1 monomers or condensates, 5 mM ATP
2a, 2b	0.1 μM FAM-A19, 0.1 μM Pab1, 1 μM Ssa2, 0.1 μM Hsp104, 0.5 μM Sis1, 0.5 μM Ydj1, 50 nM Sse1, ATP mix
2c	0.1 μM FAM-A19, 0.1 μM Pab1, 1 μM Ssa2, 0.02 μM Hsp104, 0.5 μM Sis1, ATP mix
2e	0.2 μM Pab1-Clover, 1 μM Ssa2, 0.5 μM Sis1, 0.1 μM Hsp104, 0.5 μM A90 RNA, ATP mix
3a	0.2 μM Fluc, 1 μM Ssa2, 0.1 μM Hsp104, 0.5 μM Hsp40, ATP mix
3b	20 nM Fluc, 0.75 μM Ssa2, 0.75 μM Hsp104, 0.25 μM Hsp40, 38 nM Sse1, ATP mix
3c, 3d	0.2 μM FAM-A19, 0.2 μM Pab1, 0.5 μM Ssa2, 50 nM Hsp104, 0.25 μM Sis1 (plus 0, 0.25, 0.5, 1, or 2 μM additional Sis1 or Ydj1), ATP mix
3f	0.2 μM FAM-A19 (for Pab1), 0.2 μM Pab1 or luciferase, 1 μM Ssa2, 0.1 μM Hsp104, 0.5 μM Sis1, ATP mix
5b	20 nM Fluc, 0.75 μM Ssa2, 0.75 μM Hsp104, 0.125 μM Sis1, 0.125 μM Ydj1, 0.1 μM GroEL trap, 38 nM Sse1, ATP mix
5c	0.2 μM FAM-A19, 0.2 μM Pab1, 1 μM Ssa2, 0.2 μM Hsp104, 0.5 μM Sis1, 1 μM GroEL trap, ATP mix
5d	0.1 μM FAM-A19, 0.1 μM Pab1, 1 μM GroEL trap
5f, 5g	10 nM Fluc, 1 μM Ssa2, 0.25 μM Sis1, 0.25 μM Ydj1, 1 μM Hsp104/HAP, ATP mix
5h, 5k	0.2 μM Pab1-fluorescein-ssrA, 2 μM Ssa2, 0.5 μM Sis1, 1 μM HAP, 1.5 μM ClpP, ATP mix; For ClpXP: 0.2 μM nM Pab1-fluorescein-ssrA, 0.1 μM ClpX, 1 μM ClpP
6a, 6g	Default: 0.2 μM FAM-A19, 0.2 μM Pab1, 0.5 μM Ssa2, 0.2 μM Hsp104, 0.5 μM Sis1, 0.1 μM Sse1, ATP mix
6e	0.2 μM FAM-A19, 0.14 μM Pab1, varying Ssa2, 0.02 μM Hsp104, 0.5 μM Sis1, ATP mix
S1a	15 μM Pab1 + BSA or Fluc as indicated
S1c	25 μM Pab1 + Fluc as indicated
S1d	0.1 μM FAM-A19, 0.1 μM Pab1, 0.5 μM Ssa2, 0.05 μM Hsp104, 0.1 μM Sis1, ATP mix
S2a	0.1 μM FAM-A19, 0.1 μM Pab1, 1 μM Ssa4, 0.1 μM Hsp104, 0.5 μM Sis1, 0.5 μM Ydj1, ATP mix
S3b	0.5 μM Pab1, 1.2 μM Ssa1, 0.2 μM Hsp104, 0.3 μM Sse1, 0.3 μM Ydj1, 0.3 μM Sis1, 3 mM PEP, 10 units/mL PK, 2 mM ATP
S4a	10 μM Pab1 + Hsp26 as indicated
S4c	10 μM Pab1 + Hsp26 as indicated
S4e	0.2 μM FAM-A19 + Pab1 monomer as indicated
S6c	0.1 μM Pab1-fluorescein-ssrA, 2 μM Ssa2, 0.5 μM Sis1, 1 μM Hsp104/HAP, 1.5 μM ClpP, ATP mix
S6e, S6f	0.2 μM Pab1-Clover, 1.5 μM ClpP, 1 μM Hsp104/HAP, 0.5 μM Sis1, 2 μM Ssa2, ATP mix
S6g, S6h	0.2 μM fluorescein-Pab1 or Pab1-fluorescein, 1.5 μM ClpP, 1 μM Hsp104/HAP, 0.5 μM Sis1, 2 μM Ssa2, ATP mix

*Concentrations of Hsp104/HAP, Hsp40, and GroEL indicate the concentrations for the hexamers, dimers, and 14-mers, respectively; ATP mix includes 1 μM CK, 8 mM CP, 5 mM ATP.

3.7 Competing Interests

The authors declare no competing interests.

3.8 Author contributions

HY, EP, and DAD designed fluorescence anisotropy-based Pab1 dispersal assay. HY designed and performed *in vivo* Pab1 sedimentation experiments. EP and DAD designed SEC- and sedimentation-based Pab1 dispersal assays. HY, EP, and DAD designed Pab1 condensate isolation protocol. HY, JAMB, and EP purified proteins. HY performed Pab1 dispersal assays using sedimentation, fluorescence anisotropy, and FSEC. EP designed and performed SEC-based dropout experiments. HY and DAD designed experiments with luciferase and HY performed the experiments. HY designed and performed experiments with Hsp26. HY and JAMB designed and performed experiments with HAP/ClpP/ClpX and analyzed the data together. HY analyzed the rest of the experimental data. HY collected and analyzed the literature data. HY constructed the kinetic model and performed simulation. HY wrote the first draft of the manuscript. HY and DAD edited the manuscript with the assistance and approval of all authors.

3.9 Acknowledgements

We thank the members of the Drummond lab, Tobin Sosnick, and Ruofan Chen for helpful discussions and comments on the manuscript. We also thank Zachary March for providing the original protocol for Hsp70 purification, Axel Mogk for providing the plasmid for GroEL trap, Andreas Martin for providing the plasmids for ClpX and ClpP, David Pincus and Michael Rust for their feedback on modeling, the Perozo lab for providing the FSEC instrument, and Elena Solomaha at the Biophysics Core for assistance with DLS experiments. Research reported in this publication was supported by the National Institute of General Medical Sciences and the National Institute of Environmental Health Sciences of the National Institutes of

Health (NIH) through awards to HY (award numbers T32GM007183 and F31ES030697). JAMB acknowledges fellowship support from the Helen Hay Whitney Foundation. DAD acknowledges support from the NIH (award numbers R01GM126547 and R01GM127406) and from the US Army Research Office (award number W911NF-14-1-0411). The content is solely the responsibility of the authors and does not necessarily represent the official views of the NIH.

CHAPTER 4

PRELIMINARY RESULTS

This chapter includes unpublished preliminary results.

4.1 Less efficient dispersal of larger condensates

The phase boundary of biomolecular condensates is often dependent on temperature and pH [196]. For Pab1, condensation is promoted at higher temperature and/or lower pH [138]. Interestingly, the size and morphology of Pab1 condensates formed under different temperature and pH are different (Figure 4.1A). For example, Pab1 forms many smaller condensates that are attached together like grapes when condensation is triggered by heat shock. But when condensation is triggered by a drop in pH at around room temperature, Pab1 forms much larger and spherical condensates. Pab1 condensates formed under a more physiological condition (42°C, pH 6.8) in Chapter 3 are big enough to sediment but too small to be imaged using a conventional confocal microscope or make the buffer turbid (Figure 4.1B) [176, 195]. What is the relationship between the size of condensates and the efficiency of condensate dispersal by chaperones? If condensate size is an important factor affecting dispersal efficiency, what kind of molecular mechanism would allow cells to control condensate size?

Intuitively, smaller Pab1 condensates have greater surface area to volume ratio and therefore will be dispersed much more efficiently by chaperones. To test this hypothesis, I prepared Pab1 condensates of different sizes by triggering condensation under different temperature and pH conditions. Condensates were isolated from monomers either by size exclusion chromatography (SEC) or sedimentation followed by resuspension. Smaller condensates formed at 42°C at pH 6.8 were resolubilized after a two-hour incubation in the presence of Hsp104, Ssa2/Hsp70, and Sis1/Hsp40 (Figure 4.1C and 4.1D). However, larger condensates formed at higher temperature and/or lower pH remained insoluble after incubation with chaperones.

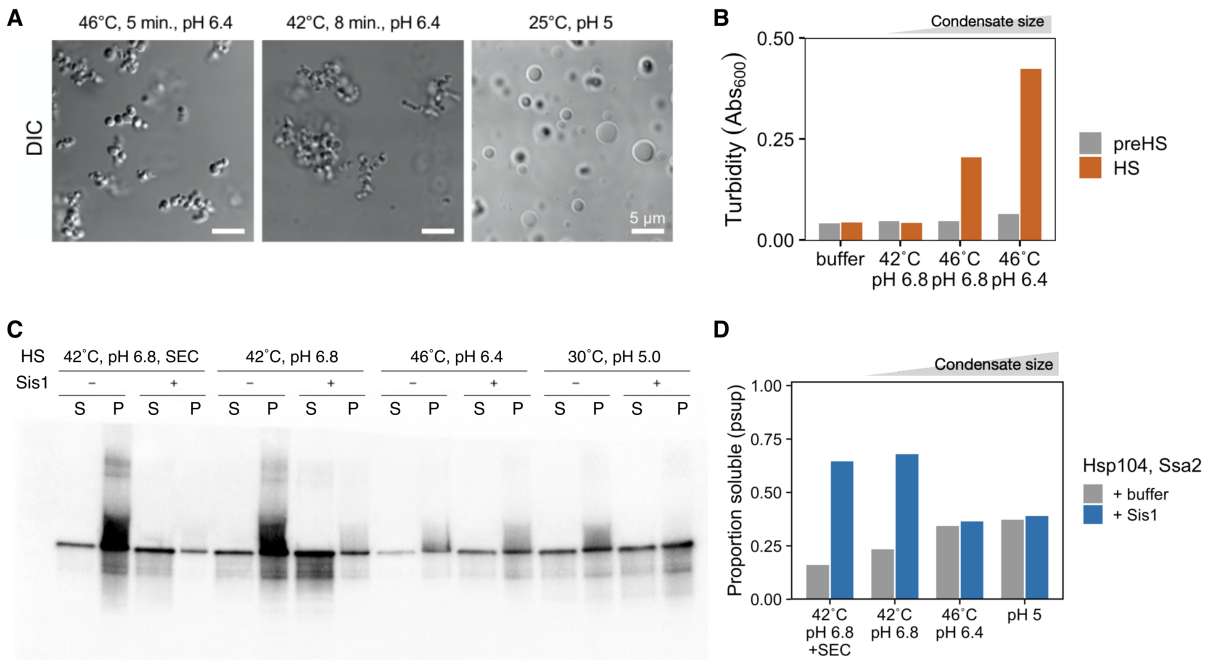

Figure 4.1: Less efficient dispersal of larger condensates.
(A) DIC images of Pab1-mRuby2 formed under different conditions, adapted from [138]. (B) Unlabeled wildtype Pab1 was treated as specified for 20 minutes and the absorbance of the sample was measured at 600 nm. Highter temperatnre and lower pH cause higher turbidity. (C) Pab1 condensates formed under the specified condition were incubated with the disaggregation system (0.1 μM Pab1, 01 μM Ssa2, 0.1 μM Hsp104, 0.5 μM Sis1) for 2 hours at 30°C, centrifuged at 100k g for 20 minutes, and analyzed by western blot to measure chaperone-dependent solubilization. Sis1 was omitted in negative controls. SEC denotes samples which have gone through size exclusion column. (D) Quantification of the western blot shown in (C). Pab1 condensates formed under higher temperature and lower pH are refractory to chaperones.

This preliminary result suggests condensates formed under different conditions are treated differently by the disaggregation system. A similar observation was reported for G6PDH aggregates: both the rate and yield of disaggregation decrease as the aggregate size increases [33]. Whether an increase in aggregate/condensate size accompanies change in the underlying structure or burial of chaperone binding sites, as proposed by [33], is unclear. Further research is required to investigate the molecular and/or physical differences between the condensates formed under different conditions, address why larger condensates are refractory to dispersal, and whether/how condensate size is controlled in cell.

4.2 Co-evolution of chaperones with their endogenous substrates

We explored the hypothesis that the molecular disaggregation system and its endogenous substrates co-evolved to maintain high dispersal efficiency. This can be tested by challenging diverse disaggregation systems with heat-induced condensates of conspecific or cross-species Pab1 variants. Through a collaboration with James Shorter's group at the University of Pennsylvania, we obtained recombinantly expressed and purified Hsp104 from six distinct species: *Chlamydomonas reinhardtii* (Cr), *Monosiga brevicollis* (Mb), *Calcarisporiella thermophila* (Ct), *Saccharomyces cerevisiae* (Sc), *Thermomyces lanuginosus* (Tl), and *Thielavia terrestris* (Tt) (Figure 4.2). The optimal growth temperatures ranged from around 25°C for Mb to 45°C for Ct, Tl, and Tt (Table 4.1).

For preliminary investigation, I dispersed ScPab1 condensates using ScHsp70 (either Ssa1 or Ssa2), ScHsp40 (Sis1), and Hsp104 from Sc or different source organisms. Dispersal was tracked by monitoring fluorescence anisotropy of labeled A19 RNA. Systems with Hsp104 from Ct, Sc, Tl, and Tt showed comparable initial rate of dispersal (Figure 4.3A). Hsp104 from Cr and Mb caused more than 50% decrease in the dispersal rate (Figure 4.3A). A positive linear correlation (r = 0.73) was observed between the mean dispersal rate and the optimal growth temperature of the source organism (Figure 4.3B).

At first glance, the data seem to suggest that Hsp104 from a source organism whose optimal growth temperature is lower than 30°C disperses ScPab1 condensates less efficiently than conspecific Hsp104. This is not clear, however, because the two species with lower

Table 4.1: Hsp104 source organism and the initial rate of Pab1 dispersal.

Source organism	**Initial rate of dispersal (1/min)**	**Optimal growth temperature (°C)**
Cr	0.05	26 [193]
Mb	0.08	25 [83]
Ct	0.18	45 [115]
Sc	0.16	30 [152]
Tl	0.18	45 [102]
Tt	0.19	45 [15]

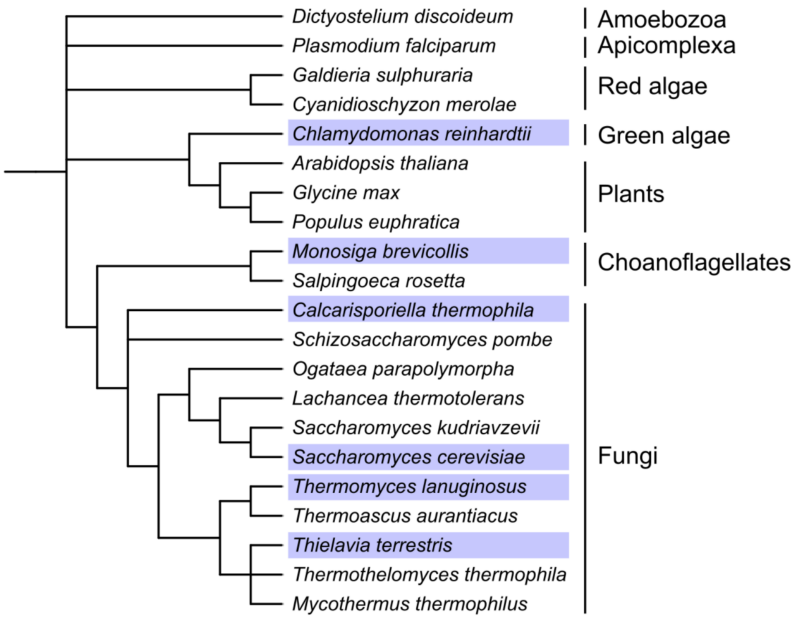

Figure 4.2: Species tree highlighting Hsp104 source organisms.
Hsp104 was purified from the highlighted organisms. The species tree was generated using phyloT (`http://phylot.biobyte.de/`) and visualized using iTOL (`http://itol.embl.de/`).

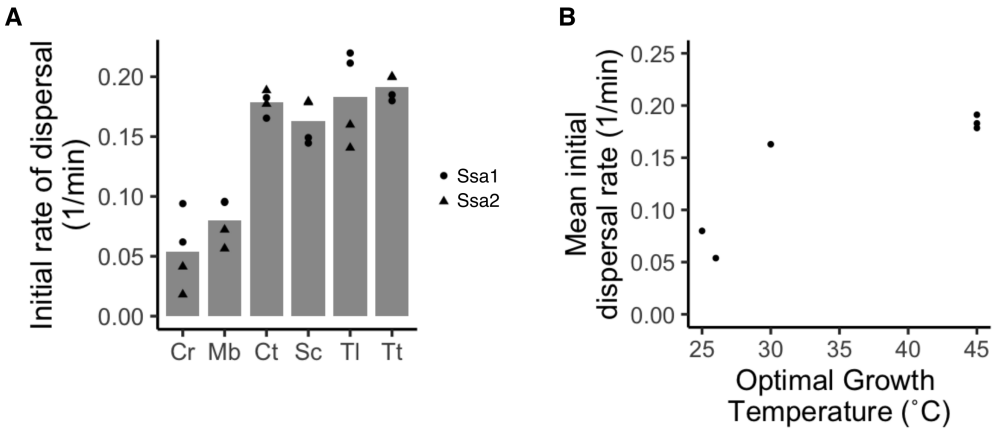

Figure 4.3: Relationship between the optimal growth temperature and the initial rate of Pab1 dispersal.
(A) Initial rate of *S. cerevisiae* Pab1 condensate dispersal quantified from fluorescence anisotropy assay. Hsp104 of the specified source organism was added to Pab1 condensates, Sis1, and Hsp70 (either Ssa1 or Ssa2) to initiate dispersal. The following concentrations of proteins were used: 0.2 μM Pab1, 0.2 μM labeled A19 RNA, 1 μM Hsp70, 0.1 μM Hsp104, and 0.5 μM Sis1. (B) The average initial rate of Pab1 condensate dispersal quantified in (A) was plotted against the optimal growth temperature of the Hsp104 source organism.

optimal growth temperatures are the species most distantly related to Sc (Figure 4.2). It is possible that larger sequence difference between chaperones from Sc and more distantly related species made cross-species Hsp104-Hsp70 interaction less compatible. Further investigation using a complete conspecific disaggregation system (e.g., MbHsp104 with MbHsp70 and MbHsp40), a stand-alone variant of Hsp104, or diverse Pab1 will help determine co-evolution of chaperones with endogenous substrates.

4.3 Measuring the effect of Sis1/DnaJ on Hsp70's affinity to CE2 peptide

Hsp40 uses its substrate binding domain and conserved J-domain to increase Hsp70's substrate specificity and affinity, respectively [80]. Sis1, a type II Hsp40, promotes Hsp70 binding to heat shock factor 1 (Hsf1), the master regulator of the HSR [42, 4]. The Hsp70 binding site on Hsf1 is known as conserved element 2 (CE2) [86] (Figure 4.4A). To biochemically recapitulate Sis1's effect on Hsp70 affinity toward Hsf1, I measured Hsp70's affinity to labeled CE2 peptides in the absence or presence of Sis1 using fluorescence polarization (Figure 4.4B-E and Table 4.2). I also repeated the experiment with bacterial Hsp70/DnaK and Hsp40/DnaJ (Figure 4.4F and 4.4G).

The result was unexpected; Sis1 interfered with Ssa2 binding to CE2 peptide. The same pattern was observed with DnaK and DnaJ. This is probably due to the artefact of using short peptides instead of full-length Hsf1. A full-length substrate is likely to have separate and/or multiple binding sites Hsp40 and Hsp70, allowing simultaneous binding. Sis1 may be competing with Hsp70 for the single binding site on the CE2 peptide. Purified full-length Hsf1 or tandem repeats of CE2 will be required to set up a better *in vitro* system for Sis1.

Detailed method: Fluorescence polarization was monitored using TECAN Spark microplate reader. Increasing concentration of Ssa2/DnaK or Sis1/DnaJ was added to 0.1 μM fluorescein-labeled CE2 peptide (5-FAM-KQRYLLKNRANS) in buffer (20 mM HEPES pH

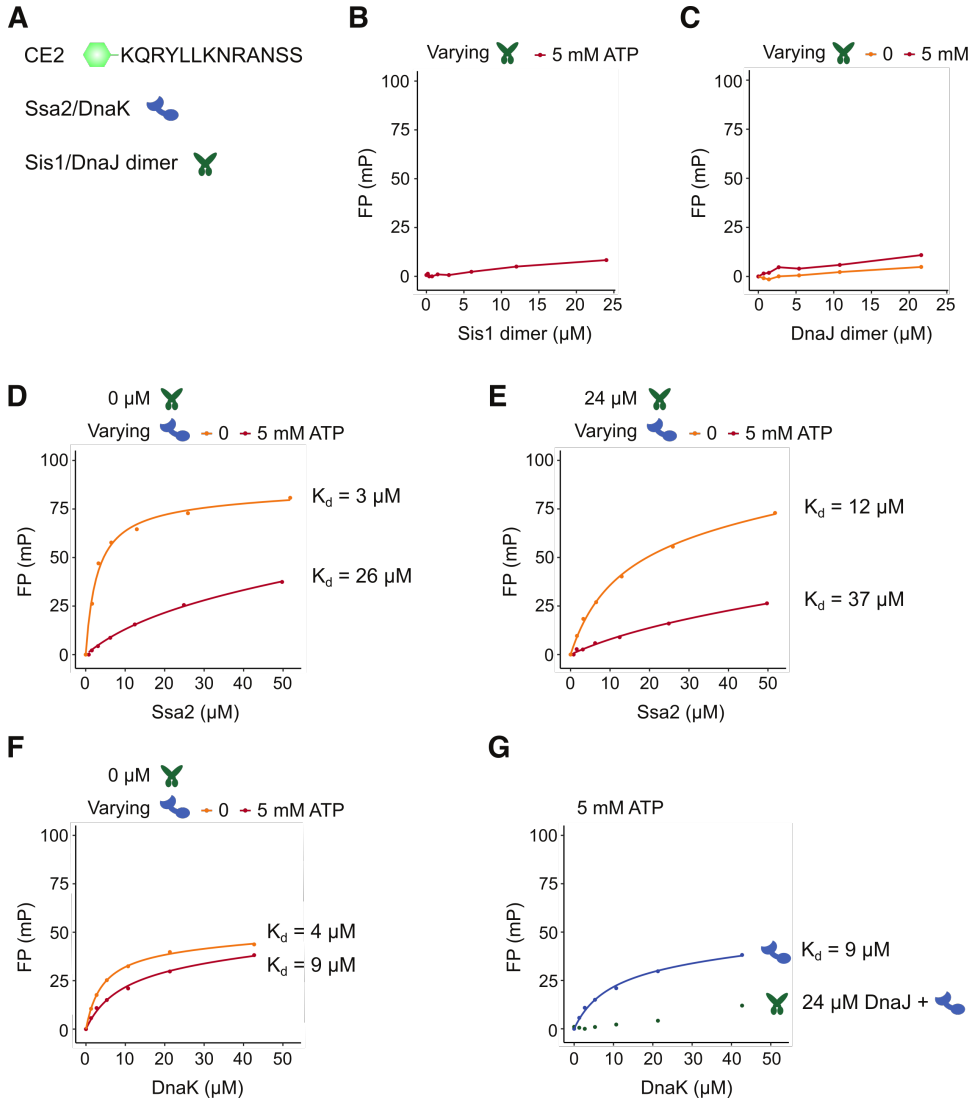

Figure 4.4: Excess Sis1 interferes with Ssa2 binding to CE2 peptide.
(A) Fluorescently labeled CE2 peptide with the shown sequence was used at 0.1 μM concentration and its fluorescence polarization was monitored. (B and C) Sis1/DnaJ does not bind the CE2 peptide. (D) Ssa2 binds CE2 peptide with about 3 μM affinity in the absence of ATP in the buffer. The affinity decreases significantly in the presence of 5 mM ATP. (E) In the presence of excess Sis1, Ssa2 affinity decreases regardless of ATP concentration. (F) DnaK binds the peptide with similar affinity as Ssa2 in the absence of ATP. The affinity decreases by about 2-fold in the presence of ATP. (G) Excess DnaJ interferes with DnaK binding to CE2 peptide. The DnaK-only data in (F) and (G) are identical data plotted in different colors for clarity.

7.4, 150 mM KCl, 2.5 mM MgCl2, 0.01 % Triton X-100, 1 mM DTT) containing either no or 5 mM ATP. After 1 hour equilibration at room temperature, fluorescence polarization was measured every minute for 60 minutes. The signal stayed steady throughout this

post-equilibration measurement. The average data were plotted and fitted to the following quadratic equation with fitting parameters K_d and g:

$$y = \frac{\max(y)}{[CE2]}\left(\frac{([CE2] + x + K_d) - \sqrt{([CE2] + x + K_d)^2 - 4([CE2] + x)}}{2}\right) + (xg) \qquad (4.1)$$

Table 4.2: CE2 peptide binding affinity and g values.

Condition	**Apparent K_d rounded to the nearest integer (μM)**	**g**
Ssa2 - ATP	3	0.06
Ssa2 + ATP	26	0.26
Ssa2 + Sis1 - ATP	12	0.25
Ssa2 + Sis1 + ATP	37	0.22
DnaK - ATP	4	0.10
DnaK + ATP	9	0.15

4.4 Efficient refolding of fully denatured Pab1

Pab1 readily refolds from completely denatured state to RNA-binding competent form upon dilution into refolding buffer with no urea (Figure 3.5D). To assess whether denatured Pab1 refolds into its native structure or some other RNA-binding competent, but nonnative structure, I compared circular dichroism (CD) of native versus refolded Pab1 (Figure 4.5A-C). Wavelength scan at room temperature showed a smooth signal between 215 nm and 240 nm for both native and refolded Pab1 (Figure 4.5B). To assess any difference in protein structure or stability between native and refolded Pab1, each protein's CD at 217 nm was monitored over a temperature range between 20°C and 70°C (Figure 4.5C). The traces from the native and refolded Pab1 showed a similar shape. The melting temperature (Tm) for refolded Pab1 was higher than that of native Pab1 by about 0.8°C (Table 4.5). This suggests two possibilities: 1) a local domain of the refolded Pab1 misfolded during refolding, leading to higher Tm for the refolded Pab1, or 2) a small population of Pab1 failed to refold into the native state and misfolded. The small difference in Tm indicates that Pab1 is able to efficiently refold into the native state most of the time in the absence of any auxiliary factors

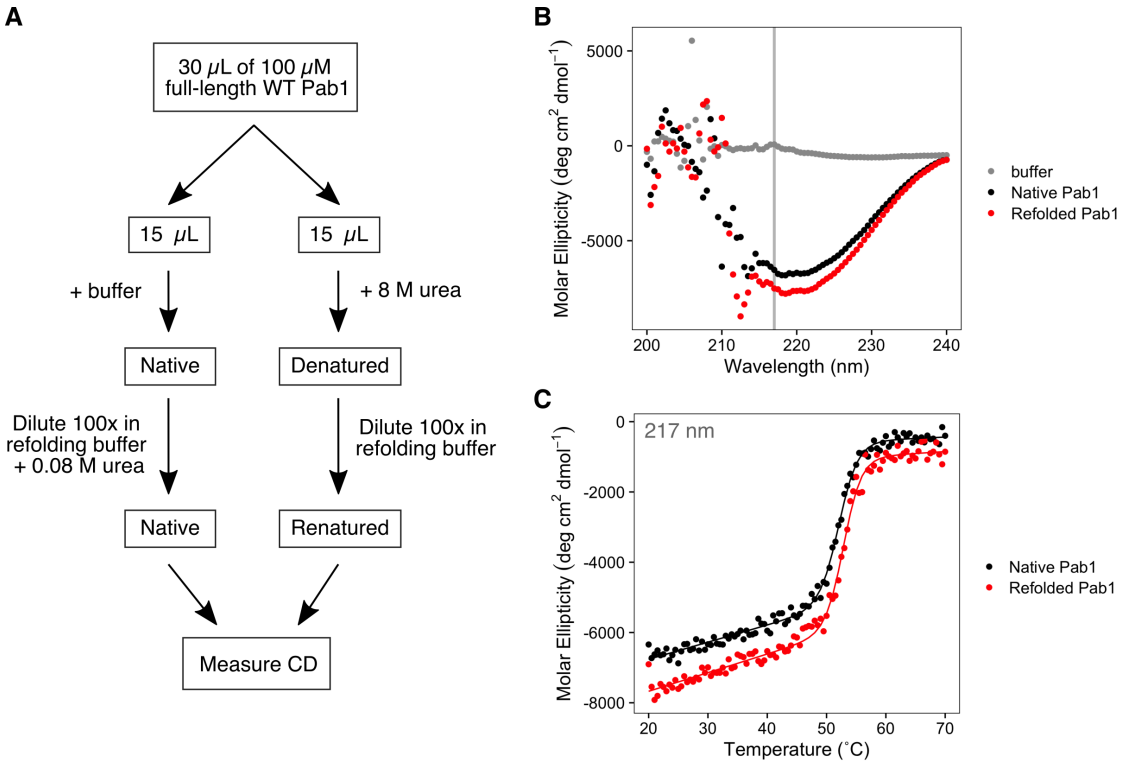

Figure 4.5: Efficient refolding of fully denatured Pab1.
(A) General workflow. The same setting and buffer condition were used for CD measurement as described in [138]. (B) Wavelength scan for native and refolded Pab1. (C) Temperature scan at 217 nm for native and refolded Pab1. The data are fitted to a two-state model with sloping baselines to extract melting temperature using R (Table 4.3).

Table 4.3: Melting temperature (Tm) of native and refolded Pab1

Pab1	Tm (°C)	Standard error
Native	52.15	0.07
Refolded	52.94	0.09

such as chaperones. Whether this efficient folding is a characteristic specific to Pab1, or an evolved trait commonly shared by all condensing endogenous proteins, remains to be determined.

4.5 Pab1 releases RNA upon condensation

Excess RNA was shown to inhibit Pab1 condensation in a previous study [138], suggesting that the same interface may be used for RNA binding and condensation for Pab1. To track

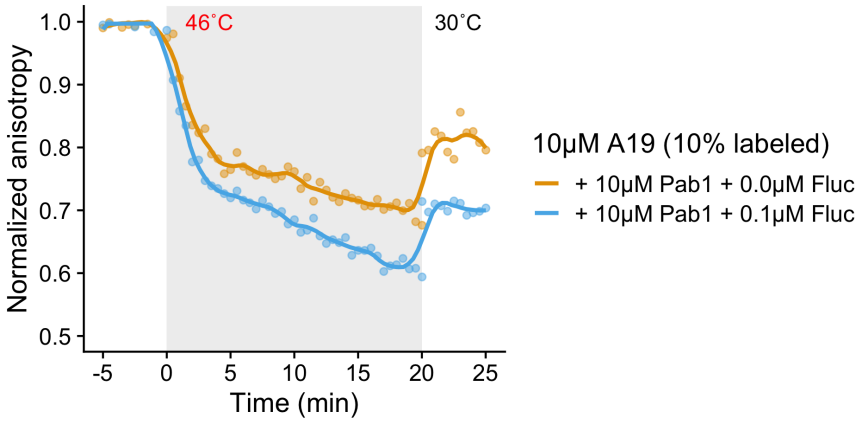

Figure 4.6: Pab1 releases RNA upon condensation.
Fluorescence anisotropy of labeled A19 RNA was monitored before, during, and after a 20 minute, 46°C treatment in the presence of Pab1. Data were collected using HORIBA Fluorolog-3 at the Biophysics Core Facility.

the fate of Pab1-bound poly(A) RNA during Pab1 condensation, I monitored fluorescence anisotropy of labeled 19-mer poly(A) RNA (A19) in the presence of Pab1 before, during, and after a 20 minute heat treatment at 46°C (Figure 4.6). The total concentration of RNA matched that of Pab1. Normalization to the pre-treatment anisotropy level showed a reduction in the anisotropy value after heat treatment, suggesting RNA release during Pab1 condensation. The magnitude of the drop was greater in the presence of a thermolabile protein firefly luciferase, which is consistent with the previous observation that misfolded protein nucleates Pab1 condensation [195] (Figure 3.8).

4.6 Artifactual co-localization of Pab1 condensates with DNA in the absence of competitors

I previously showed that Pab1 releases RNA upon condensation (Figure 4.6). However, I also noticed that when pre-assembled Pab1 condensates are added to labeled RNA, the baseline anisotropy increases slightly (Figure 3.1E). I hypothesized that this increase in anisotropy results from RNA interacting with the surface of Pab1 condensates.

To test whether poly(A) RNA associates with the surface of Pab1 condensates, I turned

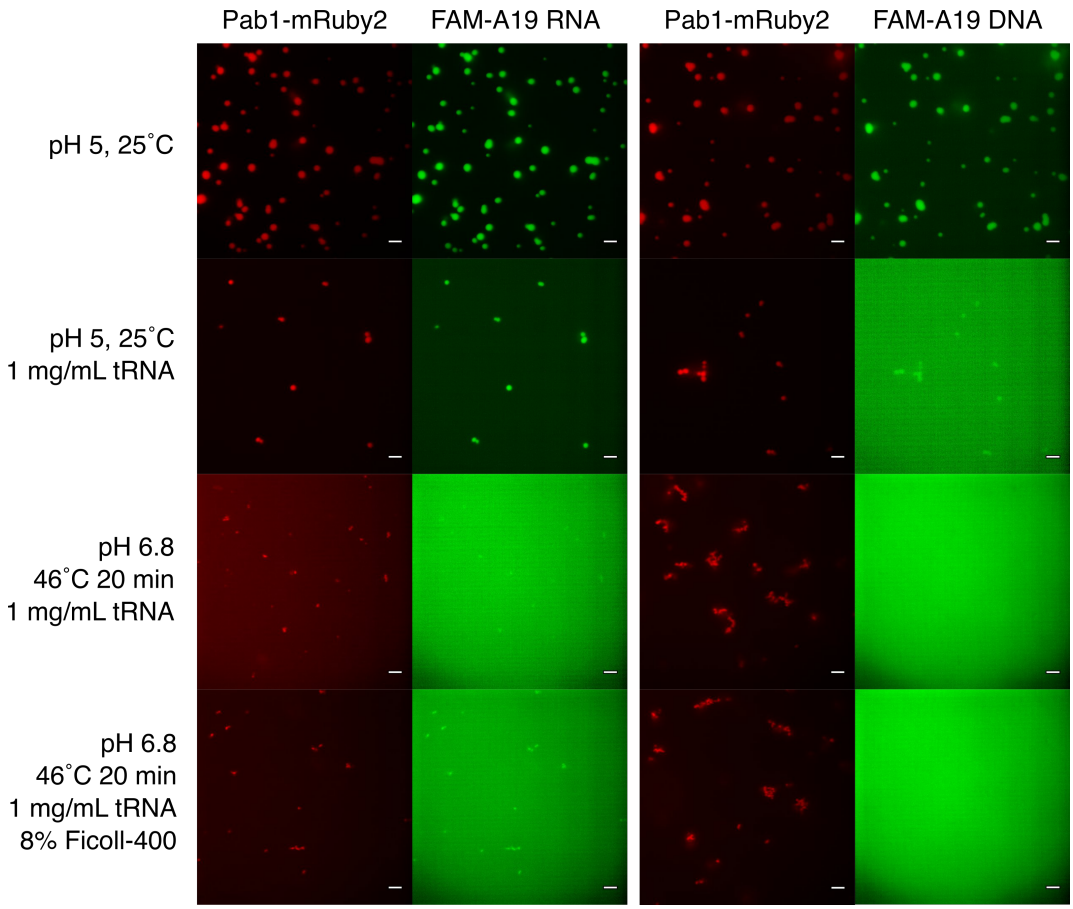

Figure 4.7: Artifactual co-localization of Pab1 condensates with DNA in the absence of competitors.
Co-localization of Pab1-mRuby2 with either fluorescein-labeled 19-mer poly(A) RNA (left) or DNA (right), in the absence or presence of 1 mg/mL tRNA as nonspecific competitors. Condensation of 10 μM Pab1 in the presence of 5 μM RNA was triggered either by pH or heat shock. Higher temperature and Ficoll were used to induce more complete Pab1 condensation, with minimal residual monomeric Pab1 in the background. The scale bar is 5 μm.

to use fluorescence microscopy. Fluorescence microscopy is a common method used in the field to assess co-condensation. As a negative control, I used poly(A) DNA to which Pab1 does not bind. Condensation of Pab1-mRuby2 in the presence of either RNA or DNA showed localization of both nucleic acids to Pab1 condensates (Figure 4.7). Co-localization of poly(A) DNA with Pab1 condensates indicated that observed co-localization is due to nonspecific interaction. When co-condensation was repeated in the presence of 1 mg/mL tRNA as a competitor, poly(A) DNA no longer co-localized to Pab1 condensates. Poly(A) RNA still showed substantial localization of pH-induced Pab1 condensates and weaker, but visible

localization to heat-induced Pab1 condensates. Whether the higher co-localization of poly(A) RNA with pH-induced Pab1 condensates is due to the larger size or higher permeability of pH-induced condensates compared to heat-induced condensates is unknown. Even with heat-induced Pab1 condensates, it was impossible to determine whether poly(A) RNA is associating with the surface of condensates. A higher resolution microscopy in the presence of excess RNA competitor, and perhaps with lower amount of labeled RNA, will help better determine how poly(A) RNA is interacting with Pab1 condensates.

The co-condensation of poly(A) DNA with Pab1 condensates in the absence of nonspecific competitor provides a cautionary example of how a poorly designed microscopy experiment can lead to a wrong conclusion. A proper negative control should always be used in experiments to prevent making a false conclusion based on nonspecific interactions.

CHAPTER 5

CONCLUSIONS AND FUTURE DIRECTIONS

This thesis opened with a review on adaptive function of environmentally induced biomolecular condensation, then explored the function of molecular chaperones as efficient dispersers of biomolecular condensates. The knowledge gained from this thesis—that chaperones can directly disperse stress-induced condensates, that stress-induced condensates are endogenous chaperone substrates, and the resolution of a long-standing puzzle in the chaperone field—exemplify how research at the interface between the burgeoning field of biomolecular condensates and the mature field of molecular chaperones can benefit both fields. In this concluding chapter, I describe some of the open questions and future directions for both fields.

5.1 Regulation of biomolecular condensates

How do chaperones affect the onset of biomolecular condensation in cells? A two-dimensional phase boundary is commonly used to describe a protein's temperature-, pH, and/or concentration-dependent *in vitro* condensation behavior [68, 196]. However, the phase boundary of a protein is likely to be affected by multiple interacting biomolecules or ligands in the highly concentrated and heterocompositional cellular environment. A heterotypic interaction-dependent modulation of the phase boundary has been proposed as the molecular basis of the directional flux of rRNA out of the nucleolus [139]. More recently, a simulation-based study showed that binding of a ligand can either stabilize or destabilize condensation of the scaffold protein depending on the valency and the binding location of the ligand [144]. In Chapter 3, Hsp26 was shown to suppress condensation of Pab1 in a concentration dependent manner [195] (Figure 3.9A-D). Whether the chaperone binding sites generally overlap with those involved in condensation, and how the change in the chaperone availability due to environmental stress, adaptation, or disease progression affects condensation of key proteins and the ensuing

biological consequences are major open questions.

The functional importance of the material state of condensates remains to be determined, but chaperones can prevent liquid-to-solid transition of a human RNA binding protein Fused in Sarcoma (FUS) [97, 17]. In mammalian cells, the exogenously expressed misfolded protein partitions into either stress granules or nucleolus and slows the internal dynamics of the respective organelle [108, 47]. Chaperone recruitment alleviates this liquid-to-solid transition. The molecular events leading to the transition from adaptive to aberrant condensates and the role of chaperones in preventing such aberrant transition are the topics of large interest in the fields of cellular stress, protein aggregation, and aging [3].

What regulates chaperone-dependent dispersal of stress-induced endogenous condensates? Is it simply the availability of chaperones, or is there a preceding molecular event which must "license" condensates for chaperone-dependent dispersal? In yeast, heat shock triggers pyruvate kinase Cdc19 to form reversible amyloids which localize to stress granules [24]. Dissolution of Cdc19 is required for Pab1 and other constituents of stress granules to be dispersed. Interestingly, Cdc19 amyloids cannot recruit and get disassembled by the Hsp104/70/40 disaggregation system unless the glycolytic metabolite fructose-1,6-bisphosphate (FBP) induces a conformational change in Cdc19 amyloids [24]. This illustrates two important regulatory mechanisms of condensate regulation in cell: 1) the hierarchical dispersal of different proteins from condensates and 2) coupling of chaperone-dependent condensate dispersal to other cellular processes such as metabolism. Biochemical reconstitution of the dispersal system using multiple different condensates or heterogeneous condensates, and measurement of the relative dispersal kinetics will help identify the hierarchical relationship between different substrates. Many metabolic enzymes in eukaryotes and prokaryotes have been previously shown to form either filamentous or spherical condensates in response to stress [131, 118, 12, 100, 5, 147, 128]. Future research identifying which of these structures require chaperones for facilitated dispersal, whether small molecules like metabolites affect their engagement with chaperones, and if so what conformational change is induced to recruit

chaperones will benefit both fundamental and translational research involving biomolecular condensates.

5.2 Regulation and specificity of molecular chaperones

Studying molecular chaperones in the presence of their endogenous substrates may help address some of the long-standing open questions in the chaperone field. One big question is how the multitude of post-translational modification (PTM) sites on chaperones are used to regulate chaperone activity and specificity [123]. For example, in budding yeast, stress-triggered phosphorylation of the site T36 on Hsp70 has shown to displace Ydj1 [178]. This suggests that the disaggregation system will preferentially target substrates with Sis1 binding sites during stress. Competition experiments using multiple endogenous substrates and phosphomimetic mutants of Hsp70 will reveal how a single or a combination of PTMs can shape the specificity of the disaggregation system. This can be combined with *in vivo* experiments to determine how the kinetics of the PTM addition and/or removal correlate with the dispersal of specific substrates.

Future research on more endogenous chaperone substrates and the PTM effect on chaperone specificity may also help us understand why eukaryotic cells often express multiple isoforms of Hsp70 [78]. Yeast has four cytosolic Hsp70 paralogs, two of which are constitutively expressed (Ssa1/2) while the others are induced upon stress (Ssa3/4). Human cells have six cytosolic Hsp70 isoforms, which are expressed in varying patterns in different tissues and developmental stages [78]. The functional specificity of these isoforms has been difficult to assess biochemically because no clear isoform-specific activity or specificity is known. A recent study in human cells showed that chemical stress triggers acetylation of stress-inducible Hsp70 and renders that Hsp70 to associate with co-chaperones to promote protein refolding [158]. As the stress persists, Hsp70 is gradually deacetylated and the deacetylated Hsp70 associates with a different co-chaperone to switch Hsp70 function from protein refolding to protein degradation [158]. Interestingly, this acetylation site is conserved across eukaryotes

in stress-inducible Hsp70 but not in constitutively-expressed Hsp70 [158]. Future work on whether and how cells utilize Hsp70 isoform-specific PTM to target misfolded aggregates or aberrant condensates for degradation will provide much insight about the chaperone system.

References

[1] Nadra Al-Husini, Dylan T Tomares, Obaidah Bitar, W Seth Childers, and Jared M Schrader. α-Proteobacterial RNA degradosomes assemble Liquid-Liquid Phase-Separated RNP bodies. *Mol. Cell*, 71(6):1027–1039.e14, September 2018.

[2] Simon Alberti, Randal Halfmann, Oliver King, Atul Kapila, and Susan Lindquist. A systematic survey identifies prions and illuminates sequence features of prionogenic proteins. *Cell*, 137(1):146–158, April 2009.

[3] Simon Alberti and Anthony A Hyman. Biomolecular condensates at the nexus of cellular stress, protein aggregation disease and ageing. *Nat. Rev. Mol. Cell Biol.*, 22(3):196–213, March 2021.

[4] Brian D Alford, Eduardo Tassoni-Tsuchida, Danish Khan, Jeremy J Work, Gregory Valiant, and Onn Brandman. ReporterSeq reveals genome-wide dynamic modulators of the heat shock response across diverse stressors. *Elife*, 10, July 2021.

[5] Sajitha A Anthony, Anika L Burrell, Matthew C Johnson, Krisna C Duong-Ly, Yin-Ming Kuo, Jacqueline C Simonet, Peter Michener, Andrew Andrews, Justin M Kollman, and Jeffrey R Peterson. Reconstituted IMPDH polymers accommodate both catalytically active and inactive conformations. *Mol. Biol. Cell*, August 2017.

[6] J P Aris and G Blobel. Identification and characterization of a yeast nucleolar protein that is similar to a rat liver nucleolar protein. *J. Cell Biol.*, 107(1):17–31, July 1988.

[7] M P Ashe, S K De Long, and A B Sachs. Glucose depletion rapidly inhibits translation initiation in yeast. *Mol. Biol. Cell*, 11(3):833–848, March 2000.

[8] Salvatore Assenza, Alberto Stefano Sassi, Ruth Kellner, Benjamin Schuler, Paolo De Los Rios, and Alessandro Barducci. Efficient conversion of chemical energy into mechanical work by hsp70 chaperones. *Elife*, 8, December 2019.

[9] Mario J Avellaneda, Kamila B Franke, Vanda Sunderlikova, Bernd Bukau, Axel Mogk, and Sander J Tans. Processive extrusion of polypeptide loops by a hsp100 disaggregase. *Nature*, 578(7794):317–320, February 2020.

[10] R Baler, W J Welch, and R Voellmy. Heat shock gene regulation by nascent polypeptides and denatured proteins: hsp70 as a potential autoregulatory factor. *J. Cell Biol.*, 117(6):1151–1159, June 1992.

[11] Salman F Banani, Hyun O Lee, Anthony A Hyman, and Michael K Rosen. Biomolecular condensates: organizers of cellular biochemistry. *Nat. Rev. Mol. Cell Biol.*, 18(5):285–298, May 2017.

[12] Rachael M Barry, Anne-Florence Bitbol, Alexander Lorestani, Emeric J Charles, Chris H Habrian, Jesse M Hansen, Hsin-Jung Li, Enoch P Baldwin, Ned S Wingreen, Justin M Kollman, and Zemer Gitai. Large-scale filament formation inhibits the activity of CTP synthetase. *Elife*, 3:e03638, July 2014.

[13] Kyle Begovich and James E. Wilhelm. An inÂ vitro assembly system identifies roles for rna nucleation and atp in yeast stress granule formation. *Molecular Cell*, 2020.

[14] Anat Ben-Zvi, Paolo De Los Rios, Giovanni Dietler, and Pierre Goloubinoff. Active solubilization and refolding of stable protein aggregates by cooperative unfolding action of individual hsp70 chaperones. *J. Biol. Chem.*, 279(36):37298–37303, September 2004.

[15] Randy M Berka, Igor V Grigoriev, Robert Otillar, Asaf Salamov, Jane Grimwood, Ian Reid, Nadeeza Ishmael, Tricia John, Corinne Darmond, Marie-Claude Moisan, Bernard Henrissat, Pedro M Coutinho, Vincent Lombard, Donald O Natvig, Erika Lindquist, Jeremy Schmutz, Susan Lucas, Paul Harris, Justin Powlowski, Annie Bellemare, David Taylor, Gregory Butler, Ronald P de Vries, Iris E Allijn, Joost van den Brink, Sophia Ushinsky, Reginald Storms, Amy J Powell, Ian T Paulsen, Liam D H Elbourne, Scott E Baker, Jon Magnuson, Sylvie Laboissiere, A John Clutterbuck, Diego Martinez, Mark Wogulis, Alfredo Lopez de Leon, Michael W Rey, and Adrian Tsang. Comparative genomic analysis of the thermophilic biomass-degrading fungi myceliophthora thermophila and thielavia terrestris. *Nat. Biotechnol.*, 29(10):922–927, October 2011.

[16] Anders Blomberg. Metabolic surprises insaccharomyces cerevisiaeduring adaptation to saline conditions: questions, some answers and a model, 2000.

[17] Edgar E Boczek, Julius Fürsch, Louise Jawerth, Marcus Jahnel, Marie Laura Niedermeier, Martine Ruer-Gruß, Kai-Michael Kammer, Laura Mediani, Jie Wang, Xiao Yan, Andrej Pozniakovski, Ina Poser, Daniel Mateju, Serena Carra, Simon Alberti, Anthony A Hyman, and Florian Stengel. HspB8 prevents aberrant phase transitions of FUS by chaperoning its folded RNA binding domain. April 2021.

[18] Jill J Bouchard, Joel H Otero, Daniel C Scott, Elzbieta Szulc, Erik W Martin, Nafiseh Sabri, Daniele Granata, Melissa R Marzahn, Kresten Lindorff-Larsen, Xavier Salvatella, Brenda A Schulman, and Tanja Mittag. Cancer mutations of the tumor suppressor SPOP disrupt the formation of active, Phase-Separated compartments. *Mol. Cell*, September 2018.

[19] Clifford P Brangwynne, Timothy J Mitchison, and Anthony A Hyman. Active liquid-like behavior of nucleoli determines their size and shape in xenopus laevis oocytes. *Proc. Natl. Acad. Sci. U. S. A.*, 108(11):4334–4339, March 2011.

[20] Stefan Bresson, Vadim Shchepachev, Christos Spanos, Tomasz Turowski, Juri Rappsilber, and David Tollervey. Stress-induced translation inhibition through rapid displacement of scanning initiation factors. May 2020.

[21] Marta Carroni, Eva Kummer, Yuki Oguchi, Petra Wendler, Daniel K Clare, Irmgard Sinning, Jürgen Kopp, Axel Mogk, Bernd Bukau, and Helen R Saibil. Head-to-tail interactions of the coiled-coil domains regulate ClpB activity and cooperation with hsp70 in protein disaggregation. *Elife*, 3:e02481, April 2014.

[22] Anil G Cashikar, Martin Duennwald, and Susan L Lindquist. A chaperone pathway in protein disaggregation. hsp26 alters the nature of protein aggregates to facilitate reactivation by hsp104. *J. Biol. Chem.*, 280(25):23869–23875, June 2005.

[23] Fabrice Caudron and Yves Barral. A super-assembly of whi3 encodes memory of deceptive encounters by single cells during yeast courtship. *Cell*, 155(6):1244–1257, December 2013.

[24] Gea Cereghetti, Caroline Wilson-Zbinden, Vera Kissling, Maren Diether, Alexandra Arm, Haneul Yoo, Ilaria Piazza, Shady Saad, Paola Picotti, David Drummond, and Others. Reversible amyloids of pyruvate kinase couple cell metabolism and stress granule disassembly. 2021.

[25] Lynne Chantranupong, Rachel L Wolfson, and David M Sabatini. Nutrient-sensing mechanisms across evolution. *Cell*, 161(1):67–83, March 2015.

[26] Valeria Cherkasov, Tomas Grousl, Patrick Theer, Yevhen Vainshtein, Christine Glässer, Cyril Mongis, Günter Kramer, Georg Stoecklin, Michael Knop, Axel Mogk, and Bernd Bukau. Systemic control of protein synthesis through sequestration of translation and ribosome biogenesis factors during severe heat stress. *FEBS Lett.*, 589(23):3654–3664, November 2015.

[27] Valeria Cherkasov, Sarah Hofmann, Silke Druffel-Augustin, Axel Mogk, Jens Tyedmers, Georg Stoecklin, and Bernd Bukau. Coordination of translational control and protein homeostasis during severe heat stress. *Curr. Biol.*, 23(24):2452–2462, December 2013.

[28] D Crews, J M Bergeron, J J Bull, D Flores, A Tousignant, J K Skipper, and T Wibbels. Temperature-dependent sex determination in reptiles: proximate mechanisms, ultimate outcomes, and practical applications. *Dev. Genet.*, 15(3):297–312, 1994.

[29] Gábor Csárdi, Alexander Franks, David S Choi, Edoardo M Airoldi, and D Allan Drummond. Accounting for experimental noise reveals that mRNA levels, amplified by post-transcriptional processes, largely determine steady-state protein levels in yeast. *PLoS Genet.*, 11(5):e1005206, May 2015.

[30] Paolo De Los Rios and Alessandro Barducci. Hsp70 chaperones are non-equilibrium machines that achieve ultra-affinity by energy consumption. *Elife*, 3:e02218, May 2014.

[31] M Delarue, G P Brittingham, S Pfeffer, I V Surovtsev, S Pinglay, K J Kennedy, M Schaffer, J I Gutierrez, D Sang, G Poterewicz, J K Chung, J M Plitzko, J T Groves, C Jacobs-Wagner, B D Engel, and L J Holt. mTORC1 controls phase separation and the biophysical properties of the cytoplasm by tuning crowding. *Cell*, 174(2):338–349.e20, July 2018.

[32] Morgan E DeSantis, Eunice H Leung, Elizabeth A Sweeny, Meredith E Jackrel, Mimi Cushman-Nick, Alexandra Neuhaus-Follini, Shilpa Vashist, Matthew A Sochor, M Noelle Knight, and James Shorter. Operational plasticity enables hsp104 to disaggregate diverse amyloid and nonamyloid clients. *Cell*, 151(4):778–793, November 2012.

[33] S Diamant, A P Ben-Zvi, B Bukau, and P Goloubinoff. Size-dependent disaggregation of stable protein aggregates by the DnaK chaperone machinery. *J. Biol. Chem.*, 275(28):21107–21113, July 2000.

[34] Shannon M Doyle, Shankar Shastry, Andrea N Kravats, Yu-Hsuan Shih, Marika Miot, Joel R Hoskins, George Stan, and Sue Wickner. Interplay between e. coli DnaK, ClpB and GrpE during protein disaggregation. *J. Mol. Biol.*, 427(2):312–327, January 2015.

[35] Mingjian Du and Zhijian J Chen. DNA-induced liquid phase condensation of cGAS activates innate immune signaling. *Science*, 361(6403):704–709, August 2018.

[36] Zhiqiang Du, Ying Zhang, and Liming Li. The yeast prion [SWI(+)] abolishes multicellular growth by triggering conformational changes of multiple regulators required for flocculin gene expression. *Cell Rep.*, 13(12):2865–2878, December 2015.

[37] Martin L Duennwald, Analisa Echeverria, and James Shorter. Small heat shock proteins potentiate amyloid dissolution by protein disaggregases from yeast and humans. *PLoS Biol.*, 10(6):e1001346, June 2012.

[38] André C Dumetz, Aaron M Chockla, Eric W Kaler, and Abraham M Lenhoff. Protein phase behavior in aqueous solutions: Crystallization, Liquid-Liquid phase separation, gels, and aggregates, 2008.

[39] Albert J Erives and Jan S Fassler. Metabolic and chaperone gene loss marks the origin of animals: Evidence for hsp104 and hsp78 chaperones sharing mitochondrial enzymes as clients. *PLoS One*, 10(2):e0117192, February 2015.

[40] N G Farny, N L Kedersha, and P A Silver. Metazoan stress granule assembly is mediated by P-eIF2 -dependent and -independent mechanisms, 2009.

[41] Ofrah Faust, Meital Abayev-Avraham, Anne S Wentink, Michael Maurer, Nadinath B Nillegoda, Nir London, Bernd Bukau, and Rina Rosenzweig. HSP40 proteins use class-specific regulation to drive HSP70 functional diversity. *Nature*, 587(7834):489–494, November 2020.

[42] Zoë A Feder, Asif Ali, Abhyudai Singh, Joanna Krakowiak, Xu Zheng, Vytas P Bindokas, Donald Wolfgeher, Stephen J Kron, and David Pincus. Subcellular localization of the j-protein sis1 regulates the heat shock response. *J. Cell Biol.*, 220(1), January 2021.

[43] Marina Feric, Nilesh Vaidya, Tyler S Harmon, Diana M Mitrea, Lian Zhu, Tiffany M Richardson, Richard W Kriwacki, Rohit V Pappu, and Clifford P Brangwynne. Coexisting liquid phases underlie nucleolar subcompartments. *Cell*, 165(7):1686–1697, June 2016.

[44] P A Fields. Review: Protein function at thermal extremes: balancing stability and flexibility. *Comp. Biochem. Physiol. A Mol. Integr. Physiol.*, 129(2-3):417–431, June 2001.

[45] Titus M Franzmann, Marcus Jahnel, Andrei Pozniakovsky, Julia Mahamid, Alex S Holehouse, Elisabeth Nüske, Doris Richter, Wolfgang Baumeister, Stephan W Grill, Rohit V Pappu, Anthony A Hyman, and Simon Alberti. Phase separation of a yeast prion protein promotes cellular fitness. *Science*, 359(6371), January 2018.

[46] Elizabeth S Freeman Rosenzweig, Bin Xu, Luis Kuhn Cuellar, Antonio Martinez-Sanchez, Miroslava Schaffer, Mike Strauss, Heather N Cartwright, Pierre Ronceray, Jürgen M Plitzko, Friedrich Förster, Ned S Wingreen, Benjamin D Engel, Luke C M Mackinder, and Martin C Jonikas. The eukaryotic CO2-Concentrating organelle is liquid-like and exhibits dynamic reorganization. *Cell*, 171(1):148–162.e19, September 2017.

[47] F Frottin, F Schueder, S Tiwary, R Gupta, R Körner, T Schlichthaerle, J Cox, R Jungmann, F U Hartl, and M S Hipp. The nucleolus functions as a phase-separated protein quality control compartment. *Science*, 365(6451):342–347, July 2019.

[48] Xuechao Gao, Marta Carroni, Carmen Nussbaum-Krammer, Axel Mogk, Nadinath B Nillegoda, Anna Szlachcic, D Lys Guilbride, Helen R Saibil, Matthias P Mayer, and Bernd Bukau. Human hsp70 disaggregase reverses Parkinson's-Linked α-Synuclein amyloid fibrils. *Mol. Cell*, 59(5):781–793, September 2015.

[49] David M Garcia, David Dietrich, Jon Clardy, and Daniel F Jarosz. A common bacterial metabolite elicits prion-based bypass of glucose repression. *Elife*, 5, November 2016.

[50] Stephanie N Gates, Adam L Yokom, Jiabei Lin, Meredith E Jackrel, Alexandrea N Rizo, Nathan M Kendsersky, Courtney E Buell, Elizabeth A Sweeny, Korrie L Mack, Edward Chuang, Mariana P Torrente, Min Su, James Shorter, and Daniel R Southworth. Ratchet-like polypeptide translocation mechanism of the AAA+ disaggregase hsp104. *Science*, 357(6348):273–279, July 2017.

[51] Kerry A Geiler-Samerotte, Michael F Dion, Bogdan A Budnik, Stephanie M Wang, Daniel L Hartl, and D Allan Drummond. Misfolded proteins impose a dosage-dependent fitness cost and trigger a cytosolic unfolded protein response in yeast. *Proc. Natl. Acad. Sci. U. S. A.*, 108(2):680–685, January 2011.

[52] S M Gisler, E V Pierpaoli, and P Christen. Catapult mechanism renders the chaperone action of hsp70 unidirectional. *J. Mol. Biol.*, 279(4):833–840, June 1998.

[53] J R Glover and S Lindquist. Hsp104, hsp70, and hsp40: a novel chaperone system that rescues previously aggregated proteins. *Cell*, 94(1):73–82, July 1998.

[54] John R Glover, Anthony S Kowal, Eric C Schirmer, Maria M Patino, Jia-Jia Liu, and Susan Lindquist. Self-Seeded fibers formed by sup35, the protein determinant of [PSI], a heritable prion-like factor of s. cerevisiae, 1997.

[55] P Goloubinoff, A Mogk, A P Zvi, T Tomoyasu, and B Bukau. Sequential mechanism of solubilization and refolding of stable protein aggregates by a bichaperone network. *Proc. Natl. Acad. Sci. U. S. A.*, 96(24):13732–13737, November 1999.

[56] Pierre Goloubinoff, Alberto S Sassi, Bruno Fauvet, Alessandro Barducci, and Paolo De Los Rios. Chaperones convert the energy from ATP into the nonequilibrium stabilization of native proteins. *Nat. Chem. Biol.*, 14(4):388–395, April 2018.

[57] Jordina Guillén-Boixet, Andrii Kopach, Alex S Holehouse, Sina Wittmann, Marcus Jahnel, Raimund Schlüßler, Kyoohyun Kim, Irmela R E A Trussina, Jie Wang, Daniel Mateju, Ina Poser, Shovamayee Maharana, Martine Ruer-Gruß, Doris Richter, Xiaojie Zhang, Young-Tae Chang, Jochen Guck, Alf Honigmann, Julia Mahamid, Anthony A Hyman, Rohit V Pappu, Simon Alberti, and Titus M Franzmann. RNA-Induced conformational switching and clustering of G3BP drive stress granule assembly by condensation. *Cell*, 181(2):346–361.e17, April 2020.

[58] Carla P Guimaraes, Martin D Witte, Christopher S Theile, Gunes Bozkurt, Lenka Kundrat, Annet E M Blom, and Hidde L Ploegh. Site-specific c-terminal and internal loop labeling of proteins using sortase-mediated reactions. *Nat. Protoc.*, 8(9):1787–1799, August 2013.

[59] Lin Guo, Hong Joo Kim, Hejia Wang, John Monaghan, Fernande Freyermuth, Julie C Sung, Kevin O'Donovan, Charlotte M Fare, Zamia Diaz, Nikita Singh, Zi Chao Zhang, Maura Coughlin, Elizabeth A Sweeny, Morgan E DeSantis, Meredith E Jackrel, Christopher B Rodell, Jason A Burdick, Oliver D King, Aaron D Gitler, Clotilde Lagier-Tourenne, Udai Bhan Pandey, Yuh Min Chook, J Paul Taylor, and James Shorter. Nuclear-Import receptors reverse aberrant phase transitions of RNA-Binding proteins with prion-like domains. *Cell*, 173(3):677–692.e20, April 2018.

[60] Randal Halfmann, Daniel F Jarosz, Sandra K Jones, Amelia Chang, Alex K Lancaster, and Susan Lindquist. Prions are a common mechanism for phenotypic inheritance in wild yeasts. *Nature*, 482(7385):363–368, February 2012.

[61] Tobias Haslberger, Jimena Weibezahn, Regina Zahn, Sukyeong Lee, Francis T F Tsai, Bernd Bukau, and Axel Mogk. M domains couple the ClpB threading motor with the DnaK chaperone activity. *Mol. Cell*, 25(2):247–260, January 2007.

[62] Tobias Haslberger, Agnieszka Zdanowicz, Ingo Brand, Janine Kirstein, Kürsad Turgay, Axel Mogk, and Bernd Bukau. Protein disaggregation by the AAA+ chaperone ClpB involves partial threading of looped polypeptide segments. *Nat. Struct. Mol. Biol.*, 15(6):641–650, June 2008.

[63] Amayra Hernández-Vega, Marcus Braun, Lara Scharrel, Marcus Jahnel, Susanne Wegmann, Bradley T Hyman, Simon Alberti, Stefan Diez, and Anthony A Hyman. Local nucleation of microtubule bundles through tubulin concentration into a condensed tau phase. *Cell Rep.*, 20(10):2304–2312, September 2017.

[64] Hidehiko Hirakawa, Suguru Ishikawa, and Teruyuki Nagamune. Ca2+ -independent sortase-a exhibits high selective protein ligation activity in the cytoplasm of escherichia coli. *Biotechnol. J.*, 10(9):1487–1492, September 2015.

[65] Alex S Holehouse and Rohit V Pappu. Functional implications of intracellular phase transitions. *Biochemistry*, January 2018.

[66] Walid A Houry, Dmitrij Frishman, Christoph Eckerskorn, Friedrich Lottspeich, and F Ulrich Hartl. Identification of in vivo substrates of the chaperonin GroEL, 1999.

[67] Nathaniel P Hoyle, Lydia M Castelli, Susan G Campbell, Leah E A Holmes, and Mark P Ashe. Stress-dependent relocalization of translationally primed mRNPs to cytoplasmic granules that are kinetically and spatially distinct from p-bodies. *J. Cell Biol.*, 179(1):65–74, October 2007.

[68] Anthony A Hyman, Christoph A Weber, and Frank Jülicher. Liquid-liquid phase separation in biology. *Annu. Rev. Cell Dev. Biol.*, 30:39–58, 2014.

[69] J Ignacio Gutiérrez, Greg Brittingham, Xuya Wang, David Fenyö, and Liam J Holt. The largest SWI/SNF polyglutamine domain is a ph sensor. April 2018.

[70] Rahmi Imamoglu, David Balchin, Manajit Hayer-Hartl, and F Ulrich Hartl. Bacterial hsp70 resolves misfolded states and accelerates productive folding of a multi-domain protein. *Nat. Commun.*, 11(1):365, January 2020.

[71] Yuji Inoue, Hideki Taguchi, Aiko Kishimoto, and Masasuke Yoshida. Hsp104 binds to yeast sup35 prion fiber but needs other factor(s) to sever it. *J. Biol. Chem.*, 279(50):52319–52323, December 2004.

[72] Christiane Iserman, Christine Desroches Altamirano, Ceciel Jegers, Ulrike Friedrich, Taraneh Zarin, Anatol W Fritsch, Matthäus Mittasch, Antonio Domingues, Lena Hersemann, Marcus Jahnel, Doris Richter, Ulf-Peter Guenther, Matthias W Hentze, Alan M Moses, Anthony A Hyman, Günter Kramer, Moritz Kreysing, Titus M Franzmann, and Simon Alberti. Condensation of ded1p promotes a translational switch from housekeeping to stress protein production. *Cell*, 181(4):818–831.e19, May 2020.

[73] Daniel G Isom, Stephani C Page, Leonard B Collins, Nicholas J Kapolka, Geoffrey J Taghon, and Henrik G Dohlman. Coordinated regulation of intracellular ph by two glucose-sensing pathways in yeast. *J. Biol. Chem.*, 293(7):2318–2329, February 2018.

[74] Hao Jiang, Shusheng Wang, Yuejia Huang, Xiaonan He, Honggang Cui, Xueliang Zhu, and Yixian Zheng. Phase transition of spindle-associated protein regulate spindle apparatus assembly. *Cell*, 163(1):108–122, September 2015.

[75] Yajun Jiang, Paolo Rossi, and Charalampos G Kalodimos. Structural basis for client recognition and activity of hsp40 chaperones. *Science*, 365(6459):1313–1319, September 2019.

[76] Meiyan Jin, Gregory G Fuller, Ting Han, Yao Yao, Amelia F Alessi, Mallory A Freeberg, Nathan P Roach, James J Moresco, Alla Karnovsky, Misuzu Baba, John R Yates, 3rd, Aaron D Gitler, Ken Inoki, Daniel J Klionsky, and John K Kim. Glycolytic enzymes coalesce in G bodies under hypoxic stress. *Cell Rep.*, 20(4):895–908, July 2017.

[77] Ryan P Joyner, Jeffrey H Tang, Jonne Helenius, Elisa Dultz, Christiane Brune, Liam J Holt, Sebastien Huet, Daniel J Müller, and Karsten Weis. A glucose-starvation response regulates the diffusion of macromolecules. *Elife*, 5, March 2016.

[78] Mehdi Kabani and Céline N Martineau. Multiple hsp70 isoforms in the eukaryotic cytosol: mere redundancy or functional specificity? *Curr. Genomics*, 9(5):338–248, 2008.

[79] Jayasankar Mohanakrishnan Kaimal, Ganapathi Kandasamy, Fabian Gasser, and Claes Andréasson. Coordinated hsp110 and hsp104 activities power protein disaggregation in saccharomyces cerevisiae. *Mol. Cell. Biol.*, 37(11), June 2017.

[80] Harm H Kampinga and Elizabeth A Craig. The HSP70 chaperone machinery: J proteins as drivers of functional specificity. *Nat. Rev. Mol. Cell Biol.*, 11(8):579–592, August 2010.

[81] Shigeko Kawai-Noma, Chan-Gi Pack, Tomoko Kojidani, Haruhiko Asakawa, Yasushi Hiraoka, Masataka Kinjo, Tokuko Haraguchi, Hideki Taguchi, and Aiko Hirata. In vivo evidence for the fibrillar structures of sup35 prions in yeast cells. *J. Cell Biol.*, 190(2):223–231, July 2010.

[82] Nancy L Kedersha, Mita Gupta, Wei Li, Ira Miller, and Paul Anderson. RNA-Binding proteins tia-1 and tiar link the phosphorylation of Eif-2α to the assembly of mammalian stress granules. *J. Cell Biol.*, 147(7):1431–1442, December 1999.

[83] Nicole King, Susan L Young, Monika Abedin, Martin Carr, and Barry S C Leadbeater. Starting and maintaining monosiga brevicollis cultures. *Cold Spring Harb. Protoc.*, 2009(2):db.prot5148, February 2009.

[84] Agnieszka Kłosowska, Tomasz Chamera, and Krzysztof Liberek. Adenosine diphosphate restricts the protein remodeling activity of the hsp104 chaperone to hsp70 assisted disaggregation. *Elife*, 5, May 2016.

[85] Thomas Kluyver, Benjamin Ragan-Kelley, Fernando Pérez, Brian Granger, Matthias Bussonnier, Jonathan Frederic, Kyle Kelley, Jessica Hamrick, Jason Grout, Sylvain Corlay, Paul Ivanov, Damián Avila, Safia Abdalla, Carol Willing, and Jupyter development team. Jupyter notebooks – a publishing format for reproducible computational workflows. pages 87–90. IOS Press, 2016.

[86] Joanna Krakowiak, Xu Zheng, Nikit Patel, Zoë A Feder, Jayamani Anandhakumar, Kendra Valerius, David S Gross, Ahmad S Khalil, and David Pincus. Hsf1 and hsp70 constitute a two-component feedback loop that regulates the yeast heat shock response. *Elife*, 7, February 2018.

[87] Susanne Kramer, Rafael Queiroz, Louise Ellis, Helena Webb, Jörg D Hoheisel, Christine Clayton, and Mark Carrington. Heat shock causes a decrease in polysomes and the appearance of stress granules in trypanosomes independently of eIF2α phosphorylation at thr169. *J. Cell Sci.*, 121(18):3002–3014, September 2008.

[88] Sonja Kroschwald, Shovamayee Maharana, Daniel Mateju, Liliana Malinovska, Elisabeth Nüske, Ina Poser, Doris Richter, and Simon Alberti. Promiscuous interactions and protein disaggregases determine the material state of stress-inducible RNP granules. *Elife*, 4:e06807, August 2015.

[89] Sonja Kroschwald, Matthias C Munder, Shovamayee Maharana, Titus M Franzmann, Doris Richter, Martine Ruer, Anthony A Hyman, and Simon Alberti. Different material states of pub1 condensates define distinct modes of stress adaptation and recovery. *Cell Rep.*, 23(11):3327–3339, June 2018.

[90] Adam G Larson, Daniel Elnatan, Madeline M Keenen, Michael J Trnka, Jonathan B Johnston, Alma L Burlingame, David A Agard, Sy Redding, and Geeta J Narlikar. Liquid droplet formation by HP1α suggests a role for phase separation in heterochromatin. *Nature*, 547(7662):236–240, July 2017.

[91] Thomas Laufen, Matthias P Mayer, Christian Beisel, Dagmar Klostermeier, Axel Mogk, Jochen Reinstein, and Bernd Bukau. Mechanism of regulation of hsp70 chaperones by DnaJ cochaperones. *Proc. Natl. Acad. Sci. U. S. A.*, 96(10):5452–5457, May 1999.

[92] Jian Li, Johnathan Labbadia, and Richard I Morimoto. Rethinking HSF1 in stress, development, and organismal health. *Trends Cell Biol.*, 27(12):895–905, December 2017.

[93] Pilong Li, Sudeep Banjade, Hui-Chun Cheng, Soyeon Kim, Baoyu Chen, Liang Guo, Marc Llaguno, Javoris V Hollingsworth, David S King, Salman F Banani, Paul S Russo, Qiu-Xing Jiang, B Tracy Nixon, and Michael K Rosen. Phase transitions in the assembly of multivalent signalling proteins. *Nature*, 483(7389):336–340, March 2012.

[94] Yuan Lin, David S W Protter, Michael K Rosen, and Roy Parker. Formation and maturation of Phase-Separated liquid droplets by RNA-Binding proteins. *Mol. Cell*, 60(2):208–219, October 2015.

[95] S Lindquist. The heat-shock response. *Annu. Rev. Biochem.*, 55:1151–1191, 1986.

[96] Yu Liu and Amy Chang. Heat shock response relieves ER stress. *EMBO J.*, 27(7):1049–1059, April 2008.

[97] Zhenying Liu, Shengnan Zhang, Jinge Gu, Yilun Tong, Yichen Li, Xinrui Gui, Houfang Long, Chuchu Wang, Chunyu Zhao, Jinxia Lu, Lin He, Ying Li, Zhijun Liu, Dan Li, and Cong Liu. Hsp27 chaperones FUS phase separation under the modulation of stress-induced phosphorylation. *Nat. Struct. Mol. Biol.*, 27(4):363–372, April 2020.

[98] Huasong Lu, Dan Yu, Anders S Hansen, Sourav Ganguly, Rongdiao Liu, Alec Heckert, Xavier Darzacq, and Qiang Zhou. Phase-separation mechanism for c-terminal hyperphosphorylation of RNA polymerase II. *Nature*, 558(7709):318–323, June 2018.

[99] Z Lu and D M Cyr. Protein folding activity of hsp70 is modified differentially by the hsp40 co-chaperones sis1 and ydj1. *J. Biol. Chem.*, 273(43):27824–27830, October 1998.

[100] Eric M Lynch, Derrick R Hicks, Matthew Shepherd, James A Endrizzi, Allison Maker, Jesse M Hansen, Rachael M Barry, Zemer Gitai, Enoch P Baldwin, and Justin M Kollman. Human CTP synthase filament structure reveals the active enzyme conformation. *Nat. Struct. Mol. Biol.*, 24(6):507–514, June 2017.

[101] Shovamayee Maharana, Jie Wang, Dimitrios K Papadopoulos, Doris Richter, Andrey Pozniakovsky, Ina Poser, Marc Bickle, Sandra Rizk, Jordina Guillén-Boixet, Titus M Franzmann, Marcus Jahnel, Lara Marrone, Young-Tae Chang, Jared Sterneckert, Pavel Tomancak, Anthony A Hyman, and Simon Alberti. RNA buffers the phase separation behavior of prion-like RNA binding proteins. *Science*, 360(6391):918–921, May 2018.

[102] R Maheshwari, G Bharadwaj, and M K Bhat. Thermophilic fungi: their physiology and enzymes. *Microbiol. Mol. Biol. Rev.*, 64(3):461–488, September 2000.

[103] Zachary M March, Oliver D King, and James Shorter. Prion-like domains as epigenetic regulators, scaffolds for subcellular organization, and drivers of neurodegenerative disease. *Brain Res.*, 1647:9–18, September 2016.

[104] Andreas Martin, Tania A Baker, and Robert T Sauer. Rebuilt AAA + motors reveal operating principles for ATP-fuelled machines. *Nature*, 437(7062):1115–1120, October 2005.

[105] Ianire Martín, Garbiñe Celaya, Carlos Alfonso, Fernando Moro, Germán Rivas, and Arturo Muga. Crowding activates ClpB and enhances its association with DnaK for efficient protein aggregate reactivation. *Biophys. J.*, 106(9):2017–2027, May 2014.

[106] Jennifer L Martindale and Nikki J Holbrook. Cellular response to oxidative stress: signaling for suicide and survival. *J. Cell. Physiol.*, 192(1):1–15, July 2002.

[107] Anna E Masser, Wenjing Kang, Joydeep Roy, Jayasankar Mohanakrishnan Kaimal, Jany Quintana-Cordero, Marc R Friedländer, and Claes Andréasson. Cytoplasmic protein misfolding titrates hsp70 to activate nuclear hsf1. *Elife*, 8, September 2019.

[108] Daniel Mateju, Titus M Franzmann, Avinash Patel, Andrii Kopach, Edgar E Boczek, Shovamayee Maharana, Hyun O Lee, Serena Carra, Anthony A Hyman, and Simon Alberti. An aberrant phase transition of stress granules triggered by misfolded protein and prevented by chaperone function. *EMBO J.*, 36(12):1669–1687, June 2017.

[109] M P Mayer, H Schröder, S Rüdiger, K Paal, T Laufen, and B Bukau. Multistep mechanism of substrate binding determines chaperone activity of hsp70. *Nat. Struct. Biol.*, 7(7):586–593, July 2000.

[110] J S McCarty, A Buchberger, J Reinstein, and B Bukau. The role of ATP in the functional cycle of the DnaK chaperone system. *J. Mol. Biol.*, 249(1):126–137, May 1995.

[111] David T McSwiggen, Mustafa Mir, Xavier Darzacq, and Robert Tjian. Evaluating phase separation in live cells: diagnosis, caveats, and functional consequences. *Genes Dev.*, 33(23-24):1619–1634, December 2019.

[112] Axel Mogk, Bernd Bukau, and Harm H Kampinga. Cellular handling of protein aggregates by disaggregation machines. *Mol. Cell*, 69(2):214–226, January 2018.

[113] Begoña Monterroso, Silvia Zorrilla, Marta Sobrinos-Sanguino, Miguel A Robles-Ramos, Marina López-Álvarez, William Margolin, Christine D Keating, and Germán Rivas. Bacterial FtsZ protein forms phase-separated condensates with its nucleoid-associated inhibitor SlmA, 2019.

[114] Kevin A Morano, Chris M Grant, and W Scott Moye-Rowley. The response to heat shock and oxidative stress in saccharomyces cerevisiae. *Genetics*, 190(4):1157–1195, April 2012.

[115] Ingo Morgenstern, Justin Powlowski, Nadeeza Ishmael, Corinne Darmond, Sandrine Marqueteau, Marie-Claude Moisan, Geneviève Quenneville, and Adrian Tsang. A molecular phylogeny of thermophilic fungi. *Fungal Biol.*, 116(4):489–502, April 2012.

[116] Richard I Morimoto. Proteotoxic stress and inducible chaperone networks in neurodegenerative disease and aging. *Genes Dev.*, 22(11):1427–1438, June 2008.

[117] Matthias Christoph Munder, Daniel Midtvedt, Titus Franzmann, Elisabeth Nüske, Oliver Otto, Maik Herbig, Elke Ulbricht, Paul Müller, Anna Taubenberger, Shovamayee Maharana, Liliana Malinovska, Doris Richter, Jochen Guck, Vasily Zaburdaev, and Simon Alberti. A ph-driven transition of the cytoplasm from a fluid- to a solid-like state promotes entry into dormancy. *Elife*, 5, March 2016.

[118] Arjun Narayanan, Anatoli Meriin, J Owen Andrews, Jan-Hendrik Spille, Michael Y Sherman, and Ibrahim I Cisse. A first order phase transition mechanism underlies protein aggregation in mammalian cells. *Elife*, 8:e39695, February 2019.

[119] Rammohan Narayanaswamy, Matthew Levy, Mark Tsechansky, Gwendolyn M Stovall, Jeremy D O'Connell, Jennifer Mirrielees, Andrew D Ellington, and Edward M Marcotte. Widespread reorganization of metabolic enzymes into reversible assemblies upon nutrient starvation. *Proc. Natl. Acad. Sci. U. S. A.*, 106(25):10147–10152, June 2009.

[120] Basile Nguyen, David Hartich, Udo Seifert, and Paolo De Los Rios. Thermodynamic bounds on the ultra- and infra-affinity of hsp70 for its substrates. *Biophys. J.*, 113(2):362–370, July 2017.

[121] Nadinath B Nillegoda, Janine Kirstein, Anna Szlachcic, Mykhaylo Berynskyy, Antonia Stank, Florian Stengel, Kristin Arnsburg, Xuechao Gao, Annika Scior, Ruedi Aebersold, D Lys Guilbride, Rebecca C Wade, Richard I Morimoto, Matthias P Mayer, and Bernd Bukau. Crucial HSP70 co-chaperone complex unlocks metazoan protein disaggregation. *Nature*, 524(7564):247–251, August 2015.

[122] Nadinath B Nillegoda, Antonia Stank, Duccio Malinverni, Niels Alberts, Anna Szlachcic, Alessandro Barducci, Paolo De Los Rios, Rebecca C Wade, and Bernd Bukau. Evolution of an intricate j-protein network driving protein disaggregation in eukaryotes. *Elife*, 6, May 2017.

[123] Nitika, Corey M Porter, Andrew W Truman, and Matthias C Truttmann. Post-translational modifications of hsp70 family proteins: Expanding the chaperone code. *J. Biol. Chem.*, 295(31):10689–10708, July 2020.

[124] Timothy J Nott, Timothy D Craggs, and Andrew J Baldwin. Membraneless organelles can melt nucleic acid duplexes and act as biomolecular filters. *Nat. Chem.*, 8(6):569–575, June 2016.

[125] D A Parsell and S Lindquist. The function of heat-shock proteins in stress tolerance: degradation and reactivation of damaged proteins. *Annu. Rev. Genet.*, 27:437–496, 1993.

[126] Avinash Patel, Liliana Malinovska, Shambaditya Saha, Jie Wang, Simon Alberti, Yamuna Krishnan, and Anthony A Hyman. ATP as a biological hydrotrope. *Science*, 356(6339):753–756, May 2017.

[127] M M Patino, J J Liu, J R Glover, and S Lindquist. Support for the prion hypothesis for inheritance of a phenotypic trait in yeast. *Science*, 273(5275):622–626, August 1996.

[128] Gopal K Pattanayak, Yi Liao, Edward W J Wallace, Bogdan Budnik, D Allan Drummond, and Michael J Rust. Daily cycles of reversible protein condensation in cyanobacteria. *Cell Rep.*, 32(7):108032, August 2020.

[129] S V Paushkin, V V Kushnirov, V N Smirnov, and M D Ter-Avanesyan. Propagation of the yeast prion-like [psi+] determinant is mediated by oligomerization of the SUP35-encoded polypeptide chain release factor. *EMBO J.*, 15(12):3127–3134, 1996.

[130] Sara Peffer, Davi Gonçalves, and Kevin A Morano. Regulation of the hsf1-dependent transcriptome via conserved bipartite contacts with hsp70 promotes survival in yeast. *J. Biol. Chem.*, 294(32):12191–12202, August 2019.

[131] Ivana Petrovska, Elisabeth Nüske, Matthias C Munder, Gayathrie Kulasegaran, Liliana Malinovska, Sonja Kroschwald, Doris Richter, Karim Fahmy, Kimberley Gibson, Jean-Marc Verbavatz, and Simon Alberti. Filament formation by metabolic enzymes is a specific adaptation to an advanced state of cellular starvation. *Elife*, April 2014.

[132] Evan T Powers, David L Powers, and Lila M Gierasch. FoldEco: a model for proteostasis in e. coli. *Cell Rep.*, 1(3):265–276, March 2012.

[133] Arpan Kumar Rai, Jia-Xuan Chen, Matthias Selbach, and Lucas Pelkmans. Kinase-controlled phase transition of membraneless organelles in mitosis. *Nature*, 559(7713):211–216, July 2018.

[134] Heike Rampelt, Janine Kirstein-Miles, Nadinath B Nillegoda, Kang Chi, Sebastian R Scholz, Richard I Morimoto, and Bernd Bukau. Metazoan hsp70 machines use hsp110 to power protein disaggregation. *EMBO J.*, 31(21):4221–4235, November 2012.

[135] Elzbieta Ratajczak, Szymon Zietkiewicz, and Krzysztof Liberek. Distinct activities of escherichia coli small heat shock proteins IbpA and IbpB promote efficient protein disaggregation. *J. Mol. Biol.*, 386(1):178–189, February 2009.

[136] Michael Reidy, Ruchika Sharma, Shankar Shastry, Brittany-Lee Roberts, Ivan Albino-Flores, Sue Wickner, and Daniel C Masison. Hsp40s specify functions of hsp104 and hsp90 protein chaperone machines. *PLoS Genet.*, 10(10):e1004720, October 2014.

[137] Bryan A Reyes, Julie S Pendergast, and Shin Yamazaki. Mammalian peripheral circadian oscillators are temperature compensated, 2008.

[138] Joshua A. Riback, Christopher D. Katanski, Jamie L. Kear-Scott, Evgeny V. Pilipenko, Alexandra E. Rojek, Tobin R. Sosnick, and D. Allan Drummond. Stress-triggered phase separation is an adaptive, evolutionarily tuned response. *Cell*, 168(6):1028 – 1040.e19, 2017.

[139] Joshua A Riback, Lian Zhu, Mylene C Ferrolino, Michele Tolbert, Diana M Mitrea, David W Sanders, Ming-Tzo Wei, Richard W Kriwacki, and Clifford P Brangwynne. Composition-dependent thermodynamics of intracellular phase separation. *Nature*, 581(7807):209–214, May 2020.

[140] F Ritossa. A new puffing pattern induced by temperature shock and DNP in drosophila. *Experientia*, 18(12):571–573, December 1962.

[141] F Ritossa. Discovery of the heat shock response. *Cell Stress Chaperones*, 1(2):97–98, June 1996.

[142] Rina Rosenzweig, Shoeib Moradi, Arash Zarrine-Afsar, John R Glover, and Lewis E Kay. Unraveling the mechanism of protein disaggregation through a ClpB-DnaK interaction. *Science*, 339(6123):1080–1083, March 2013.

[143] RStudio Team. *RStudio: Integrated Development Environment for R*. RStudio, Inc., Boston, MA, 2018.

[144] Kiersten M Ruff, Furqan Dar, and Rohit V Pappu. Ligand effects on phase separation of multivalent macromolecules. *Proc. Natl. Acad. Sci. U. S. A.*, 118(10), March 2021.

[145] Kiersten M Ruff, Stefan Roberts, Ashutosh Chilkoti, and Rohit V Pappu. Advances in understanding Stimulus-Responsive phase behavior of intrinsically disordered protein polymers. *J. Mol. Biol.*, 430(23):4619–4635, November 2018.

[146] R Russell, R Jordan, and R McMacken. Kinetic characterization of the ATPase cycle of the DnaK molecular chaperone. *Biochemistry*, 37(2):596–607, January 1998.

[147] Shady Saad, Gea Cereghetti, Yuehan Feng, Paola Picotti, Matthias Peter, and Reinhard Dechant. Reversible protein aggregation is a protective mechanism to ensure cell cycle restart after stress. *Nat. Cell Biol.*, 19(10):1202–1213, October 2017.

[148] Benjamin R Sabari, Alessandra Dall'Agnese, Ann Boija, Isaac A Klein, Eliot L Coffey, Krishna Shrinivas, Brian J Abraham, Nancy M Hannett, Alicia V Zamudio, John C Manteiga, Charles H Li, Yang E Guo, Daniel S Day, Jurian Schuijers, Eliza Vasile, Sohail Malik, Denes Hnisz, Tong Ihn Lee, Ibrahim I Cisse, Robert G Roeder, Phillip A Sharp, Arup K Chakraborty, and Richard A Young. Coactivator condensation at super-enhancers links phase separation and gene control. *Science*, 361(6400), July 2018.

[149] Alan B Sachs, R W Davis, and R D Kornberg. A single domain of yeast poly (a)-binding protein is necessary and sufficient for RNA binding and cell viability. *Mol. Cell. Biol.*, 7(9):3268–3276, 1987.

[150] Shambaditya Saha, Christoph A Weber, Marco Nousch, Omar Adame-Arana, Carsten Hoege, Marco Y Hein, Erin Osborne-Nishimura, Julia Mahamid, Marcus Jahnel, Louise Jawerth, Andrej Pozniakovski, Christian R Eckmann, Frank Jülicher, and Anthony A Hyman. Polar positioning of Phase-Separated liquid compartments in cells regulated by an mRNA competition mechanism. *Cell*, 166(6):1572–1584.e16, September 2016.

[151] Makoto Saito, Daniel Hess, Jan Eglinger, Anatol W Fritsch, Moritz Kreysing, Brian T Weinert, Chunaram Choudhary, and Patrick Matthias. Acetylation of intrinsically disordered regions regulates phase separation. *Nat. Chem. Biol.*, 15(1):51–61, December 2018.

[152] Z Salvadó, F N Arroyo-López, J M Guillamón, G Salazar, A Querol, and E Barrio. Temperature adaptation markedly determines evolution within the genus saccharomyces. *Appl. Environ. Microbiol.*, 77(7):2292–2302, April 2011.

[153] D Schmid, A Baici, H Gehring, and P Christen. Kinetics of molecular chaperone action. *Science*, 263(5149):971–973, February 1994.

[154] Hermann Broder Schmidt and Dirk Görlich. Nup98 FG domains from diverse species spontaneously phase-separate into particles with nuclear pore-like permselectivity. *Elife*, 4, January 2015.

[155] Hermann Broder Schmidt and Dirk Görlich. Transport selectivity of nuclear pores, phase separation, and membraneless organelles. *Trends Biochem. Sci.*, 41(1):46–61, January 2016.

[156] Annika Scior, Alexander Buntru, Kristin Arnsburg, Anne Ast, Manuel Iburg, Katrin Juenemann, Maria Lucia Pigazzini, Barbara Mlody, Dmytro Puchkov, Josef Priller, Erich E Wanker, Alessandro Prigione, and Janine Kirstein. Complete suppression of htt fibrilization and disaggregation of htt fibrils by a trimeric chaperone complex. *EMBO J.*, 37(2):282–299, January 2018.

[157] Piali Sengupta and Paul Garrity. Sensing temperature. *Curr. Biol.*, 23(8):R304–7, April 2013.

[158] Ji Hae Seo, Ji-Hyeon Park, Eun Ji Lee, Tam Thuy Lu Vo, Hoon Choi, Jun Yong Kim, Jae Kyung Jang, Hee-Jun Wee, Hye Shin Lee, Se Hwan Jang, Zee Yong Park,

Jaeho Jeong, Kong-Joo Lee, Seung-Hyeon Seok, Jin Young Park, Bong Jin Lee, Mi-Ni Lee, Goo Taeg Oh, and Kyu-Won Kim. ARD1-mediated hsp70 acetylation balances stress-induced protein refolding and degradation. *Nat. Commun.*, 7:12882, October 2016.

[159] Fabian Seyffer, Eva Kummer, Yuki Oguchi, Juliane Winkler, Mohit Kumar, Regina Zahn, Victor Sourjik, Bernd Bukau, and Axel Mogk. Hsp70 proteins bind hsp100 regulatory M domains to activate AAA+ disaggregase at aggregate surfaces. *Nat. Struct. Mol. Biol.*, 19(12):1347–1355, December 2012.

[160] Maya Shamir, Yinon Bar-On, Rob Phillips, and Ron Milo. SnapShot: Timescales in cell biology. *Cell*, 164(6):1302–1302.e1, March 2016.

[161] Yongdae Shin and Clifford P Brangwynne. Liquid phase condensation in cell physiology and disease. *Science*, 357(6357), September 2017.

[162] James Shorter. The mammalian disaggregase machinery: Hsp110 synergizes with hsp70 and hsp40 to catalyze protein disaggregation and reactivation in a cell-free system. *PLoS One*, 6(10):e26319, October 2011.

[163] James Shorter and Susan Lindquist. Hsp104 catalyzes formation and elimination of self-replicating sup35 prion conformers. *Science*, 304(5678):1793–1797, June 2004.

[164] Bernhard Sielaff and Francis T F Tsai. The m-domain controls hsp104 protein remodeling activity in an Hsp70/Hsp40-dependent manner. *J. Mol. Biol.*, 402(1):30–37, September 2010.

[165] Kobi Simpson-Lavy, Tianchang Xu, Mark Johnston, and Martin Kupiec. The std1 activator of the Snf1/AMPK kinase controls glucose response in yeast by a regulated protein aggregation. *Mol. Cell*, 68(6):1120–1133.e3, December 2017.

[166] Wilton T Snead and Amy S Gladfelter. The control centers of biomolecular phase separation: How membrane surfaces, PTMs, and active processes regulate condensation. *Mol. Cell*, 76(2):295–305, October 2019.

[167] Alexandra Stolz and Dieter H Wolf. Endoplasmic reticulum associated protein degradation: a chaperone assisted journey to hell. *Biochim. Biophys. Acta*, 1803(6):694–705, June 2010.

[168] Amy R Strom, Alexander V Emelyanov, Mustafa Mir, Dmitry V Fyodorov, Xavier Darzacq, and Gary H Karpen. Phase separation drives heterochromatin domain formation. *Nature*, 547(7662):241–245, July 2017.

[169] Xiaolei Su, Jonathon A Ditlev, Enfu Hui, Wenmin Xing, Sudeep Banjade, Julia Okrut, David S King, Jack Taunton, Michael K Rosen, and Ronald D Vale. Phase separation of signaling molecules promotes T cell receptor signal transduction. *Science*, 352(6285):595–599, April 2016.

[170] Lijun Sun, Jiaxi Wu, Fenghe Du, Xiang Chen, and Zhijian J Chen. Cyclic GMP-AMP synthase is a cytosolic DNA sensor that activates the type I interferon pathway. *Science*, 339(6121):786–791, February 2013.

[171] Elizabeth A Sweeny and James Shorter. Mechanistic and structural insights into the Prion-Disaggregase activity of hsp104. *J. Mol. Biol.*, 428(9 Pt B):1870–1885, May 2016.

[172] M Tanabe, A Nakai, Y Kawazoe, and K Nagata. Different thresholds in the responses of two heat shock transcription factors, HSF1 and HSF3. *J. Biol. Chem.*, 272(24):15389–15395, June 1997.

[173] Daniela Teixeira, Ujwal Sheth, Marco A Valencia-Sanchez, Muriel Brengues, and Roy Parker. Processing bodies require RNA for assembly and contain nontranslating mRNAs. *RNA*, 11(4):371–382, April 2005.

[174] Peter Tessarz, Axel Mogk, and Bernd Bukau. Substrate threading through the central pore of the hsp104 chaperone as a common mechanism for protein disaggregation and prion propagation. *Mol. Microbiol.*, 68(1):87–97, April 2008.

[175] H Theyssen, H P Schuster, L Packschies, B Bukau, and J Reinstein. The second step of ATP binding to DnaK induces peptide release. *J. Mol. Biol.*, 263(5):657–670, November 1996.

[176] Catherine G Triandafillou, Christopher D Katanski, Aaron R Dinner, and David Allan Drummond. Transient intracellular acidification regulates the core transcriptional heat shock response. *eLife*, 9:e54880, August 2020.

[177] H L True and S L Lindquist. A yeast prion provides a mechanism for genetic variation and phenotypic diversity. *Nature*, 407(6803):477–483, September 2000.

[178] Andrew W Truman, Kolbrun Kristjansdottir, Donald Wolfgeher, Naushaba Hasin, Sigrun Polier, Hong Zhang, Sarah Perrett, Chrisostomos Prodromou, Gary W Jones, and Stephen J Kron. CDK-dependent hsp70 phosphorylation controls G1 cyclin abundance and cell-cycle progression. *Cell*, 151(6):1308–1318, December 2012.

[179] Jens Tyedmers, Maria Lucia Madariaga, and Susan Lindquist. Prion switching in response to environmental stress. *PLoS Biol.*, 6(11):e294, November 2008.

[180] Sophia Ungelenk, Fatemeh Moayed, Chi-Ting Ho, Tomas Grousl, Annette Scharf, Alireza Mashaghi, Sander Tans, Matthias P Mayer, Axel Mogk, and Bernd Bukau. Small heat shock proteins sequester misfolding proteins in near-native conformation for cellular protection and efficient refolding. *Nat. Commun.*, 7(1):13673, November 2016.

[181] R Martin Vabulas, Swasti Raychaudhuri, Manajit Hayer-Hartl, and F Ulrich Hartl. Protein folding in the cytoplasm and the heat shock response. *Cold Spring Harb. Perspect. Biol.*, 2(12):a004390, 2010.

[182] Edward W J Wallace, Jamie L Kear-Scott, Evgeny V Pilipenko, Michael H Schwartz, Pawel R Laskowski, Alexandra E Rojek, Christopher D Katanski, Joshua A Riback, Michael F Dion, Alexander M Franks, Edoardo M Airoldi, Tao Pan, Bogdan A Budnik, and D Allan Drummond. Reversible, specific, active aggregates of endogenous proteins assemble upon heat stress. *Cell*, 162(6):1286–1298, September 2015.

[183] Robert W Walters, Denise Muhlrad, Jennifer Garcia, and Roy Parker. Differential effects of ydj1 and sis1 on hsp70-mediated clearance of stress granules in saccharomyces cerevisiae. *RNA*, 21(9):1660–1671, September 2015.

[184] Stephanie C Weber and Clifford P Brangwynne. Inverse size scaling of the nucleolus by a concentration-dependent phase transition. *Curr. Biol.*, 25(5):641–646, March 2015.

[185] Eilika U Weber-Ban, Brian G Reid, Andrew D Miranker, and Arthur L Horwich. Global unfolding of a substrate protein by the hsp100 chaperone ClpA. *Nature*, 401(6748):90–93, September 1999.

[186] G Weitzel, U Pilatus, and L Rensing. The cytoplasmic ph, ATP content and total protein synthesis rate during heat-shock protein inducing treatments in yeast. *Exp. Cell Res.*, 170(1):64–79, May 1987.

[187] Gabriele Weitzel, Ulrich Pilatus, and Ludger Rensing. Similar dose response of heat shock protein synthesis and intracellular ph change in yeast, 1985.

[188] Anne S Wentink, Nadinath B Nillegoda, Jennifer Feufel, Gabrielė Ubartaitė, Carolyn P Schneider, Paolo De Los Rios, Janosch Hennig, Alessandro Barducci, and Bernd Bukau. Molecular dissection of amyloid disaggregation by human HSP70. *Nature*, 587(7834):483–488, November 2020.

[189] Florian Wilfling, Joel T Haas, Tobias C Walther, and Robert V Farese, Jr. Lipid droplet biogenesis. *Curr. Opin. Cell Biol.*, 29:39–45, August 2014.

[190] Frank Wippich, Bernd Bodenmiller, Maria Gustafsson Trajkovska, Stefanie Wanka, Ruedi Aebersold, and Lucas Pelkmans. Dual specificity kinase DYRK3 couples stress granule condensation/dissolution to mTORC1 signaling. *Cell*, 152(4):791–805, February 2013.

[191] Jeffrey B Woodruff, Beatriz Ferreira Gomes, Per O Widlund, Julia Mahamid, Alf Honigmann, and Anthony A Hyman. The centrosome is a selective condensate that nucleates microtubules by concentrating tubulin. *Cell*, 169(6):1066–1077.e10, June 2017.

[192] Jiaxi Wu, Lijun Sun, Xiang Chen, Fenghe Du, Heping Shi, Chuo Chen, and Zhijian J Chen. Cyclic GMP-AMP is an endogenous second messenger in innate immune signaling by cytosolic DNA. *Science*, 339(6121):826–830, February 2013.

[193] Bo Xie, Shawn Bishop, Dan Stessman, David Wright, Martin H Spalding, and Larry J Halverson. Chlamydomonas reinhardtii thermal tolerance enhancement mediated by a

mutualistic interaction with vitamin b12-producing bacteria. *ISME J.*, 7(8):1544–1555, August 2013.

[194] Huafeng Xu. Cochaperones enable hsp70 to use ATP energy to stabilize native proteins out of the folding equilibrium. *Sci. Rep.*, 8(1):1–15, September 2018.

[195] Haneul Yoo, Jared A M Bard, Evgeny Pilipenko, and David Allan Drummond. Chaperones directly and efficiently disperse stress-triggered biomolecular condensates. *SSRN Electron. J.*, 2021.

[196] Haneul Yoo, Catherine Triandafillou, and D Allan Drummond. Cellular sensing by phase separation: Using the process, not just the products. *J. Biol. Chem.*, 294(18):7151–7159, May 2019.

[197] Hyun Young Yu, Thomas Ziegelhoffer, Jerzy Osipiuk, Szymon J Ciesielski, Maciej Baranowski, Min Zhou, Andrzej Joachimiak, and Elizabeth A Craig. Roles of intramolecular and intermolecular interactions in functional regulation of the hsp70 j-protein co-chaperone sis1. *J. Mol. Biol.*, 427(7):1632–1643, April 2015.

[198] Huaiying Zhang, Shana Elbaum-Garfinkle, Erin M Langdon, Nicole Taylor, Patricia Occhipinti, Andrew A Bridges, Clifford P Brangwynne, and Amy S Gladfelter. RNA controls PolyQ protein phase transitions. *Mol. Cell*, 60(2):220–230, October 2015.

[199] Xu Zheng, Joanna Krakowiak, Nikit Patel, Ali Beyzavi, Jideofor Ezike, Ahmad S Khalil, and David Pincus. Dynamic control of hsf1 during heat shock by a chaperone switch and phosphorylation. *Elife*, 5, November 2016.

[200] Szymon Żwirowski, Agnieszka Kłosowska, Igor Obuchowski, Nadinath B Nillegoda, Artur Piróg, Szymon Zietkiewicz, Bernd Bukau, Axel Mogk, and Krzysztof Liberek. Hsp70 displaces small heat shock proteins from aggregates to initiate protein refolding. *EMBO J.*, 36(6):783–796, March 2017.